TITLE DIFFUSION-CONTROLLED REACTIONS IN GOLD/LEAD-TIN SOLDER SYSTEMS

AUTHOR El Babi HANNECH

INSTITUTION and DATE University of Warwick 1989

DIFFUSION-CONTROLLED REACTIONS IN GOLD/LEAD-TIN SOLDER SYSTEMS

by

El Bahi HANNECH

A thesis submitted to the University of Warwick for obtention of the degree of Doctor of Philosophy

Department of Physics
University of Warwick
Coventry CV4 7AL

October 1989

I dedicate this thesis

to all my family and friends

TABLE OF CONTENTS

Figures

Tables

ACKNOWLEDGEMENTS

I would like to thank:

Dr. C. R. Hall for his supervision,

S. York, G. Smith and D. Lee of the Physics Department for their technical help,

The Algerian Government for its financial support during the period of this study.

DECLARATION

This thesis is submitted to the University of Warwick in support of my application for obtention of the degree of Ph.D. It contains an account of my own work at the Department of Physics of the University of Warwick, during the period October 1985 to October 1989,under the supervision of Dr. C. R. Hall. No part of it has been used previously in a degree thesis submitted to this or any other university. The work described in this thesis is the result of my own independent research except where acknowledged in the text.

El Bahi Hannech

October 1989

ABSTRACT

Au/PbSn joints are widely used in the microelectronics industry. Intermetallic formation in Au/60Sn-40wt.%Pb and in Au/62Sn-36Pb-2wt.%Ag systems has been studied in the temperature range 80°C-160°C using diffusion couples. Interdiffusion between Au films and 60Sn-40wt.%Pb solder doped with 2 wt.% zinc has also been studied but at 125°C only, also using diffusion couples. The intermetallic phases were identified by Energy Dispersive X-ray Analysis (EDAX) in the Scanning Electron Microscope (SEM) and found to be gold-tin compounds. The predominant phases were found to be $AuSn_4$ and $AuSn_2$ but all the phases predicted in that range of temperatures by the equilibrium phase diagram of the Au-Sn system were present in the couples after long annealing times. The kinetics of the intermetallic layers were determined and an activation energy for the growth of the layer of $AuSn_4$ of 0.84 ± 0.02 eV was found.

The effect of both silver and zinc on the growth rates of the intermetallic layers were determined. It was found that both additives reduce the intermetallic layer growth rates. In addition to the Au-Sn intermetallics, a compound layer of composition $Au_{0.3}Sn_{0.3}Zn_{0.4}$ forms between the $AuSn_4$ layer and the solder in the Au/PbSnZn system.

The tensile strengths of the joints, before and after aging, were also evaluated and the weak bounds within the joints identified. It was found that the weak bonds within a Au/PbSn joint, with or without silver in the solder, were the intermetallic layer interfaces. The joint tensile strength is not weakened by the increase of the intermetallic layer thicknesses with aging time. Joint weakening occurs after degradation of the gold film of the joint, but that happens a long aging time after the depletion of the gold film. The joint made with the zinc containing solder was found to lose strength rapidly after aging. The weak area of the joint is the solder/wire interface.

Chapter 1: INTRODUCTION

When two metals A and B which form intermediate alloy phases with each other are put in contact, layers of the intermediate phases grow between the two metals due to interdiffusion and chemical reaction between the metals. Experimental evidence of such reaction diffusion has been given for various bimetal couples [1,2]. Questions of fundamental interest are whether all the phases predicted by the equilibrium phase diagram of A and B grow and what the growth kinetics of the phase layers look like. The understanding of the reaction mechanism is both of academic and technological interest. It is of technological interest in the coating of one metal with another for corrosion protection for example, in the fabrication of integrated circuits where systems composed of two or more metal layers are often used, and in the bonding of different metals, as the reaction products may weaken the joints, increase their electrical resistance or delaminate a layer.

Solder bonding is extensively used in the microelectronics industry . It has proved to be a very convenient technique for interconnecting components with printed circuit boards, whose use within the microelectronics industry is very well known, the components being required to form a functional sub-assembly. A hybrid integrated circuit with some components indicated is shown in Fig. 1.1. Unlike the passive components (resistors, capacitors), which are generally formed and interconnected by deposition, the active components are fabricated separately then attached to the thin film network, commonly by soldering. The solder bond, however, has always been of concern, especially as the formation of brittle intermetallic

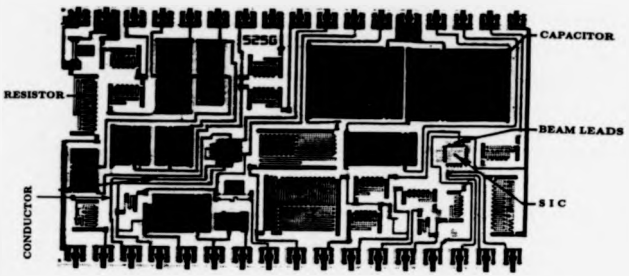

Fig. 1. 1 Hybrid integrated circuit with thin film components and silicon integrated circuits (SIC) (after reference no. 3). The resistors and capacitors are usually connected to the thin film conductor during their deposition on to the circuit board but the SIC are separately fabricated and then connected to the film network by a bonding process, often by soldering.

compounds between the solder and conductor constituents has been reported [4,5] as factors of mechanical problems, and catastrophic failures associated with the wire bonds connecting integrated circuits to printed circuits were widely experienced. Bond failure problems also occurred within joints made by other known wire bonding processes (thermo-compression at about 300°C, ultrasonic bonding at room temperature). It was shown [6] that when a pure gold wire was bonded to an aluminium metallization, or an aluminium wire to a gold surface, by thermocompression, the joint was first good, but on long-aging Au-Al intermetallic compounds plus voids formed and the joint weakened.

Because of the desirable features of the soldering process (solder is a relatively low cost material, soldering is compatible with automatic assembly, possibility of bond repair) much effort has been devoted into investigating the suitability of different solders to thin films.

1.1 Au/PbSn solder joints

Because gold is universally used in the microelectronics applications because of its outstanding properties (excellent conductor of electricity and heat, very resistant to tarnishing and oxidation at room and elevated temperatures, easily solderable, can readily be bonded and deposited onto a substrate by practical production methods, easily etched and delineated in an appropriate chemical product) Au/solder joints have been the subject of studies starting more than two decades ago. The gold used by the microelectronics industry is generally found in the form of electroplated thin films and wires. The gold thin films are used to form the conducting paths of the printed circuits and also the interconnection pattern of the integrated circuits. In some cases the gold film is only used as a coating for another metallisation in order to have non tarnishing surfaces which, even after storage, remain readily solderable. Gold wires are widely used as flying leads to components. Eutectic or near eutectic Sn-Pb solders are almost universally used in soldering the electronic components to printed circuits.

This is because tin-lead alloys have excellent melting properties and bond to many common substrates like gold, iron and copper and are corrosion resistant. The active constituent is tin which promotes dissolution of the substrate metals, the lead not only acting as a diluent but also having the beneficial effect of producing a stronger alloy and a lower melting temperature than the parent metals. The equilibrium phase diagram of the Pb-Sn system is shown in Fig. 1.2. Eutectic (63 Sn-37wt.%Pb) or near eutectic tin-lead solders are used in order to minimize the soldering temperature and to eliminate the whisker growth the tin-lead alloys are prone to. Furthermore, PbSn solders are relatively cheap and alloy readily at a conveniently low temperature with gold and many other substrate metals. This latter feature is very important for the electronics industry where exposure to high temperatures could disrupt the increasingly complex circuits.

During the soldering process gold is dissolved into the molten solder. The rate of dissolution of Au into molten tin-lead is very high (about 1 μm/s at 200°C) [5]. At room temperature the solid solubility of Au in tin-lead is negligible but several intermetallic compounds between gold and lead (Au_2Pb and $AuPb_2$) [6] and tin ($AuSn_4$, $AuSn_2$, $AuSn$, Au_2Sn, δ-phase(10 to 18.5at.%Sn) and $Au_{10}Sn$) [9] exist. In the 5-10 wt.% range, Au in 60wt.%Sn-40%Pb solder has previously been found [4,5] to produce brittle intermetallic compounds and potentially unreliable bonds. Acicular $AuSn_4$ crystals and $AuPb_2$ dendrites formed and produced a brittle weak solder joint when the gold content exceeded 5% by weight in PbSn solder [4]. Because of this potential problem gold films thicker than 1.5 μm have been considered unacceptable for producing reliable solder joints [10]. More recently, the reliability of 60wt.%Sn-40%Pb solder bonds to thin trilayer films of Ti/Pd/Au have been evaluated by aging the joints at elevated temperatures and then measuring the bond strength [12-15]. The gold thickness was within the 1.5 - 5 μm range and because of the rapid dissolution of Au into molten tin-lead solder reported earlier complete dissolution of the gold film was expected [12] to occur during the

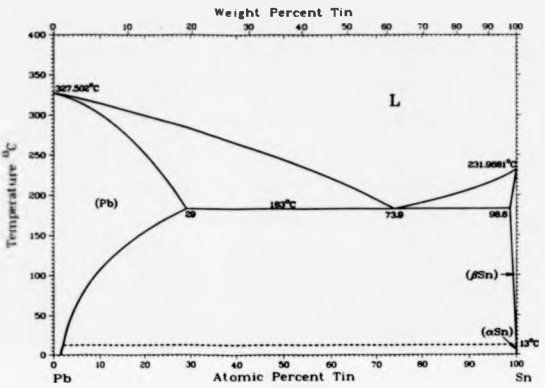

Fig. 1. 2 Equilibrium phase diagram of PbSn alloys[7].

soldering process, which would give an Au concentration in the solder less than the 5% limit which was reported to produce weak solder bonds. It was shown that initially and after mild aging (50°C) acicular $AuSn_4$ formed in the solder and disappeared during accelerated temperature aging; layers of the Cu-Sn intermetallic compounds, Cu_3Sn and Cu_6Sn_5, were detected at the solder/copper wire interface after temperature aging. Analysis of fracture surfaces after pull testing aged solder joints implicated [12-14] intermetallic growth with bond weakening. From measurements of joint strength as a function of time at different temperatures an activation energy for the weakening process was determined [12,13] by proceeding as follows. After an end of joint life was chosen as that time t when the solder bond strength decreased by one standard deviation below the initial value, an Arrhenius graph, $\log T$ versus $\log t$ was constructed, with T the annealing temperature; from that graph the activation energy was determined. The end of life extrapolated to 50°C was found to exceed [12,13] 40 years. In another work [15] on similar samples the solder life time (the time required for the pull strength to fall from 5.8 to 4.0 lb.) was found to be 114 years at 80°C.

1.2 Au/solder joints

Various solders have also been investigated in order to find a suitable one for making reliable bonds to gold surfaces. 50 wt.%indium-50Pb alloy has been reported [16] to dissolve gold more slowly than eutectic tin-lead solder does. However, it has been found [17] that the $AuIn_2$ intermetallic compound rapidly formed between the gold film and the solder in as little as 12 hours at 125°C. When that solder was used to attach sapphire circuits to gold plated copper, aluminium, or Kovar packages, as a result of the $AuIn_2$ formation, the solder joint was extremely shock sensitive and hybrid microcircuits assembled with 50In-50Pb solder and aged at 100°C for one year suffered catastrophic failures [17]. The eutectic solders 88Au-12Ge, 80Au-20Sn, 90Sn-10Au, 85Pb-15Au, and the off-eutectic solder 60Sn-36Pb-4Ag

have also been found to produce intermetallic compounds by solid-state reaction with gold plating [18]. The presence of AuSn, $AuSn_2$, $AuSn_4$, and voids at the plating/solder interface, were revealed when gold/Sn-Au solder metallographic samples aged at 125°C were examined in the scanning electron microscope and chemically analysed. $AuSn_2$ and $AuSn_4$ intermetallic compounds were detected at the interface of Sn-Pb-Ag solder, and $AuPb_2$ intermetallic compound was detected at the interface of Pb-Au solder. Leap shear measurements made on samples subjected to temperature cycles between -55 and 125°C before and after thermal aging have shown that the joints made with the Sn-Au solder failed catastrophically within 10^3 hours at 100°C when the joined materials had dissimilar thermal expansion. Analysis of the fracture surfaces of samples annealed for 120 hours at 125°C showed that Sn-Au, Pb-Au, and Sn-Pb-Ag solders failed between the gold plating and the intermetallic region whereas Au-Ge and Au-Sn solders failed within the solder. When the joined materials had similar coefficients of thermal expansion the projected life times for all the solders were >10 years at 100°C.

1.3 Growth mechanisms of Au-Sn intermetallics in Au/Sn thin film joints

Because Au/Sn thin films are often used as metallizations on GaAs and on Ga-As-Al semiconductor devices, interdiffusion in the Au/Sn system has been extensively studied [19–20]. The studies mainly focused on the joint microstructure, the growth kinetics of the resulting phases, and on the diffusion mechanism of Au and Sn in the phases. In those studies, however, the materials consisted of very thin films (less than 5000 $\AA$) obtained by evaporation and interdiffused at room temperature. For a number of reasons [20] diffusion in thin films may differ from the ordinary diffusion which occurs in bulk specimens. The factors which may cause diffusion in thin films to differ from that which occurs in bulk specimens include

the high densities of low temperature short circuits such as grain boundaries and dislocations that generally thin films contain, the short distances over which the diffusion often occurs under the influence of large concentration gradients, the disordered or metastable structure that thin films often possess since they are often produced under highly non equilibrium conditions at relatively low temperatures.

The evaporated Au/Sn thin film couples appeared to readily [20,21] interdiffuse even at room temperature leading to the formation of Au-Sn phases. It has been found [23] that AuSn and $AuSn_4$ were formed at early stages of the interdiffusion and that a transformation of $AuSn_4$ into AuSn took place in the presence of excess gold and of AuSn into $AuSn_2$ and $AuSn_4$ in the presence of excess tin; the transformation of $AuSn_2$ into $AuSn_4$ seemed to take place very slowly. At room temperature the phases had a layered structure but after annealing at about 200°C a single phase or a mixture of two of the Au-Sn phases or $AuSn_4$ and Sn, depending on the relative thickness of the evaporated gold and tin films, existed. The use of various thickness combinations in Au/Sn thin film couples have permitted [27] detection of four intermetallics (δ-phase, AuSn, $AuSn_2$, and $AuSn_4$) which exist in the equilibrium phase diagram of the Au-Sn system. Room temperature interdiffusion in evaporated Au/Sn films, studied [22] by the in-situ backscattering of 2.0 MeV ^4He ions showed that the growth of the AuSn phase followed a parabolic growth rate law; the growth rate constant was found to be about 9×10^{-15} cm^2 s^{-1} at 20°C. Implanted argon ions into Au/Sn thin films, used as Kirkendall markers, and Rutherford backscattering spectroscopy have shown [28] that gold diffuses through the AuSn phase layer three times faster than tin does. The diffusion of gold atoms through the AuSn phase is believed [29] to occur along the grain boundaries of the AuSn; an activation energy of 0.59 ± 0.06 eV for the diffusion was determined [29] for the temperature range between -170 and +50°C. The growth of the AuSn phase was found parabolic with diffusion time as reported elsewhere [22] but that of the $AuSn_4$ phase was found

to be linear with time[29].

1.4 Cu/PbSn joints

Copper is also a metal used in the microelectronics industry. Upon soldering PbSn solders to Cu metal intermetallic layers of Cu-Sn form [31-34]. With 60Sn-40Pb solder two intermetallic layers, Cu_3Sn and Cu_6Sn_5, form [31-34]. In addition to these interfacial intermetallics, Cu_6Sn_5 precipitates were found in the bulk solder region of the solder joint [33]. The effect of the intermetallics has been reported [32] to decrease the tensile strength of the joint considerably, e.g. the tensile strength of the Cu/60Sn-40Pb joint was decreased by 50% as the Cu_6Sn_5 layer increased from approximately 3 to 12 μm. The joint failure was found to occur within the Cu_6Sn_5 intermetallic layer during either tensile [32] or shear [31] tests of the joint.

1.5 Void formation in metallic joints

Interdiffusion in metallic joints may result not only in intermetallic growth but also in void formation. Two other sources of void development in the interconnect metallization regions of integrated circuits are moisture corrosion and electromigration (the mass transport in a conductor under an applied electric field [35,36]). Concentration gradient diffusion induced voids are known as the Kirkendall effect: when two species having a large difference in their bulk diffusivities interdiffuse, voids form on the side of the couple from which the faster diffusing atom originates. In a two component system with compounds formed by binary diffusion each metal has to diffuse through the layer of intermetallic compound(s) to reach the other interface. Since the diffusion rates of the reacting metals through the layer may be different, the diffusion rate discrepancy may cause a vacancy build up which will condense to produce voids at one of the metals/intermetallic layer interface. In this case it is not the difference in the diffusivities of the metals in each other which leads to void formation

but the discrepancy of their diffusivities through the layer of intermetallic compound(s). In a multiphase system, voids could occur at each metal/compound layer interface since the phase layer boundaries may act as sinks for the diffusing atoms as a result of reactions at the boundaries and thus each metal may flow into the compound layer faster than either is flowing out the other interface.

Void formation leads to greater than normal thermal and electrical resistance and causes the joint to weaken and eventually to fail. It is believed [6] that the development of voids which occurs on the gold side in gold-aluminium bonds is the cause of joint weakening and failure. In a report on room temperature interdiffusion in Au/Sn used in a metallization on Ga/Al/As light emitting diodes it was concluded [24] that the adhesion problem which occurs between Au/Sn/Al metallization and Ga/Al/As during the fabrication of light emitting diodes is due to high tensile stress resulting from void formation.

1.6 The reasons and aim of this work

Although much work has been done to study the growth mechanisms of the Au-Sn intermetallics, the studies have been limited to Au/Sn thin film joints only. The tensile strength after aging of a joint between PbSn solder and a gold plated surface has been studied in the particular case where during the joint fabrication the gold film completely dissolves into the molten solder. The formation of Au-Sn intermetallics by solid-state reactions in a Au/PbSn joint and their effect on the tensile strength of the joint has not been studied, nor the effect of additives in the solder on the growth rates of the intermetallic layers. Therefore, the aim of this work is to:

1) Determine the growth kinetics of the phase layers which grow between electroplated thin gold films and 60Sn-40Pb bulk solder at different temperatures (chapter 3).

2) Determine the effects of additives such as Ag and Zn in the solder on the growth rates

of the phase layers (chapters 3 and 4).

3) Determine the Au/solder joint strength after temperature aging and relate changes to the observed changes in the microstructure (chapter 6).

Chapter 2: EXPERIMENTAL TECHNIQUES

This chapter describes the methods used to prepare the gold films, to make the Au/solder joints and to prepare them for microscopical examination. The Scanning Electron Microscope (SEM) and the Energy Dispersive X-ray Analysis (EDAX) technique which were used for this examination are also described.

2.1 Preparation of the gold films

For the present work the gold films were prepared by electroplating. The material (the substrate) onto which the films were deposited was Al_2O_3 alumina.

2.1.1 Substrate cleaning

Before using the substrates for the subsequent metal deposition they were thoroughly cleaned. Substrate cleanliness is very important for good adhesion between the deposit and the substrate surface. A good bond was needed at this point to ensure that during pull strength test of the film/solder joint the film did not strip off the substrate. The following procedure was used to clean the substrates which consisted of wafers of 99.99% Al_2O_3 ceramic, 1 mm thick and 50 mm square. Each substrate was suspended for 10 minutes in ultrasonically agitated trichlorhethylene, rinsed with deionised water, suspended for 10 minutes in ultrasonically agitated phosphate-free detergent solution (decon^{90}), and then rinsed in deionised water and held for 15 minutes in running deionised water. Thereafter it was washed in deionised water agitated ultrasonically for 5 minutes and blow dried with N_2 gas. Finally it was rinsed in hot

methyl alcohol and blow dried with nitrogen gas.

2.1.2 Preliminary coating

To make gold electroplating possible the substrate had first to be rendered conductive. This was achieved by a process of vacuum metallization. Before starting the metallization process the substrate was heated up to 400°C and kept for 1 hour in the vacuum chamber pumped down to 10^{-6} torr. The preheating is desirable to outgass the substrate as this is found to improve the coating adherence. Then a thin layer, about 400 $\AA$ in thickness, of 80-20 nickel chromium alloy was deposited onto the substrate. The metals were deposited from a resistively heated tungsten wire (Fig. 2. 1). During evaporation the pressure in the vacuum rose to about 10^{-4} torr and the substrate was kept at 400°C. The desired deposit was obtained in a few seconds. Assuming the evaporation was isotropic the thickness d of the deposit was determined by the mass m of alloy evaporated and the distance L (about 60 mm) from the source to the substrate (Fig. 2. 1). This first evaporation is critical in providing good adherent films of gold on the substrate . While noble metals like gold do not adhere firmly to aluminium oxide , oxide formers like chromium do. The correlation between the adhesion of metals on a Al_2O_3 substrate and the free energy of formation, Δf, of their oxide has been shown [37]: the more negative Δf the greater the adhesion. In this case, the adherence between the substrate and the deposited film is thought [38] to be achieved by an alumino-chromate layer which forms as a result of some chemical reaction between the chromium and the aluminium oxide. This adherence was found to be poor when the deposition occurred at room temperature but satisfactory at 400°C.

Without removing the substrate from the vacuum, a second layer, about 400 $\AA$ in thickness, consisting of pure gold was immediately deposited over the nickel-chromium layer in the same manner. This gold film protects the nickel-chromium underlayer from oxidation on

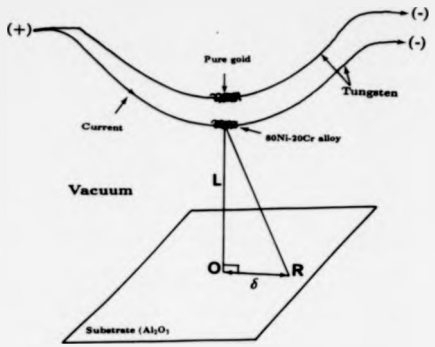

Fig. 2. 1 The nickel-chromium alloy and the gold were successively evaporated in a vacuum chamber from 2 resistively heated tungsten wires. The thickness d of a deposit at point R of the substrate is equal to $\frac{m}{4\pi L^2(1+(\frac{\delta}{L})^2)^{\frac{3}{2}}}$ where m is the mass of the material wrapped over the tungsten wire and evaporated by passing a current through the wire, L the distance from the material being evaporated down to the substrate and δ the distance indicated on the figure.

removal of the substrate from the vacuum chamber and gives a good surface for the subsequent gold electroplating. After the evaporation was complete the substrate was allowed to cool to room temperature in a vacuum of 10^{-5} torr or less and the sample kept in the vacuum until required.

2.1.3 Electroplating

Electroplating is the deposition of a metal from a solution of its ions or ion complexes by electrolysis. The choice of the electrolyte and the operating parameters (temperature, pH, concentration, etc...) to make a deposit is based upon the properties of the deposit wanted. For integrated circuit applications electrodeposited gold must be of high density and electrical conductivity to maximise signal transmission, and have a suitably smooth surface. Other features of the electrodeposit such as hardness, wear resistance, porosity, stress are of lesser importance but must meet minimum standards for the layer to be usable.

The most important complexes of gold used in gold plating baths are [39] cyanide and sulphide complexes of Au of which the potassium derivatives are $KAu(CN)_2$ and $K_3Au(SO_3)_2$.

Various possibilities have been discussed for the discharge of a metal ion from a ion complex [40]. The deposition of Au is thought [39] to occur in the following manner when the complex used is $KAu(CN)_2$ or $K_3Au(SO_3)_2$. Positive ions are attracted by the cathode to a region near its surface known as the Helmholtz double layer. The negatively charged ions such as the $Au(CN)_2^-$ present in the gold cyanide bath which approach this double layer become polarised in the electric field of the cathode. Within the Helmholtz layer the complex breaks up:

$$Au(CN)_2^- \longrightarrow Au^+ + 2\,CN^- \text{ in a cyanide bath.}$$

$$Au(SO_3)_2^{3-} \longrightarrow Au^+ + 2\,SO_3^{2-} \text{ in a sulphate bath.}$$

Finally the metal released from the complex in the form of the metal cation is neutralised

and deposited on the cathode (substrate).

Immediately after its removal from the vacuum chamber where the preliminary coating took place, the substrate was put into a gold plating bath and electroplated with Au up to the required film thickness. The Au solution used and the electroplating parameters are given in Table 2.1 and the typical microstructure of the Au films is shown in Fig. 2.2. Gold films prepared under identical conditions to those set out in this table were reported [43] to be of very high purity (99.99% Au), with low porosity, to have a density of 19 g/cm^3 and a contact resistance equal to 0.3 milliohms; film hardness in the range 110-130 V.P.N was also reported [41].

2.2 Preparation of gold discs

The evaporation and plating process gives an approximately uniform coating of gold on the substrate. For the purpose of this investigation the gold was required in the form of 2 mm diameter islands on the substrate, which were obtained as follows. A positive photoresist material, UV sensitive, was applied by a spinning technique to the gold surface and exposed to ultra-violet light via a mask. The exposed resist was removed in a suitable solvent, then the unprotected gold surface etched in an appropriate chemical solution (1g of Iodine + 25g of Potassium iodine per 50 c.c of distilled water). After cleaning and inspection in an optical microscope to ensure that all the uncoated metal had been removed, the unexposed resist was removed, leaving the desired gold pattern, i.e. 2 mm gold discs.

2.3 Preparation of gold film/solder joints

Solders of different compositions were used to make joints for diffusion studies and joints for the tensile tests. Two solders, 60Sn-40wt.%Pb and 62Sn-36Pb-2wt.%Ag, were supplied and one was made in the laboratory by adding 2wt.% zinc in the 60Sn-40wt.%Pb solder. The ready-made solders were in the form of cream for the SnPbAg and in the form of wire

Table 2. 1 Gold film electroplating conditions.

Solution	$KAuCN_2$ (68% Au) in solution made up of Aurall 292M* (75%/volume) and deionised water (25%)
Solution density	10g/l
Temperature	57°C
Cathode current density	0.2 Ampere/dm^2
Agitation	mechanical
Anode	platinum plated titanium
Deposition rate	0.104 g/Amp. minute (85% cathode efficiency)

* Aurall 292M is a commercial plating preparation sold by Lea Ronal.

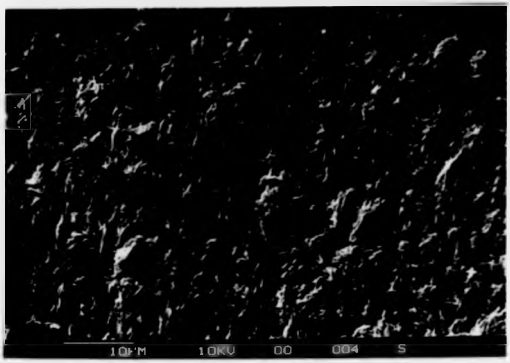

Fig. 2.2 SEM micrograph showing the typical microstructure of thin gold films electrodeposited onto Al_2O_3 substrate in the conditions set out in Table 2. 1.

for the PbSn. The laboratory-made solder, PbSnZn, was in the form of a disc 2 to 3 mm thick.

As noted in the previous chapter, gold dissolves very rapidly in molten tin-lead solder, and so joints to gold have to be made very quickly. For making a gold/solder couple the surface of the gold disc, 2 mm in diameter, was covered with a suitable amount of the solder cream and this was heated until it became liquid. As soon as this occurred, the heat (supplied by a temperature controlled soldering iron set at about 250°C) was removed and solidification occurred within a second or so. When the solder was not in the form of cream it was melted on the soldering iron first and then put on the gold surface. A special flux was used when gold/PbSnZn couples were manufactured.

To test the bond strength of the joints, copper wires, 0.5 mm diameter, were soldered to the 2 mm diameter gold films. Because copper has bad solderability when it is not new because of its quick oxidation,the wires were coated with solder before soldering them to the gold films. This was done by steeping the extremity to be attached for a few seconds in molten alloy of the solder to be used. If this had not been done the wire bonding would have required a longer soldering time which would have resulted in greater dissolution of the Au film by the molten solder.

2.4 The Scanning Electron Microscope (SEM)

The scanning electron microscope was the chief experimental tool used to study the microstructure and composition of the samples used in this investigation.

2.4.1 Working principles

A schematic diagram of a scanning electron microscope is shown in Fig. 2.3. When used to examine a solid the SEM can yield optimum results only if the working principles are fully

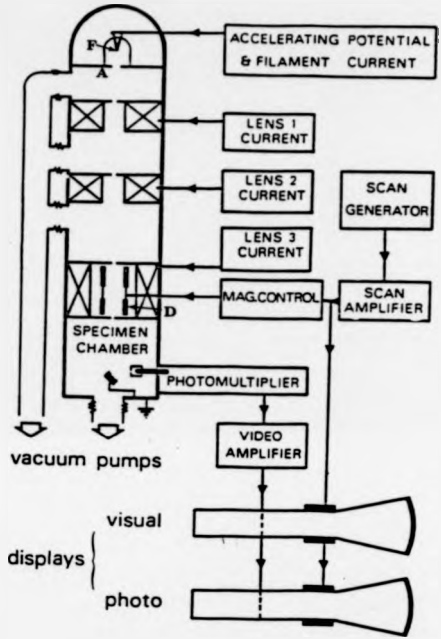

Fig. 2. 2 Schematic diagram of a scanning electron microscope[42]. A beam of high energy electrons is emitted into the microscope when the filament (F) is heated by the passage of a current and held at a high negative potential with respect to the anode A and the rest of the microscope. The electron beam is focused onto the specimen by the condenser lenses and across it by the deflector coils D.

understood. The basic principles of operation may be described as follows. An electron beam is moved over the specimen surface in a sequence of closely spaced lines. The electrons emitted from the surface are collected by a detector which converts them into an electrical signal. This signal is amplified and then used to modulate the brightness of a cathode-ray tube (CRT) beam which is moving in synchronism with the scanning beam over the specimen. The variation in electron emission or backscattered electrons from point to point on the specimen surface, due to variations in composition or topography for example, builds up the image on the recorder. The SEM can be operated in secondary or in backscattered electron imaging mode. In the secondary electron mode the contrast is formed by the variation in the number of secondary electrons which are collected from different areas of the specimen. The electron detector which has a voltage applied to it, variable from -30 to +250 V, is used with a positive bias to attract these electrons because of their low energy (of the order of 20 eV). In the backscattered mode the image is formed by detection of the backscattered electrons by the specimen. Since the number of these electrons increases with the atomic number of the target, contrast due to compositional variations may be produced.

2.4.2 Magnification

The magnification of the SEM image is determined by the ratio of the sizes of rasters (areas) scanned on the specimen surface and on the display screen. For example, if the image on the CRT screen is 100 mm across, magnification of 100× is obtained by scanning an area on the specimen surface 1 mm across. Magnification of 10× is obtained by scanning an area of the specimen surface 10 mm across. One consequence is that high magnifications are easy to obtain with the SEM, while very low magnifications are difficult. With an ordinary SEM magnifications up to 300 000× can be obtained, the lowest being 20×.

2.4.3 Resolution

The resolution is an important quantity for the microscope; it can be defined as the minimum distance between two adjacent features of the specimen that can be observed individually. With a specimen with sufficient contrast the resolution is at best equal to the diameter of the electron beam where it strikes the specimen surface. This can be as small as 5 nm. However the resolution obtained in practice is much worse than this. Firstly because of the spreading of the beam inside the sample and secondly because of insufficient contrast given by the specimen surface. A relation between specimen contrast, c, and resolution, the distance d between two adjacent features that can be observed separately, has been given [42]:

$$d^2 \geq \frac{144N^2e}{\alpha^2\tau Bf\pi^2[c^2 - 36(\sigma_g/g)^2]}, \tag{2.1}$$

where N is the number of lines per frame, e the electronic charge, α the beam divergence, τ the time to scan a whole frame, B the brightness of the beam, c the contrast, g the gain of the amplification system, σ_g the standard deviation of g of its mean value, f the number of electrons that are emitted from the specimen per incident electron.

This shows that the resolution improves with an increased time τ for one frame scan, with increased contrast in the specimen and with an increased value of the final aperture size. N is normally fixed at 1000 lines, B is fixed by the gun (filament) used and f by the specimen and the mode of contrast chosen.

Detailed texts describing the SEM are available [42–44].

2.5 Energy Dispersive X-ray Analysis (EDAX)

2.5.1 Principles of operation

The EDAX technique is based on the detection of the X-rays emitted by the sample at the time of its irradiation by the electron beam. The detector generally used in this technique

is a lithium-drifted silicon crystal. A schematic diagram of an energy dispersive X-ray spectrometer containing a lithium-drifted silicon detector is illustrated in Fig. 2. 4. Placed in the specimen chamber at a distance of about 15 mm from the sample, it is irradiated by X-rays coming from the specimen area under the primary electron beam. Each X-ray incident on the detector creates some free electrons by photoelectric absorption and subsequent electron-electron interaction. The number of free electrons produced is proportional to the energy of the absorbed X-ray quantum. So, knowing the energy necessary to raise an electron to the conduction band (equal to 3.8 eV in Si) and the number of electrons created gives the energy of the X-ray. An applied potential across the silicon crystal causes the electrons to travel to an anode, from which they are transferred to a field effect transistor. This transistor transforms the very tiny currents into voltage pulses. The amplitude of the pulse is a linear function of how much energy was collected, in other words, of the X-ray energy. The voltage pulses are passed into a multichannel analyser (MCA), separated on the basis of their amplitudes and stored in memory channels. The resulting spectrum can be displayed on a cathode-ray tube and the peaks can be identified, as shown by Fig. 2. 5, allowing thereby a qualitative analysis of any area of interest of the specimen surface.

2.5.2 Quantitative analysis

Quantitative analysis of a material of unknown composition can be achieved from measurements of the intensities of characteristic X-rays emitted by the elements present in the material. The most widely used method for converting X-ray intensities into elemental concentration is the ZAF method. One version of this method is to compare between the intensity of the characteristic radiation from the specimen, I_A, with that from a pure element or well defined compound standard, $I_{A'}$ under identical external conditions of excitation. Then the

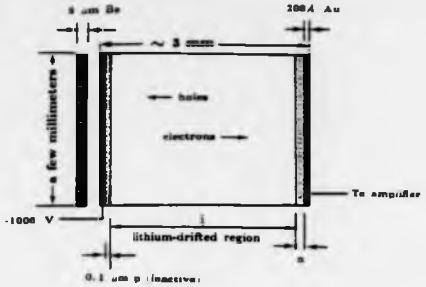

Fig. 2. 4 Schematic diagram of a typical lithium-drifted silicon detector of an energy dispersive X-ray spectrometer. The detector is a p-i-n junction. The beryllium layer (or Be window) is for maintaining the vacuum integrity of the detector, the gold layer for establishing the electrical contact and the p-layer (called silicon dead layer) for eliminating the loss of charge which occurs in the region of the silicon near the surface.

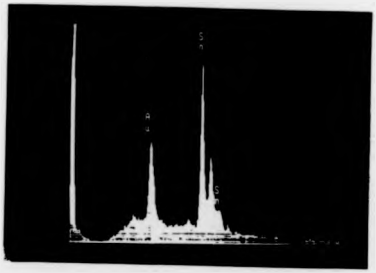

Fig. 2. 5 Display on a cathode-ray tube (CRT) of the X-Ray spectrum collected from a small area within the diffusion zone of a Au/PbSn diffusion couple using an energy dispersive X-Ray spectrometer (EDS) and a multichannel analyser (MCA). The area was excited with a 15 KV electron beam. The elements present in the area could be identified. The peaks which are seen are of the emission lines M and (L_{α_1}, L_{β_1}) of Au and Sn elements respectively. The composition of the area ,calculated from the intensities of these lines according to the procedure outlined in sub-section 2.5.2, is $AuSn_4$.

intensity ratio $I_A/I_{A'}$ is written in the form:

$$(\frac{I_A}{I_{A'}})_{measured} = ZAFC_A, \tag{2.2}$$

where C_A is the weight fraction of the element A present in the specimen and Z, A and F are correction factors which are discussed below. A similar equation with different values of Z, A and F holds for the elements B, C, etc... present in the specimen.

An alternative version of the ZAF method, which does not rely on standards, depends on measurement of the ratios I_A/I_B, I_B/I_C, *etc*... for all the different elements present in the specimen. The total concentration is then assumed to sum 100%. The procedure also requires correction for atomic number, absorption and fluorescence effects. It is this procedure, called standardless analysis, which was used here.

***Atomic number correction**

The intensity of an X-ray signal is proportional to the number of its quanta produced per electron incident. Quanta of the radiation being measured are produced by the ionization of atoms along the electron path inside the material through electron-atom collisions. If there are dn_A ionizations of A atoms in an element of electron path dx for which the electron energy falls from E to $E - dE$, then:

$$dn_A = \frac{N\rho C_A}{A_A} Q_A(E)dx, \tag{2.3}$$

where N is Avogadro's number, A_A is the atomic weight of element A which is present at weight fraction C_A in a specimen of density ρ, and $Q_A(E)$ is the ionization cross-section of an atom A for the line (K, L or M) being measured. n_A is given by integration of dn_A along the useful electron path, of length x_t, in the target (the total length traversed by the electron from the time it enters the surface until its energy drops below the minimum energy

for ionization of the line measured).

$$n_A = \frac{N\rho C_A}{A_A}\int_0^{z_c} Q_A(E)dx \tag{2.4}$$

$$= \frac{N\rho C_A}{A_A}\int_{E_0}^{E_c} \frac{Q_A(E)dE}{(dE/dx)} \tag{2.5}$$

$$= \frac{NC_A}{A_A}\int_{E_0}^{E_c} \frac{Q_A(E)}{S_A(E)}dE, \tag{2.6}$$

where $S_A(E) = -\frac{1}{\rho}\frac{dE}{dx}$ is the electron stopping power of the sample, E_0 is the initial energy of the electron (given by the accelerating voltage of the microscope), and E_c is the minimum electron energy for ionization of the line measured.

Not all the incident electrons, however, produce n_A quanta. Some of them are back-scattered by the sample before their energy falls to E_c (Fig. 2.6) and so do not produce the maximum number of quanta, n_A, of which they are capable. The effective current of electrons contributing to the generation of the X-ray quanta is $R_A P$ where P is the incident electron current and R_A an effective current factor or back-scatter factor of the sample.

The characteristic X-ray intensity generated in the sample is therefore given by:

$$I_A = \frac{NC_A}{A_A}R_A P\omega\beta\int_{E_0}^{E_c} \frac{Q_A(E)}{S_A(E)}dE, \tag{2.7}$$

where ω is the fluorescence yield of the X-ray line (K, L or M) being measured (the fraction of the ionizations of the line being measured which lead to photon emission), β is the fraction of the emitted characteristic X-ray intensity that is in the line being measured. S and R depend upon both the radiation being measured and the atomic number of the specimen.

The intensity ratio, $I_A/I_{A'}$, of X-rays produced by the element A of a multi-element specimen to that in a pure element standard is then:

$$\frac{I_A}{I_{A'}} = C_A\frac{R_A}{R_{std.}}\frac{\int_{E_0}^{E_c}\frac{Q_A(E)}{S_A(E)}dE}{\int_{E_0}^{E_c}\frac{Q_{std.}(E)}{S_{std.}(E)}dE}, \tag{2.8}$$

where the numerator relates to the production of characteristic X-rays from element A in the specimen and the denominator to the production of the same wavelength radiation in the standard.

Fig. 2. 6 Typical electron paths in a solid. One electron backscattered before its energy E had fallen below the minimum energy of ionisation of the solid atoms, E_C, and one electron which had terminated its path in the specimen are shown.

The atomic number factor, Z, is given by:

$$Z = \frac{R_A}{R_{std.}} \frac{\int_{E_0}^{E_c} \frac{Q_A(E)}{S_A(E)} dE}{\int_{E_0}^{E_c} \frac{Q_{std.}(E)}{S_{std.}(E)} dE} \tag{2.9}$$

In the absence of absorption and fluorescence:

$$(I_A/I_{A'})_{measured} = C_A Z. \tag{2.10}$$

For the evaluation of Z there exist analytical expressions and tables for R, S and Q. Values of R for an angle of incidence, α, of the electron beam on the specimen surface of 90° [45] and 45° [46], derived from experimental electron backscattering data, have been tabulated and an analytical expression for any incidence angle, α, has been proposed [47]. Analytical expressions for the stopping power [45,47], S, and the ionisation cross-section [48,49], Q, have also been published.

Absorption correction, A

The radiation produced in the specimen suffers absorption as it emerges, and consequently the intensity that is measured, I_A^m, is less than that which is produced. For a specimen having a density ρ and a mass absorption coefficient $(\frac{\mu}{\rho})$ for the radiation being measured, the X-ray intensity generated in a small element of mass thickness $d(\rho z)$ at a depth ρz below the surface (see Fig. 2.7) is given by:

$$dI_A = C_A \phi_A(\rho z) d(\rho z), \tag{2.11}$$

where $\phi_A(\rho z)$ is the distribution in depth of the X-ray radiation being measured from the specimen. In the case where the electron beam strikes the specimen at normal incidence the X-rays have a path length within the sample of $\rho z \csc\theta$, where θ is the X-ray take-off angle, and the fraction emitted at this angle is therefore $C_A \phi_A(\rho z) \exp[(-\frac{\mu}{\rho})\rho z \csc\theta] d(\rho z)$. The emitted intensity, I_A, is thus:

$$I_A = C_A \int_0^\infty \phi_A(\rho z) \exp(-\chi \rho z) d(\rho z) \equiv C_A F(\chi), \tag{2.12}$$

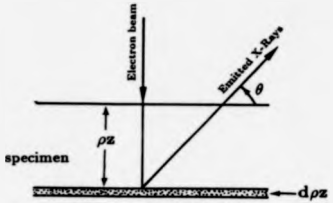

Fig. 2.7 At a take-off angle θ the X-Rays generated in a small element of thickness $d(\rho z)$ at a depth ρz below the specimen surface have a path length within the sample equal to ρz cosec θ. Because of X-Ray absorption within the specimen the intensity of the emitted X-Rays, I_{em}, is less than that of the X-Rays produced in the element $d(\rho z)$, I_{pr}; $I_{em} = I_{pr} \exp[-(\frac{\mu}{\rho}) \rho z \text{ cosec } \theta]$ where $\frac{\mu}{\rho}$ is the mass absorption coefficient of the specimen.

where $\chi = \frac{\mu}{\rho} \csc\theta$ and $F(\chi)$ the defined integral.

Thus, the primary emitted intensity ratio when a pure element standard is used is:

$$\frac{I_A}{I_{A'}} = C_A \frac{F_A(\chi)}{F_{std.}(\chi)}. \tag{2.13}$$

This may be rewritten:

$$\frac{I_A}{I_{A'}} = C_A \frac{F_A(0)}{F_{std.}(0)} \frac{f_A(\chi)}{f_{std.}(\chi)}, \tag{2.14}$$

where $f(\chi) = \frac{F(\chi)}{F(0)} = \frac{\text{intensity emitted}}{\text{intensity produced}}$. $F(0)$ is the value $F(\chi)$ takes when there is zero absorption so that $C_A F(0)$ is the generated intensity. It follows that the ratio $\frac{F_A(0)}{F_{std.}(0)}$ is the atomic number correction Z. The ratio $\frac{f_A(\chi)}{f_{std.}(\chi)}$, which contains the attenuation terms, is known as the absorption correction factor A. In the absence of fluorescence:

$$\left(\frac{I_A}{I_{A'}}\right)_{measured} = C_A Z A. \tag{2.15}$$

For the evaluation of A several authors [50–53] have proposed analytical expressions for the function $f(\chi)$. The most recent publication [53] presents a function for use with tilted specimens.

***Fluorescence correction, F**

X-rays produced in the sample by the incident electron beam (X-rays characteristic of other elements present in the specimen and/or X-rays of the continuum spectrum) may be absorbed by atoms of element A. This will happen if the X-ray energy is greater than the minimum energy for ionization of the line of the element A being measured E_c. In this case, fluorescent X-rays arise from A atoms and contribute to the intensity of the radiation being measured, resulting in radiation intensity of A different (higher) from that produced directly by the electron beam and which is related to the concentration C_A of A by the expression given above. The fluorescent enhancement is greatest when the energy of the radiation causing fluorescence is just greater than E_c and when a small concentration of A is being measured.

If I_A^f is the contribution to the intensity measured from the specimen due to fluorescence of A caused by X-rays, the ratio of the total characteristic X-ray intensity emitted by the specimen, I_A^s, to that emitted by a pure element standard, $I_{A'}$, is given by:

$$\frac{I_A^s}{I_{A'}} = \frac{I_A + I_A^f}{I_{A'}}, \tag{2.16}$$

where I_A is the primary (direct excitation by the beam) intensity emitted by the sample; I_A^f is the X-ray intensity emitted by the alloy due to fluorescence. Rewriting the equation above one obtains:

$$\frac{I_A^s}{I_{A'}} = \frac{I_A}{I_{A'}} + \frac{I_A^f}{I_A}\frac{I_A}{I_{A'}} \tag{2.17}$$

$$= \frac{I_A}{I_{A'}}(1 + \frac{I_A^f}{I_A}). \tag{2.18}$$

The ratio $\frac{I_A}{I_{A'}}$ is equal to $C_A Z A$, so:

$$(\frac{I_A^s}{I_{A'}})_{measured} = C_A Z A (1 + \frac{I_A^f}{I_A}) \equiv C_A Z A F, \tag{2.19}$$

where $F = (1 + \frac{I_A^f}{I_A})$ is the fluorescence correction factor. If there are several wavelengths present which cause fluorescence of the element A the correction is obtained by computing the sum of the different contributions. In this case F is given by:

$$F = (1 + \sum_j \frac{I_{jA}^f}{I_A}). \tag{2.20}$$

A formula for $\frac{I_A^f}{I_A}$ for absorption of characteristic radiation has been theoretically derived [54] and a simplified version of it has been given [55]. These formulas have been reported [56] to give the most accurate fluorescent corrections.

2.6 Preparation of metallographic specimens

One of the main objectives of this work was to study the microstructure of the interface between the Au film and the solder, the compositions of the various layers formed and the

kinetics of their growth. The study was carried out on metallographically prepared cross-sections using a scanning electron microscope (SEM) and an energy dispersive X-ray analyser (EDAX) fitted to the microscope.

2.6.1 Effects of the surface state on SEM-EDAX analysis of specimens

Considerable care in the specimen preparation for microscopical examination is necessary to obtain satisfactory results, particularly when quantitative measurements are desired. The surface to be examined must be clean and representative of the bulk material. Furthermore, the surface must be smooth and flat otherwise misleading effects can arise. Fig. 2.8 illustrates what may happen with a non smooth surface. Some electrons from the point A (Fig. 2.8a) are prevented from reaching the collector and consequently the point A will appear on the image screen darker than normal. As a consequence contrast between the point A and its environment will appear and may swamp the atomic number contrast that would have been present with a good surface. Such topographic contrast may lead to incorrect interpretations. Secondly, some of the X-ray signal from the point under analysis (Fig. 2.8b) may be intercepted and absorbed at B; or points like C and B may fluoresce under the effect of this signal (or backscattered electrons) and add to the measured X-ray intensity a component that has nothing to do with the area under the electron beam and whose analysis is required. Since the elemental concentrations are determined from measurements of the intensities of characteristic X-rays (see sub-section 2.4.2) these effects cause errors in the analytical results. It has been reported [57] that 1/2 μm groove in magnesium can cause a 10% error at a 20° take-off angle.

An uneven surface causes variations in the path lengths for X-rays emerging from the specimen surface, as illustrated in Fig. 2.9, and so causes changes in the X-ray intensities and this may lead to false analytical results. The effect of the surface roughness on X-ray

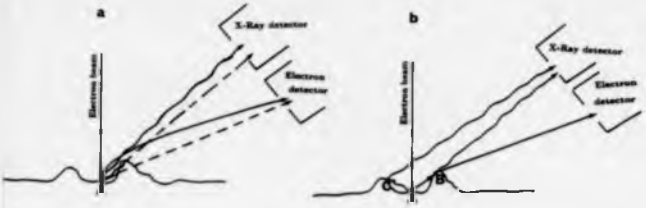

Fig. 2. 8. Effect of the roughness of the surface of a specimen on electron imaging and on X-ray analysis: (a) Some electrons and X-rays generated at point A are prevented by point B from reaching the electron and X-ray detecto rs; consequently, X-ray intensities measured from the point A will be reduced, and this point will appear darker on the image screen. (b) Fluorescent X-rays and secondary electrons are generated at points C and B by X-rays and electrons given off at the point A; consequently atomic number contrast is enhanced and X-ray intensities measured are also enhanced and the presence of incorrect elements may be indicated.

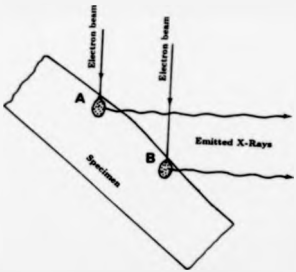

Fig. 2. 9. Effect of an even surface on X-Ray analysis. The figure shows that before emerging from the specimen X-rays generated in the region A and the region B travel different distances within the sample. Because the amount of absorption of a radiation depends on the distance covered within the material, and its wavelength, it is very likely that the ratio of the intensities of two radiations measured from the point A will be different from that measured from the point B, even if the compositions are the same at A and B.

intensities is bigger in materials of high mass absorption coefficient and smaller at the higher take-off angles. A change of 1° in the orientation of the surface gives [58] about 3% change in X-ray intensity, due to changed absorption, for a specimen with absorption coefficient $\frac{\mu}{\rho}$ = 1000 cm^2/g and a take-off angle of 20°. For a take-off angle of 75° the corresponding change in X-ray intensity is less than 0.1% [58].

The need to have a flat and smooth surface for either microscopical examination and quantitative analysis is thus clear.

2.6.2 Polishing

After a joint was given the required thermal treatment, it was sectioned across the couple interface and one or both of the cross-sections were polished for SEM examination. In order to avoid major surface damage, particularly that leading to cracking within the intermetallic compound layer formed by the reactions, the sectioning was done with great care. The soft solder and Au film were first cut by means of a razor blade; then the substrate was fractured along this cut after being grooved, on the other side, by means of a diamond file. To be polished the cross-sections were fixed with araldite on a piece of wax, large enough to be handled (Fig. 2.10). The surface regions of the section damaged by the cutting were removed by grinding which was carried out by hand through a sequence of operations using successively 600, 800, 1000 and 1200 grit papers with water as a lubricant. The sample was washed abundantly with water each time before progressing to the next finer grit size abrasive. The objective of this was to remove as many as possible of the loose particles that might otherwise become embedded into the specimen surface and cause scoring of the surface later in the polishing. The pressure applied to the specimen during this operation was extremely light otherwise the surface was badly smeared owing to the softness of the metals. The grinding was followed by mechanical polishing done by hand on a succession of polishing

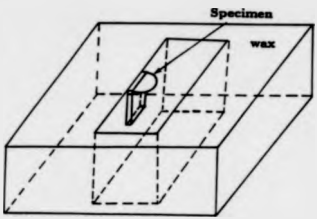

Fig. 2. 10 Schematic diagram of a Au/Solder cross-section mounted onto a specimen holder for mechanical polishing.

cloths coated with diamond powder paste and a special lubricant. It was started with powder of 6 μm, then 2 μm, and finished with 1 μm. After each operation the specimen was again abundantly washed with water. The final preparation stage was electrolytic polishing which was necessary to obtain a surface smooth and representative of the bulk material. This is because chemical analysis of specimens prepared without electropolishing gave compositions far different from the known composition of the solder used due to the smearing of a thin layer of tin over the surface. The conditions under which the electrolytic polishing was carried out were similar to those proposed in reference 59:

Solution : 80% of ethyl alcohol + 20% of perchloric acid of density 1.2,

Current density (A/dm^2): $\sim$ 130

Voltage (Volt) : 18,

Temperature : <20°C,

Time (second) : $\sim$ 4.

The electrodes were placed horizontally with a tin foil as cathode.

Immediately after removal from the electrolyte the specimen was rinsed and ultrasonically washed in acetone for a few minutes, then blow-dried. To prevent it from charging in the microscope, the sample surface was coated in a vacuum unit with a thin (100-200 $\AA$) conducting layer of carbon. The loss of measured intensity of X-ray caused by the absorption of X-rays and the attenuation of the electron beam within a coated layer depends on the take-off angle, the accelerating voltage, and the thickness of the coated layer [60]. For a carbon layer 250 $\AA$ thick the absorption of incident electrons within the carbon layer is 5% at an accelerating voltage of 10 kV and 1% at 20 kV for a take-off angle of 30°; for the same layer thickness and take-off angle the absorption of X-rays is 1.8% for a wavelength of the radiation equal to K Na (11.9 $\AA$) and 0.875% for a wavelength equal to K Fe (1.93 $\AA$) [60]. So, if the wavelengths of the characteristic X-ray radiations whose intensities are measured

are short or only comparable the absorption of the radiations in a carbon layer 250 $\AA$ or less thick is negligible in the first case and comparable in the second case. The X-ray absorption within the carbon layer would not then affect the accuracy of the X-ray microanalysis. The absorption of the intensity of the incident electrons within the coated layer cancels out in the standardless method where the elemental concentrations are determined from the ratios of the intensities measured. It is the loss of energy by the incident electrons within the coated layer which can affect the analyses. For a carbon layer 100 to 200 $\AA$ thick that loss must be negligible.

Chapter 3: INTERDIFFUSION IN Au/PbSn JOINTS

This chapter describes the observations on diffusion between electroplated Au thin films and the 60wt.%Sn-40Pb alloy at different annealing temperatures.

3.1 Sample preparation and heat treatment

Au/PbSn diffusion couples were manufactured as follows. To make a joint, a piece of solder wire of composition 60wt.%Sn-40Pb was used to form a molten drop of solder on a soldering iron which was preset at 250°C. This was quickly applied to the gold film. The latter was a 2 mm diameter thin electrodeposit on Al_2O_3 substrate obtained as described in chapter 2. After a very short time (about 1 second or so) the soldering iron was removed and the couple allowed to cool down in air to room temperature. The approximate shape and size of the completed gold/solder system is shown in Fig. 3.1.

A typical SEM micrograph of a metallographic cross-section of an as- prepared couple is shown in Fig. 3.2. It can be seen that intimate contact between the materials as required for diffusion studies exists. A thin layer, about 2 μm thick, can be seen at the joint interface in the micrograph. EDX analysis in the SEM showed that this layer was composed of Au-Sn intermetallic phases. The needle-like grains lying in the solder region next to the joint interface have the composition corresponding to the $AuSn_4$ phase. They may be due to gold which dissolved in the molten solder and precipitated subsequently upon cooling or may have been detached and deposited there during the mechanical polishing.

Interdiffusion in Au/PbSn joints can be expected to result in the formation of intermetallic

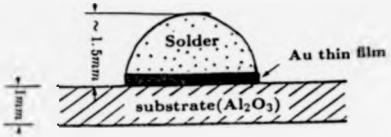

Fig. 3. 1. Schematic diagram of a diffusion couple used for studies of reaction diffusion between a gold film and the 60Sn-40Pb solder.

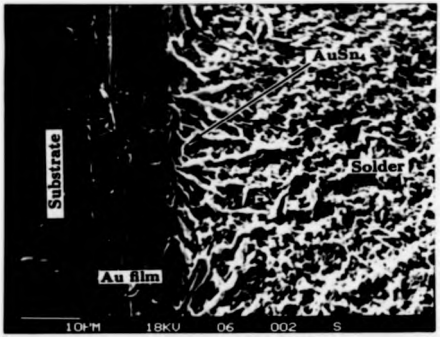

Fig. 3. 2. SEM micrograph of a cross-section of an as-prepared Au/60Sn-40Pb diffusion couple after mechanical and electrolytical polishing of the cross-section.

compounds since Au forms intermetallic phases with Sn and Pb (see Fig. 3.3a and b). To produce these phases and determine their growth kinetics the diffusion process was accelerated by heating the couples at elevated temperatures (80, 125,140 and 160°C). The choice of the range of annealing temperatures [80-160°C] was dictated by the following factors. At temperatures lower than 80°C, the thicknesses of the reaction products layers are so small that their accurate determination by the SEM is not possible. At temperatures above 160°C, the rate of the reaction is so high that the gold film is consumed after too short a time. For each annealing temperature investigated a set of diffusion couples were heated for different lengths of time. The temperature in the furnace was measured by a thermocouple which was situated very near the sample and which was connected to an automatic controller which controlled the power to the furnace to keep the temperature constant. The annealing temperatures were accurate to ± 2°C. The samples were simply annealed in air. Since the diffusion zone is not exposed to air during the heat treatment the oxidation process which could affect the diffusion coefficients and consequently the growth rates of the intermetallics is not expected to occur. The diffusion of the air elements into the solder is limited to its outer region and cannot have any effect on the processes occurring much deeper in the sample, at the gold/solder interface, during the annealing times used. As shown by Fig. 3.1 the gold film is completely protected from the air by the alumina substrate. Scanning electron microscope micrographs of diffusion zones did not show any evidence of oxidation. The amount of solder bonded to the Au film and the preparation conditions (temperature of the molten solder, soldering time) of the joints were kept the same for all the samples.

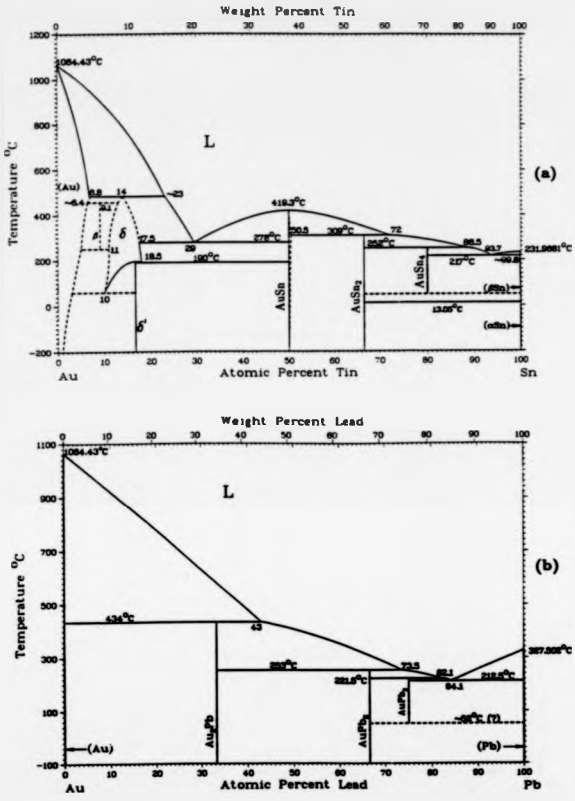

Fig. 2.2 Equilibrium phase diagrams of Au-Sn[9] (a) and Au-Pb[8] (b) alloys.

3.2 Joint microstructure after aging

3.2.1 The reaction products

The typical microstructure of a Au/40Pb-60wt%Sn joint annealed at an elevated temperature is shown in Figs. 3.4a-d. The SEM micrographs in Figs. 3.4a and b were taken before electropolishing the cross-section of the joint and those in Figs. 3.4c and d were taken after. The backscattered electron images in Figs. 3.4b and d clearly display the various regions of the joint: the substrate, the gold film, the solder, and the two layers between the gold film and the solder. These layers are products of interdiffusion in the joint. Compositional analyses carried out on the layer surfaces in the SEM, using an EDX analyser coupled to a computer, revealed that the layers were composed of gold-tin intermetallic phases which exist in the phase equilibrium diagram of Au-Sn alloys shown in Fig. 3.3a. In this diagram, five stable intermetallic phases ($AuSn_4$, $AuSn_2$, AuSn, $\delta'(Au_5Sn)$ and δ) are shown to exist in the temperature range [80-160°C]. The layer next to the solder observed in Figs. 3.4b and d is $AuSn_4$. The boundary between this intermetallic layer and the solder is better seen on the SEM micrographs taken after electropolishing the cross-section (Figs. 3.4c and d) than on those taken before (Figs. 3.4a and b) and best seen on Fig. 3.4c. The layer next to the $AuSn_4$ is $AuSn_2$. The very thin layer, 1.5 to 2 μm thick, which can be seen on Fig. 3.4b between the gold film and the $AuSn_2$ intermetallic layer is made up, from right to left on the figure, of a layer of AuSn and a layer of gold richer phase(s). It has not been possible to know whether the layer contained δ' phase (Au_5Sn) or δ' and δ phases. This is because the gap between the compositions of these two phases is of the order or less than the error in the analytical results which is so high because of the thinness of the layer. For convenience, this layer will be called in what follows δ-layer.

The $AuSn_4$ and the $AuSn_2$ phases were detected in the early stages of diffusion while the AuSn and δ layers were only detectable after long annealing times which were greater at

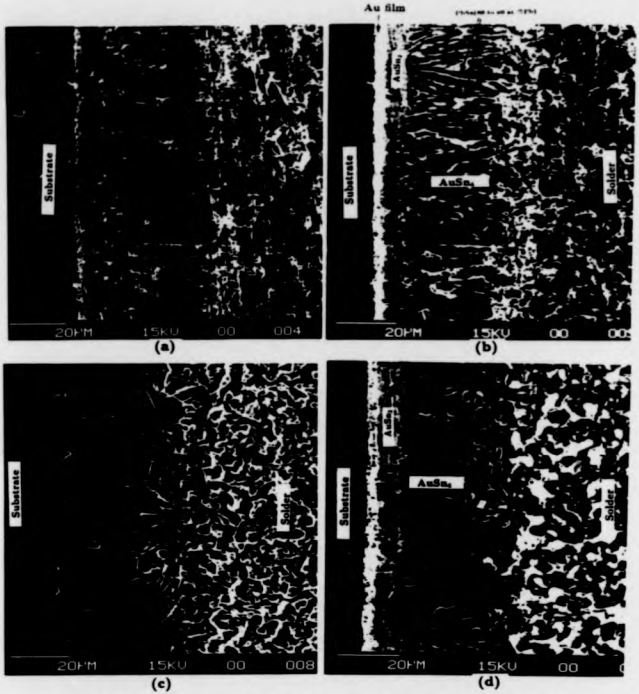

Fig. 3. 4. SEM micrographs of a metallographic cross-section of a Au/60Sn-40Pb diffusion couple annealed at 160°C for 7 hours: (a) and (b) before electro-polishing the cross-section, (c) and (d) after; (a) and (c) secondary electron images, (b) and (d) backscattered electron images.

the lower temperatures. At the 160°C annealing temperature the AuSn phase was detected after 3 hours of annealing and the δ-layer after 6 hours. At the 125°C temperature the AuSn and the δ-layer were detected after 18 and 40 hours of annealing respectively. At the 80°C diffusion temperature they were detected only after as long as 700 and 1000 hours respectively. It is possible that these phases formed in the early stages of diffusion but because of very slow growth rates they did not attain sufficient thicknesses to be detected. It is also possible that a thin film of the gold layer smeared over the intermetallic layers during the polishing and hindered their detection. A Au/PbSn couple aged for 16 hours at 125°C and strained to fracture in a direction perpendicular to the layer surfaces revealed the presence of the AuSn phase and δ-layer within the joint as the latter fractured at the $AuSn_4/AuSn_2$ and at AuSn/δ-layer interfaces. This may well prove that the AuSn and the δ-layer had formed in the early stages of annealing but were not detectable in the metallographically prepared cross-sections examined in the SEM because the phase layers were too thin at these stages. Up to the longest anneal time used, their thicknesses, determined from SEM-EDAX examination of metallographically prepared cross-sections, remained very small ($\leq$ 1 μm each) at all annealing temperatures.

The phase layer boundaries are not visible on the specimen surface examined under the SEM apart from that between $AuSn_2$ and $AuSn_4$ and occasionally that between $AuSn_2$ and AuSn which can only be seen when forming the backscattered electron image. The gold film and the intermetallic product layer are also more readily distinguishable using atomic number contrast than on the secondary electron image. However, the apparent boundary position in the image does not always coincide with the unreacted gold/intermetallic compound interface due to an overlapping of the two layers which occurs during the mechanical polishing of the sample. A thin layer of the gold film is often smeared over the intermetallic compound. Although the specimens were mechanically polished by moving them in a direction parallel

to the interface between the layers the problem always occurred. Its magnitude could be minimized by taking care in the specimen preparation.

The particles which appear white on the surface of the $AuSn_4$ layer, in Fig. 3.4b, were analysed by X-ray analysis in the SEM and found to be PbSn rich in Pb (80 to 90 at. Pb%). As can be seen in this figure such particles do not occur on the surfaces of the other intermetallic phases nor on the gold film surface. Such particles are not seen in the SEM picture, shown in Figs. 3.4c and d, which were taken after electropolishing the surface of the same cross-section shown in Figs. 3.4a and b. The PbSn particles could have arrived by transfer from the solder region of the couple during the mechanical polishing of the cross-section as suggested by Fig. 3.5 or they could be left in the intermetallic layer as a consequence of the reaction between the gold and the tin at the $AuSn_4$/solder interface. Their shape supports the second alternative. If they had been brought by polishing it might be expected that they would be elongated along the direction of polishing which was parallel to the layer interfaces whereas they almost all lie along the normal to that direction, consistent with the cellular growth of the $AuSn_4$ layer/solder interface.

The different phase layers were also analysed by the electron beam in the SEM. Both spot and scan analyses were performed. Scan analyses were performed by scanning the electron beam over the layer surface and spot analyses were done by focusing the electron beam on the layer surface. Because insufficient amounts of the AuSn and δ layers were present, only spot analyses were carried out on these phase layers. Spot analyses revealed a range of solubilities of lead in the intermetallic phases from 0 to 2 at. %. This range was obtained by performing analyses on different points of each phase. These lead concentrations were also obtained by carrying out spot analyses on the grain phases using the fracture surfaces mentioned above. Scan analyses performed on the surface of the $AuSn_4$ intermetallic layer revealed about 8 at. % lead before electropolishing the joint cross-section and about

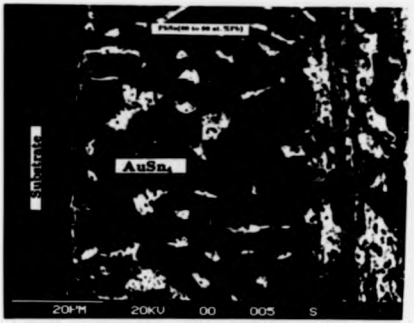

Fig. 3. 5. SEM micrograph (backscattered electron image) of a mechanically polished cross-section of a Au/60Sn-40Pb diffusion couple annealed at an elevated temperature until complete degradation of the gold film and transformation of all Au-Sn phases into $AuSn_4$ had occurred. Note the presence of PbSn particles over the whole layer of $AuSn_4$.

1 at. %Pb after. The lead detected in the intermetallic layer before the electropolishing came mainly from the PbSn particles which were left in the intermetallic layer during the interfacial reaction since the average Pb concentration in the grains of the $AuSn_4$ phase is only about 1 at. %. During the electropolishing the PbSn particles dissolved off. Scan analyses done on the surface of the $AuSn_2$ intermetallic layer revealed about 1.3 at. % lead before and after electropolishing. Within experimental error this lead concentration corresponds to the average Pb concentration in the grains of the $AuSn_2$ phase.

3.2.2 The grain structures of the intermetallic phases

The grain structure of the intermetallic phase layers is not revealed when a mechanically polished specimen is observed under the scanning electron microscope as the layers suffer plastic deformation. The electrolyte solution, mainly used to remove the smeared solder over the sample surface, does not etch the intermetallic compounds to reveal their grain structure. Specimens fractured rather than cut and polished would have allowed grain structure observation. Unfortunately, each time it was tried to fracture a sample across the Au/Solder interface it failed because the solder came off the substrate. But samples annealed and pulled to fracture in a direction perpendicular to the substrate (see chapter 6) allowed observation of grain phase structure because the pulled samples fractured at the phase boundaries. In Figs. 3.6a-d, the grain structures of the $AuSn_4$ (Fig. 3.6a), the $AuSn_2$ (Fig. 3.6b), the AuSn (Fig. 3.6c) and the δ-layer (Fig. 3.6d) are shown. The annealing temperature was 125°C and the annealing time was 16 hours (Fig. 3.6a,b) and 25 hours (Figs. 3.6c,d). The mean grain size of the $AuSn_4$ and the $AuSn_2$ phases are about 3 and 2.7 μm respectively; those of the AuSn phase and the δ-layer are less than 1 μm.

The microstructures of these phases have been observed at different annealing temperatures and diffusion times in similar joints and shown in sub-section 4.3.2 of the next chapter.

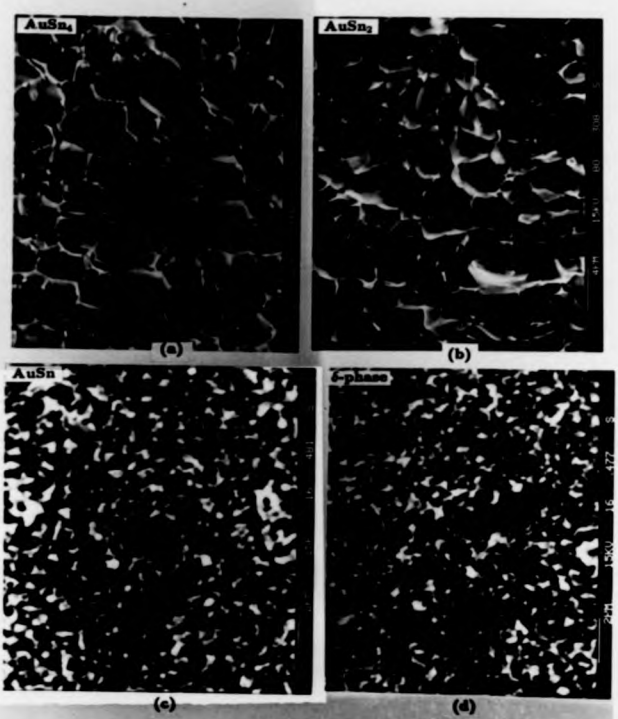

Fig. 3. 6. SEM micrographs showing the grain structure, in a Au/60Sn-40Pb joint annealed at 125°C, of (a) $AuSn_4$ phase layer at the boundary between this layer and that of $AuSn_2$ phase, (b) $AuSn_2$ phase layer at this boundary, (c) AuSn phase layer at the boundary between this layer and that of δ-phase, (d) δ-phase layer at this boundary. The annealing time was 16 hours, (a) and (b), and 25 hours, (c) and (d).

3.2.3 The compositions of the intermetallic phases

The equilibrium phase diagram for Au-Sn alloys (Fig. 3.3a) shows the homogeneity ranges of the different Au-Sn phases. According to that phase diagram the δ phase is homogeneous in the range from 10 up to 16.5 at. %Sn, the AuSn in the range 50 to 50.5 at. %Sn, the $AuSn_2$ at 66.7 at. %Sn, the $AuSn_4$ at 80 at. %Sn and the Au_5Sn (δ') at 16.7 at. %Sn.

The atomic percentage compositions of the $AuSn_4$, $AuSn_2$, and AuSn phases formed by interdiffusion in the Au/PbSn system are given in Table 3.1. The range of compositions detected in the δ-layer is also given in this table. The compositions were determined in the SEM by energy dispersive X-ray analysis. The analyses were carried out on metallographic sections, at different points across the phase layers, and on the phase layer interfaces. The ranges of compositions given in Table 3.1 represent the different compositions detected in the phase layers.

The accuracy in the measurement of chemical composition using an energy dispersive spectrometer has been determined [61]. For that, materials of known composition were analysed in an electron probe and the relative errors, $\frac{\Delta C}{C}$, were calculated using $\frac{\Delta C}{C} = \frac{C_{cal} - C_{true}}{C_{true}}$ where C_{cal} was calculated from the measured X-ray intensity ratio $\frac{I_A}{I_{A'}} = ZAFC_{cal}$ (see subsection 2.4.2). Based on the data obtained it has been concluded [61] that a relative error of better than $\pm$ 4% of the amount present could be expected at concentrations above 10 wt. %; for concentrations below 5 wt. % the standard deviation was 16% with no error less than 6%.

3.2.4 The microstructure of the solder

The microstructure of the 60Sn-40Pb solder, before aging, is shown in Fig. 3.7. The compositions of the crystallites revealed by X-ray analysis in the SEM are different from those given at room temperature by the equilibrium phase diagram of the Pb-Sn system shown in Fig. 1.2.The EDX analyses of the dark particles observed in Fig. 3.7 gave Sn concentrations,

Table 2. 1 Compositions of the intermetallic phases which have formed in Au/60Sn-40Pb diffusion couples annealed in the temperature range [80 - 160°C], determined by X-ray analysis in the SEM.

Phase	at.%Sn	at.%Au	at.%Pb
δ-layer	11 - 20	80 - 88	0.5 - 1.8
AuSn	49 - 52	46 - 49	0 - 2
$AuSn_2$	66 - 68	30 - 33	0 - 2
$AuSn_4$	79.5 - 81.5	17 - 18.5	0 - 2

in atomic percent, in the range [12-32]; those of the light areas observed on the same figure gave Sn concentrations, also in atomic percent, in the range [97.5-99]. For several reasons such as interaction volume, roughness of the sample surface, errors in the analytical results exist but even so these show that the solder is in a non-equilibrium state.

This non-equilibrium state of the phases is due to the rapid cooling of the alloy from above the melting point to room temperature during the joint preparation. Under equilibrium conditions the compositions of the phases change by solid-state diffusion as the temperature falls below the eutectic temperature. Because the alloy is brought quickly to room temperature there is not enough time for diffusion to change significantly the compositions of the crystallites. This metastable structure persists at room temperature as the solid state diffusion is very slow under these conditions.

Annealed Au/PbSn samples have shown a depletion of tin ahead of the intermetallic compound. The depleted region is a few micrometers wide and lead contents of up to 60 atomic percent were found in that region after long annealing times. The depletion of tin is understandable. The intermetallic compound grows at the expense of Au and Sn only, and lead does not react; Au atoms which reach the solder, after diffusing through the compound, react with Sn atoms to form $AuSn_4$ and at the same time there is a flux of tin atoms which diffuse from the solder towards the gold film. Thus a tin depleted region forms ahead of the intermetallic compound. The depletion is not replenished from the bulk of the solder because of the slow diffusion of tin within the solder shown by the non equilibrium composition of the solder.

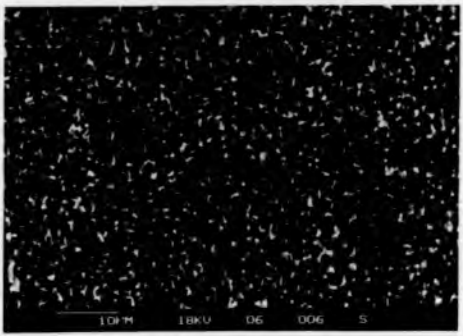

Fig. 3.7. SEM micrograph (backscattered electron image) of the 60Sn-40Pb solder in an as-prepared Au/60Sn-40Pb diffusion couple after polishing of a cross-section of the joint (the cross-section was not electro-polished).

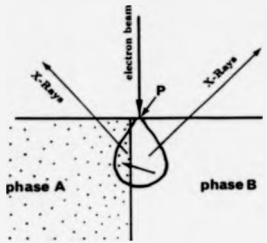

Fig. 3. 8 This figure shows that although the electron beam is focused on the phase B, at P, X-Rays are collected from both phase A and B because of the spreading of the electrons into the sample and possibly fluorescence of atoms of A by primary X-Rays generated in B. Therefore the apparent concentration at P is different from the concentrations of phases A and B, so that it can not be known whether the point belongs to the phase A or the phase B. Thus an uncertainty on the boundary position arises.

PAGINATION ERROR

Page 35

Uncertainties in the measurement of the intermetallic layer thicknesses are inevitable. They result from both the specimen polishing and the irregularities of the layer interfaces. Mechanical polishing leads to an overlapping of the layers, particularly the soft gold layer and the intermetallic compound, and consequently the boundary positions are blurred. Furthermore, during mechanical polishing particles of the intermetallic phases, mainly of $AuSn_4$, detach from the compound layers and embed in the solder region next to the $AuSn_4$ layer/solder interface. This creates a doubt on the interface position and therefore uncertainty in the layer thickness arises. That constitutes a source of uncertainty in measuring the $AuSn_4$ layer thickness greater than the irregularities of the layer boundaries. Figure 3.9 of a sample annealed then transverse fractured suggests that the irregularities of the boundaries between the gold film and the intermetallic compound and between the $AuSn_2$ and $AuSn_4$ observed on Fig. 3.4 occurred during polishing, by overlapping of the layers.

3.3.2 Growth kinetics of the intermetallic layers

To plot the layer thicknesses against annealing time at a temperature of interest, in order to determine the layer growth kinetics, several Au/PbSn diffusion couples were heated at the same temperature for different lengths of time. After a couple was given the desired anneal time it was removed from the furnace and coded, then cut across the interface. A cross-section of the sample, after being carefully polished, was examined in the SEM, and the layer thicknesses were determined as described above.

The phase layer thicknesses are plotted as a function of the annealing time in Figs. 3.10-13 for the four different temperatures investigated (80, 125, 140 and 160°C) respectively. The uncertainties in the measured thicknesses are indicated by error bars. It can be seen from those graphs that after a certain annealing time t_1 the rate of growth of the $AuSn_4$ phase layer slows down and that of the layer of the other intermetallics appears to become zero. This

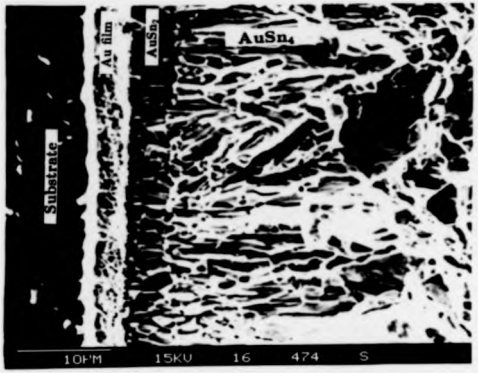

Fig. 3. 9. SEM micrograph of a Au/60Sn-40Pb diffusion couple annealed at 80°C for 500 hours then fractured through the diffusion zone showing the shapes, straight lines, of the phase layer boundaries.

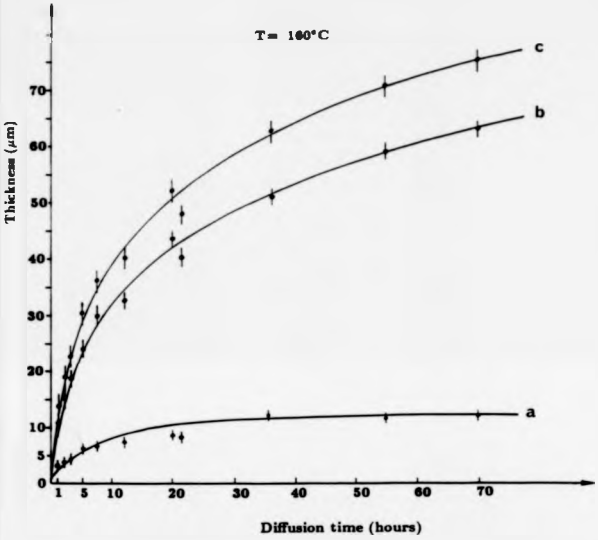

Fig. 3. 10 Variation with time at 160°C diffusion temperature of the thicknesses of the intermetallic layers in a Au/60Sn-40Pb diffusion couple; (a) $AuSn_2$, AuSn and δ-layer, (b) $AuSn_4$, (c) all the intermetallic phases.

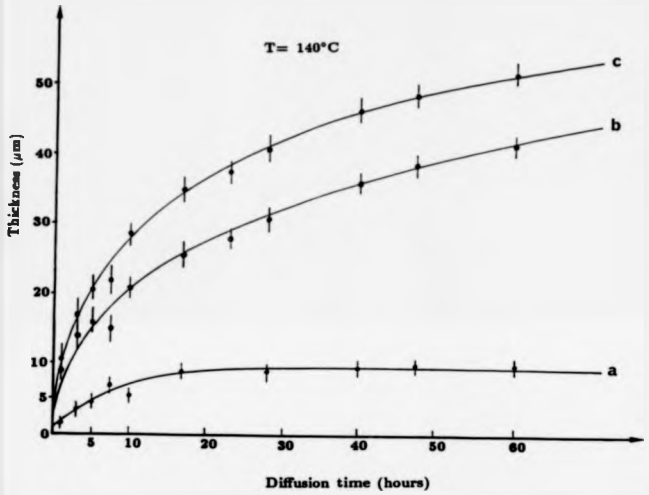

Fig. 3. 11 Variation with time at 140°C diffusion temperature of the thicknesses of the intermetallic layers in a Au/60Sn-40Pb diffusion couple; (a) $AuSn_2$, AuSn and δ-layer, (b) $AuSn_4$, (c) all the intermetallic phases.

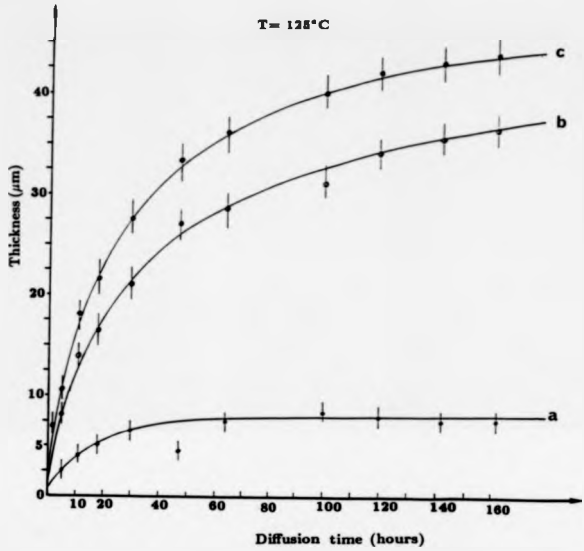

Fig. 3.12 Variation with time at 125°C diffusion temperature of the thicknesses of the intermetallic layers in a Au/60Sn-40Pb diffusion couple; (a) $AuSn_2$, AuSn and δ-layer, (b) $AuSn_4$, (c) all the intermetallic phases.

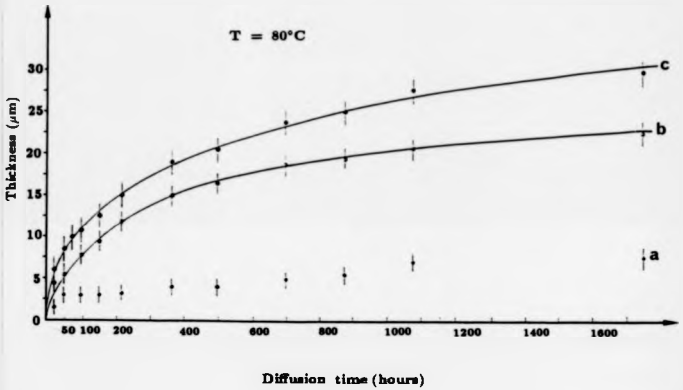

Fig. 3. 13 Variation with time at 80°C diffusion temperature of the thicknesses of the intermetallic layers in a Au/60Sn-40Pb diffusion couple; (a) $AuSn_2$, AuSn and δ-layer, (b) $AuSn_4$, (c) all the intermetallic phases.

behaviour is observed at all the temperatures investigated. The time t_1 falls with increasing temperature but the higher the temperature the greater the $AuSn_4$ layer thickness attained at t_1. Thus, two stages in the variation of the thickness of an intermetallic layer with the annealing time can be distinguished: the initial stage (for $t < t_1$) and the late stage (for $t > t_1$).

- The initial stage

Figures 3.14-17 show that to a good approximation straight lines can be fitted to the experimental points over the initial stage of the layer growth if the layer thicknesses are plotted against $t^{1/2}$ where t is the annealing time. This means that the layer growths are parabolic. The straight lines do not pass through the origins because of the initial thicknesses of the phase layers which arise during the soldering process as shown in Fig. 3.2. The total thickness of the phase layers which grow during this process was estimated from SEM examination of as-prepared samples to be about 2 μm.

The parabolic law of growth is usually expressed in this way:

$$d^2 = Kt \qquad (3.1)$$

where d is the layer thickness, t the annealing time and K the growth rate constant of the layer. From the figures d versus $t^{1/2}$ the parabolic rate constants were determined for the different temperatures. The best fits gave the values reported in Table 3.2.

- The late stage

When the intermetallic layers reach certain thicknesses (which increase with increasing temperature) their growth rates change. At each diffusion temperature the change appears to occur at the same time for the two layers. In this late stage the $AuSn_4$ layer continues to grow while the thickness of the other layer remains constant with the annealing time. As can be seen on Figs. 3.10-13 the growth of that layer is slower than it is in the early stage.

Table 3. 2 Growth rate constants of intermetallic layers in Au/60Sn-40Pb diffusion couples during the initial stage of interdiffusion.

Annealing temperature (°C)	K (cm^2/s)	K ($AuSn_4$) (cm^2/s)
80		$(1.76 \pm 0.2) \times 10^{-12}$
125	$(3.78 \pm 0.3) \times 10^{-12}$	$(0.38 \pm 0.06) \times 10^{-10}$
140	$(0.125 \pm 0.02) \times 10^{-10}$	$(1 \pm 0.10) \times 10^{-10}$
160	$(0.156 \pm 0.02) \times 10^{-10}$	$(3.00 \pm 0.30) \times 10^{-10}$

K is the growth rate constant of the layer of ($AuSn_2$ + AuSn + δ-layer).

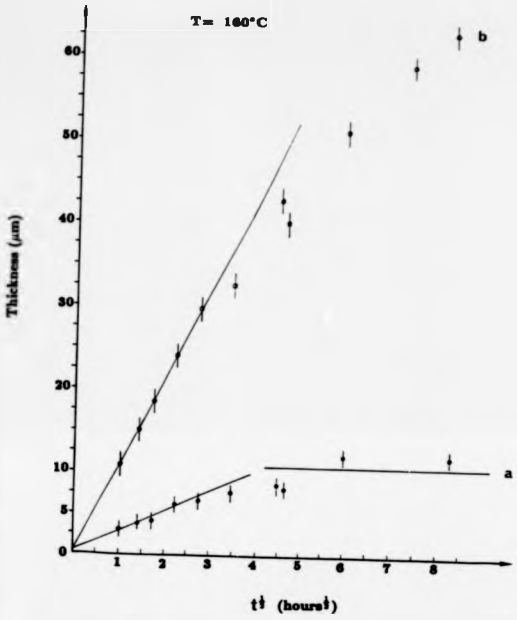

Fig. 3. 14 Plot of the thicknesses of the intermetallic layers in a Au/60Sn-40Pb diffusion couple against the square root of the diffusion time at 160°C; (a) $AuSn_2$, AuSn and δ-layer, (b) $AuSn_4$.

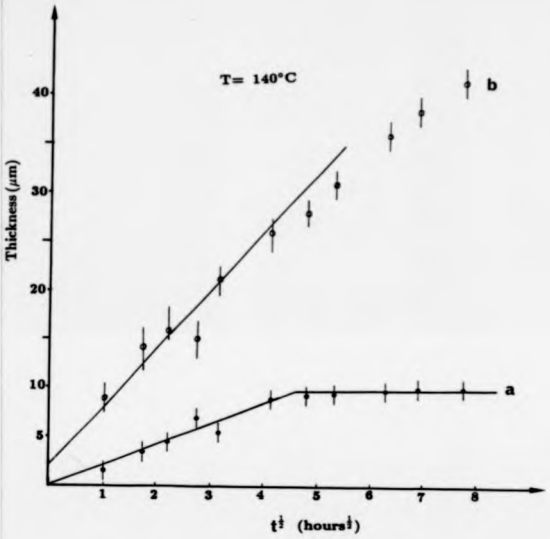

Fig. 3. 15 Plot of the thicknesses of the intermetallic layers in a Au/60Sn-40Pb diffusion couple against the square root of the diffusion time at 140°C; (a) $AuSn_2$, AuSn and δ-layer, (b) $AuSn_4$.

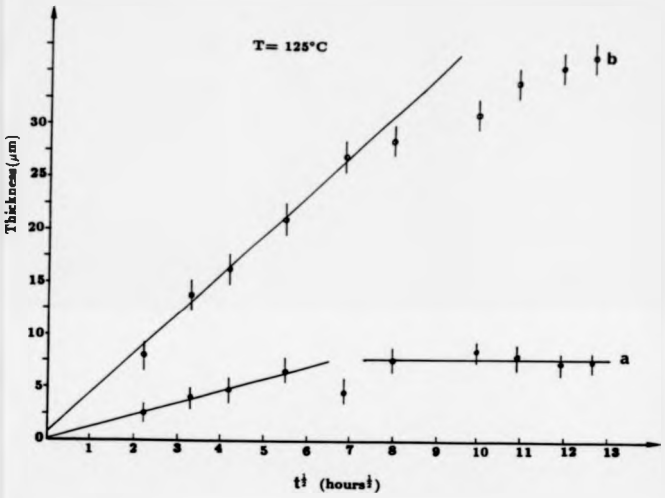

Fig. 2.16 Plot of the thicknesses of the intermetallic layers in a Au/60Sn-40Pb diffusion couple against the square root of the diffusion time at 125°C; (a) $AuSn_2$, AuSn and δ-layer, (b) $AuSn_4$.

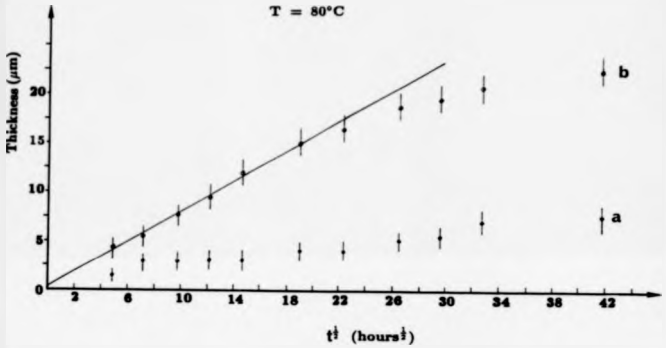

Fig. 3. 17 Plot of the thicknesses of the intermetallic layers in a Au/60Sn-40Pb diffusion couple against the square root of the diffusion time at 80°C; (a) $AuSn_2$, AuSn and δ-layer, (b) $AuSn_4$.

3.4 Dissolution rate of the gold film

It is possible to determine the amount of gold consumed in the Au/PbSn joint as a function of annealing time of the couple from the quantities of the reaction products. The amount of Au in a layer of Au_nSn_y phase is the product of the volume of this layer and the density of the phase times the mass concentration of Au in the phase. The volume is equal to the layer thickness times its area. Since in the joint the different layers have equal areas, the thickness $L(t)$ of consumed gold at a time t can be expressed as follows, assuming that the product layers are free from pores and inclusions.

$$\rho_{Au} L_{Au}(t) = \sum_{i}^{n} \rho_i C'_{Au} L_i(t) \qquad (3.2)$$

where $L_i(t)$ is the thickness of the phase layer i of density ρ_i at the annealing time t, C'_{Au} is the mass concentration of Au in the phase i, ρ_{Au} is the density of pure Au, and n the number of phases present. ρ_{Au}, ρ_i and C'_{Au} are given in Table 3.3 for the different phases. The thickness of consumed gold calculated with the formula given above and the ρ'_{Au} given in Table 3.3 is a bit overestimated. Firstly, because of the presence of Pb grains in the intermetallic layers, particularly in the $AuSn_4$ layer. Secondly, because of the presence of lead in the intermetallic phases which affects the densities of the phases. Thirdly, because the concentrations of Au in the phases which grow by diffusion in the joint are slightly smaller than those given by the equilibrium phase diagram of the Au-Sn system from which C_{Au} were calculated.

For the reasons given earlier it was not possible to measure the thicknesses of the δ-layer and AuSn layer. The data plotted in Figs. 3.10-13 include the thicknesses of these layers and that of $AuSn_2$ as indicated. Since the δ-layer and AuSn layer are very thin ($\leq$ 1 μm each) $L_{Au}(t)$ is not much underestimated by including those layers with the $AuSn_2$ ($\Delta L_{Au}^{max} \approx$ 0.2 μm). With this approximation the consumed gold thicknesses could be calculated and plotted against annealing time (see Fig. 3.18) for each of the temperatures studied. From

Table 3. 3 Parameters relative to Au-Sn equilibrium phases.

phase	C_{Au} (%)	density (g/cm^3)	structure[62]	number of atoms per unit cell[62]
Au	100	19.3	fcc	4
AuSn	62.4	11.732	hexagonal	4
$AuSn_2$	45.35	10.1	orthorhombic	24
$AuSn_4$	29.32	9.227	orthorhombic	20

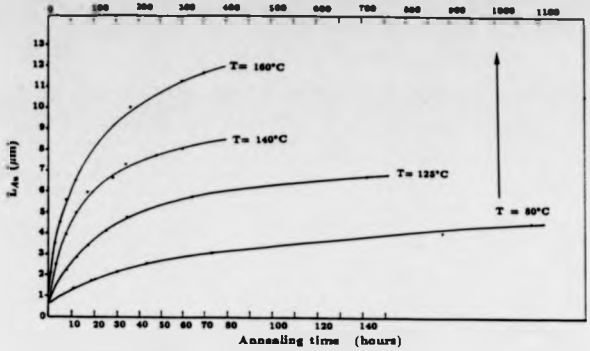

Fig. 3. 18 Thickness of the gold layer consumed through compound formation with tin in a Au/60Sn-40Pb joint versus the annealing time at various temperatures.

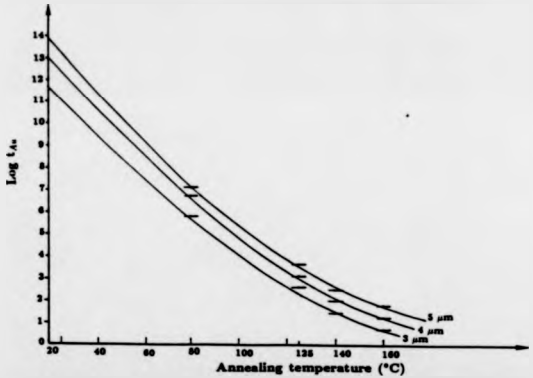

Fig. 3. 19 Plot of Log t_{Au} versus the annealing temperature of a Au/60Sn-40Pb joint for various thicknesses of the starting gold film where t_{Au} is the anneal time necessary to transform all the gold film of the joint into Au-Sn intermetallics (gold film life time). t_{Au} at a studied temperature is given, in the axis-system of Fig. 3. 18, by the abscissa of the point of intercept of the horizontal line of ordinate equal to the starting gold film thickness with the corresponding curve drawn in that figure.

those plots the life time t_{Au} of a Au film of given initial thickness can be estimated for each temperature. In order to illustrate the temperature dependence of gold film life time, values of t_{Au} are shown in Fig. 3. 19 for several starting thicknesses. With the object of estimating t_{Au} at room temperature (25°C), L_{Au}-annealing temperature curves were extrapolated to 25°C. The gold film life time was found to be 7, 27 and 60 years for starting Au film thicknesses of 3, 4 and 5 μm respectively.

3.5 Activation energy of layer growth

It was seen in sub-section 3. 3. 2 that the variation of the thickness of a product layer with annealing time at a temperature T can be expressed in the following form:

$$d^2 = Kt \tag{3.3}$$

where k is the growth rate constant at the temperature T. It is of interest to know the temperature dependence of K. For this purpose, the growth rate constants of the intermetallic layers which are reported in Table 3. 2 were displayed in an Arrhenius graph, $\log K$ versus inverse absolute temperature, in Fig. 3. 20. To a very good approximation a straight line fits to the experimental points of K_{AuSn_4}; the experimental points of the growth constant of the other intermetallic layer could not be reasonably fitted by a straight line. Thus the growth rate constant, $K_{Au_5Sn_4}$, can be written in the form:

$$K_{Au_5Sn_4} = K_0 e^{-E_a/k_B T} \tag{3.4}$$

where K_0 is a constant, k_B is Boltzmann's constant, T is the absolute temperature, and E_a is the activation energy of the layer growth.

The activation energy E_a is given by the slope of the line on the Arrhenius plot and K_0 by the intercept of the line with the vertical axis. The least squares method which was used to fit the line to the experimental points yielded and activation energy $E_a = 0.84 \pm 0.02$ eV. In

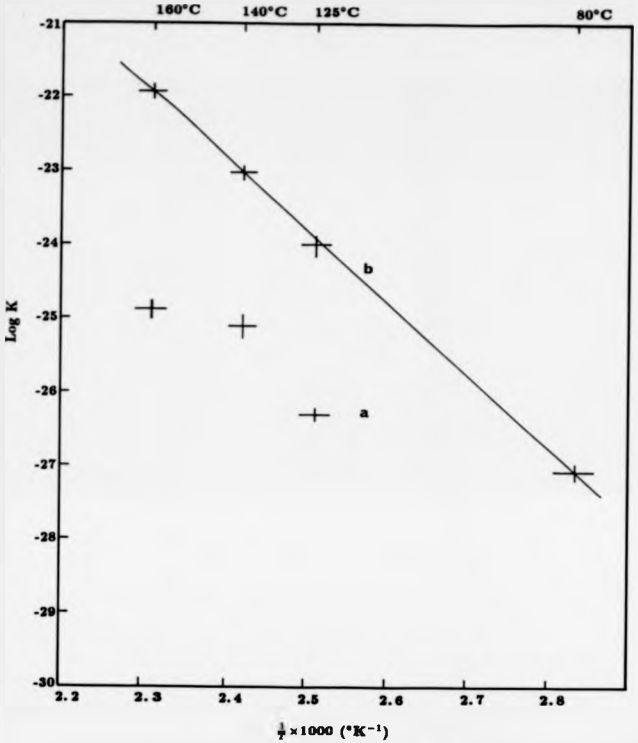

Fig. 3. 20 Log K versus the inverse of the diffusion temperature where K is the parabolic growth constant, in a Au/60Sn-40Pb diffusion couple, of (a) ($AuSn_2$ + AuSn + δ) layer, (b) $AuSn_4$ layer. The straight line through the points of K_{AuSn_4} which was fitted by the least squares method yielded an activation energy $E_a = 0.84 \pm 0.02$ eV. The points corresponding to the second layer could not be reasonably fitted by a straight line.

the range [80-160°C] the temperature dependence of K_{AuSn_4} (in cm^2/s) may be represented by the following equation:

$$K_{AuSn_4} = 1.7e^{-0.84/k_BT} \tag{3.5}$$

with k_BT expressed in eV.

3.6 Summary

Interdiffusion between gold films and 60Sn-40wt.%Pb solder has been studied at 160, 140, 125 and 80°C using diffusion couples. The intermetallic layers which formed between the gold films and the solder were identified by X-ray analysis in the SEM. Four intermetallic layers were found to occur at those temperatures. Three intermetallic layers were identified as $AuSn_4$, $AuSn_2$ and AuSn. The 4 th intermetallic layer which was detected between the gold films and the AuSn layer could not be known whether it was δ' (Au_5Sn) or made up of layers of δ' and δ phases of the Au-Sn system. The predominant phases were $AuSn_4$ and $AuSn_2$ with $AuSn_4$ predominating over $AuSn_2$. The two other intermetallic layers appeared in the diffusion zone after a certain diffusion time which increased with decreasing temperature and their thicknesses remained very small (≤ 1 μm) at all diffusion times and temperatures. The thickness of the $AuSn_4$ layer and the total thickness of the 3 others intermetallic layers were measured at different diffusion times and temperatures. Two stages in the layer growths were observed. In the first stage, both layers grew parabolically with the diffusion time. In the second stage, the $AuSn_4$ layer continued to grow but at a slower growth rate than in the first stage while the thickness of the layer of the other intermetallics remained constant with the diffusion time. An activation energy of growth of the $AuSn_4$ layer related to the early stage of 0.84 ± 0.02 eV was determined.

Chapter 4: INTERDIFFUSION IN Au/PbSnAg JOINTS

4.1 Introduction

The object of this study was to observe the effect of a small proportion of silver on the growth rates of the reaction products in the Au/PbSn joints. Therefore the solder used was the same as in the previous chapter plus silver. The composition by weight of the solder was 62% Sn, 36% Pb and 2% Ag. The exact melting temperature of this alloy is not known and might be a bit lower than that of the eutectic (63-37wt. %) tin-lead alloy which is 183°C since a recent study has shown that the PbSn eutectic temperature decreases by 3.3°C by the addition of 1 wt. % silver [63]. It is known however that silver has a beneficial effect on the hardness, the tensile and the shear strengths of the tin-lead alloys [64].

4.2 Sample preparation and heat treatment

The solder was supplied in the form of a paste which is a mixture of solder powder and flux. To fabricate a joint, a small quantity of the solder was heat melted over the gold disc, of the same diameter (2 mm) as in the previous study, by using a soldering iron. The latter was removed as soon as the paste melted. Although the reaction between solid gold and molten solder was very short in time, a layer of Au-Sn intermetallic phases formed at the gold/solder interface after solidification of the joint, as can be seen when a polished cross-section of the as-processed sample is observed in the scanning electron microscope. The thickness of the intermetallic layer is approximately 2 μm. To make comparison possible between the previous

study and this one, the amount of solder per bond was kept the same.

As in the previous case of the pure tin-lead solder, the interdiffusion in the samples was accelerated by heating them, using the same general method and annealing temperatures as those used for silver-free couples.

4.3 Joint microstructure after aging

4.3.1 The reaction products

SEM examination along with energy dispersive X-ray analysis of metallographic cross-sections of annealed joints revealed the growth between the gold film and the solder of all the phase layers reported in the previous chapter, i.e. $AuSn_4$, $AuSn_2$, AuSn and a layer of δ' (Au_5Sn) or δ' and δ phases of the Au-Sn system. All these phases exist in the equilibrium phase diagram of the Au-Sn system in the temperature range [80 - 160°C] (Fig. 3.3a). As in the previous chapter we called this last cited layer δ-layer. This layer and that of AuSn became detectable only after long annealing times which were greater at the lower temperatures as in the case without silver in the solder (chapter 3). Their presence within the diffusion zone, which was difficult to detect with accuracy because of their small thicknesses (1 μm each) which approach the spatial resolution of the electron beam, was confirmed by analyses of the fracture surfaces of joints annealed and strained to fracture in a direction perpendicular to the layer interfaces. These pull-to-fracture tests and examination of the fracture surfaces also showed these phases form earlier than when they became detectable on polished specimens X-ray analysed in the SEM.

The typical microstructure of a Au/PbSnAg joint annealed at an elevated temperature is shown in Figs. 4.1a-d. The SEM micrographs in Figs. 4.1a and b were taken before electropolishing the joint cross-section and those in Figs. 4.1c and d were taken after. The various regions of the joint are clearly revealed in the backscattered electron images shown

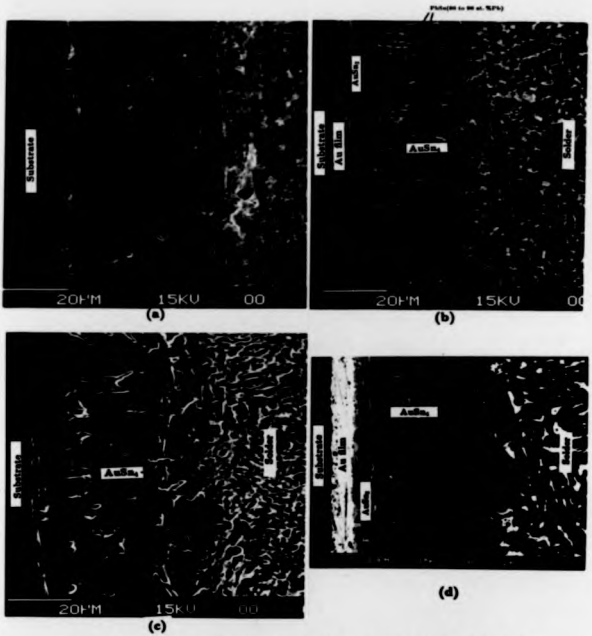

Fig. 4. 1. SEM micrographs of a metallographic cross-section of a Au/62Sn36Pb2Ag diffusion couple annealed at 160°C for 7 hours: (a) and (b) before electro-polishing the cross-section, (c) and (d) after; (a) and (c) secondary electron images, (b) and (d) backscattered eletron images.

in Figs. 4.1b and d. It can be seen that the solder/reaction compound interface is best delineated after electropolishing, which is beneficial for layer thickness measurements.

The two layers between the gold film and the solder observed in Figs. 4.1b and d are the reaction products of the starting materials of the couple. Their identification, made by X-ray analysis in the SEM, showed that the layer next to the solder was $AuSn_4$ as before. This intermetallic compound of Au and Sn was detectable in the initial stages of interdiffusion. The layer between the gold film and the $AuSn_4$ intermetallic layer was found to contain, from right to left on the figures, layers of $AuSn_2$ and AuSn phases and δ-layer lying parallel to the gold film boundary. These intermetallic compound layers are not distinguishable from one another on the SEM micrographs. The $AuSn_2$ phase constitutes almost the whole of that layer, since the AuSn layer and δ-layer which were detected only after long annealing times (which were greater at the lower temperatures) are very thin (≤ 1 μm each).

The particles which appear white in Fig. 4.1b over the $AuSn_4$ intermetallic layer, and which were observed in the case of joints made with pure PbSn solder (sub-section 3.2.1), are PbSn rich in lead (80 to 90 at. % Pb). For the reason given in sub-section 3.2.1 of the previous chapter it is believed that those particles were left in the intermetallic layer as a consequence of the reaction between the gold and the tin at the $AuSn_4$/solder interface.

The solubility of lead in the intermetallic layers was also investigated by carrying out X-ray analyses in the SEM. The analytical results were similar to those obtained in the previous case. About 8 at. % Pb were detected in the $AuSn_4$ layer before electropolishing the cross-section and about 1 at. % Pb after. In the other intermetallic layers the lead concentration was about 1.3 at. % either before or after electropolishing. The solubility of lead in the grain phases themselves was investigated by performing point analyses over the intermetallic layer surfaces. From zero up to 2 at. % Pb were detected in the grain phases of each intermetallic layer. Similar results were obtained when analysing on the

fracture surfaces mentioned above. Scan analyses carried out over these surfaces gave variable amounts of lead in the intermetallic layers. For instance, at 80°C annealing temperature the atomic concentration of lead found in the $AuSn_4$ layer, at the $AuSn_2/AuSn_4$ interface, was in the range [3-5%] after 188 hours of annealing, 4% after 266 hours, and 2% after 500 hours. The lead concentration in the $AuSn_2$ intermetallic layer, also at the $AuSn_2/AuSn_4$ interface, detected after 50, 188, 262, 500 hours of annealing was 1.5 to 1.9 at.%. The lead concentration detected in the other intermetallic layers was about these amounts.

4.3.2 The grain structures of the intermetallic phases

The grain structure of the intermetallic phase layers is not revealed when a mechanically polished transverse section is observed under the scanning electron microscope as the layers suffer plastic deformation. However, it has been possible to observe the phase grain structures by examining the fracture surfaces of pulled joints since it has been found (see chapter 6) that after aging the joints break during pull testings at the intermetallic layer interfaces. The change of the interface of fracture within the joint with aging time permitted observation of the grain structure of different Au-Sn phases. However, the observed grain structures are only those at the phase layer interfaces. In Figs. 4.2-5 the grain structures of some phases formed at 50, 80 and 125°C, pictured at different annealing times, are shown. Two observations have been made from the SEM examination of the phase grain structures. First, the phase grain sizes increase with increasing annealing time which is obvious in comparing Fig. 4.2a with Fig. 4.2b and Fig. 4.3a with Fig. 4.3b.

The second observation is the increase of the phase grain sizes with the annealing temperature. This observation is obvious if one compares the grain structure of the $AuSn_2$ grown at 50°C (Fig. 4.2a), 80°C (Fig. 4.3a) and 125°C (Fig. 4.5a)

(a)

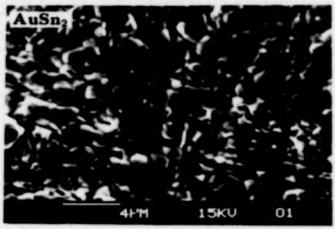

(b)

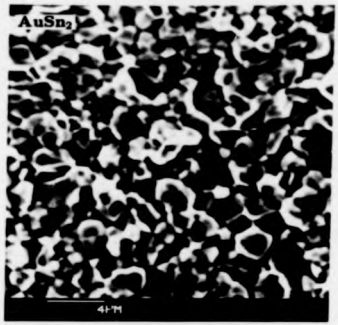

Fig. 4. 2. SEM micrographs showing the grain structure of the $AuSn_2$ phase layer, at the boundary between this layer and that of $AuSn_4$, grown by reaction diffusion in a Au/62Sn36Pb2Ag joint annealed at 50°C for (a) 100 hours, (b) 10434 hours.

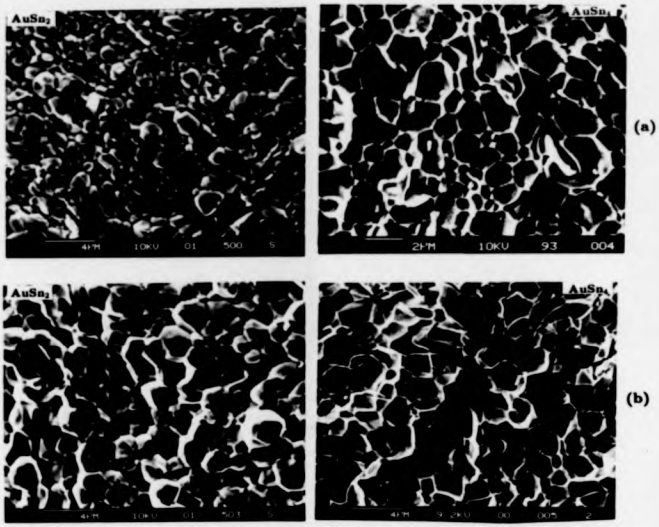

Fig. 4. 3. SEM micrographs showing the grain structures of the $AuSn_2$ and $AuSn_4$ phase layers, at the layer interface, grown by reaction diffusion in a Au/62Sn36Pb2Ag joint annealed at 80°C for (a) 50 hours, (b) 501 hours.

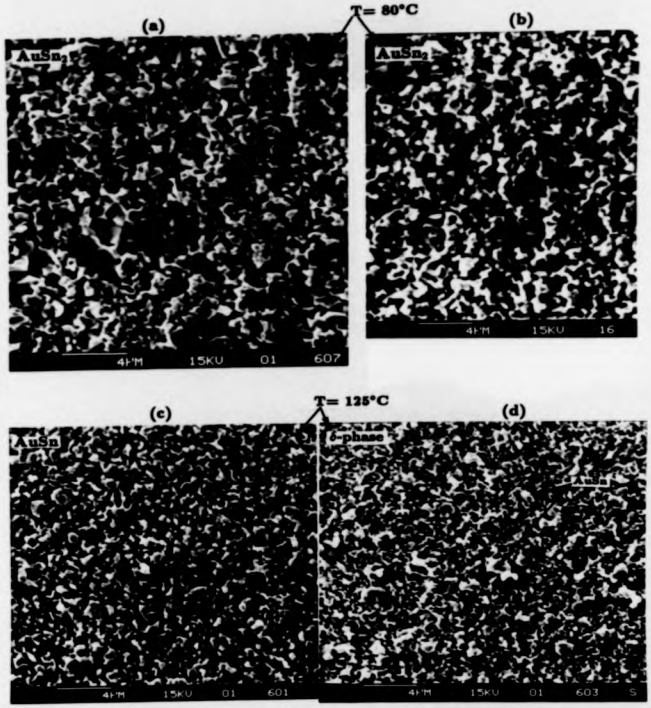

Fig. 4. 4 SEM micrographs showing the grain structure, in a Au/PbSnAg joint annealed at elevated temperatures, of (a) and (b) $AuSn_2$ layer at the boundary between this layer and that of AuSn, (c) AuSn layer within the layer itself, (d) δ-phase layer at the boundary between this layer and that of AuSn. The annealing time was (a) 650 hours (b) 1053 hours (c) 47 hours (d) 10 hours.

(a)

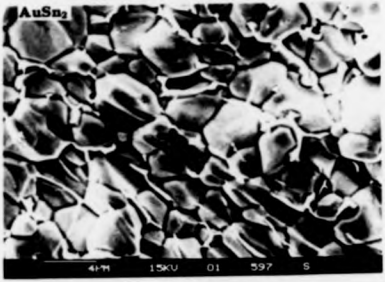

(b)

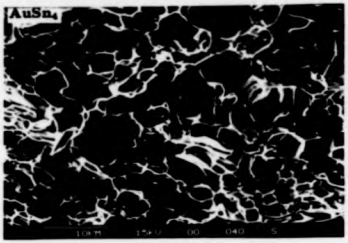

Fig. 4. 5. SEM micrographs showing the grain structure of (a) the $AuSn_2$ phase layer, (b) the $AuSn_4$ phase layer, at the phase layer interface, grown by reaction diffusion in a Au/62Sn36Pb2Ag joint annealed at 125°C for 47 hours.

4.4 growth kinetics of the intermetallic layers

In order to determine the growth kinetics, the layer thicknesses were measured at different annealing times, using the same procedure described in section 3.3. A set of Au/PbSnAg diffusion couples were heated for different lengths of time. For each anneal time the layer thicknesses were determined using SEM and EDX analyser as described in sub-section 3.3.1. As before, only the thickness of the $AuSn_4$ layer and the total thickness of the other intermetallic layers were measured at different diffusion times.

In Figs. 4.6-8 are plotted the intermetallic layer thicknesses as a function of diffusion time for different temperatures, 160, 125 and 80°C. It can be seen that all those figures show the same pattern of layer growth as that shown by Figs. 3.10-13 for the case of pure tin-lead solder. During the early stage of annealing, layer growth is apparently parabolic. Later, the $AuSn_4$ layer continues to grow but a slower growth rate than in the early stage while the total thickness of the other intermetallic layers appears to become constant with aging time. The change-over of the growth rate of the $AuSn_4$ layer is more obvious on the figures corresponding to the higher temperatures. The time t_1 which ends the first stage and which decreases with increasing temperature does not appear to differ substantially from that in a silver free-sample annealed at the same temperature. In this case, again two stages in the layer growths can be distinguished.

-The initial stage

Figures 4.9-11 show that to a good approximation the layer thicknesses are proportional to $t^{1/2}$ up to a certain diffusion time t which is approximately 12 hours at 160°C, 50 at 125°C and 500 at 80°C. This confirms that the layer growths are parabolic during the initial period of annealing time. From the graphs of layer thicknesses versus $t^{1/2}$, the parabolic rate constants were determined for each layer for the different temperatures. The growth rate of a layer is given by the square of the slope of the line on the corresponding thickness-$t^{1/2}$ plot

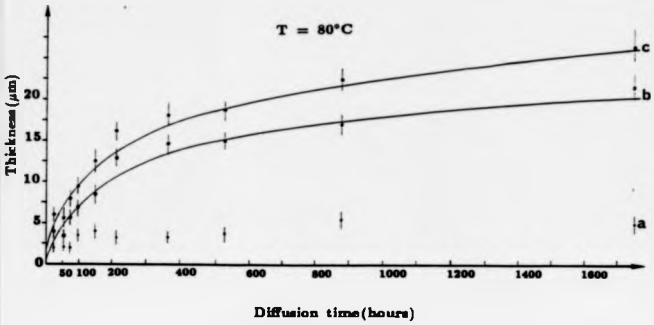

Fig. 4.6 Variation with time at 80°C diffusion temperature of the thicknesses of the intermetallic layers in a Au/62Sn36Pb2Ag diffusion couple; (a) $AuSn_2$, AuSn and δ-layer, (b) $AuSn_4$, (c) all the intermetallic phases.

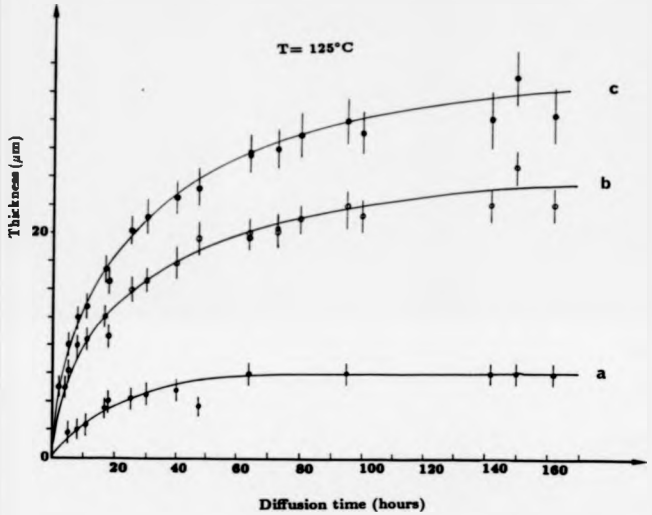

Fig. 4. 7 Variation with time at 125°C diffusion temperature of the thicknesses of the intermetallic layers in a Au/62Sn36Pb2Ag diffusion couple; (a) $AuSn_2$, AuSn and δ-layer, (b) $AuSn_4$, (c) all the intermetallic phases.

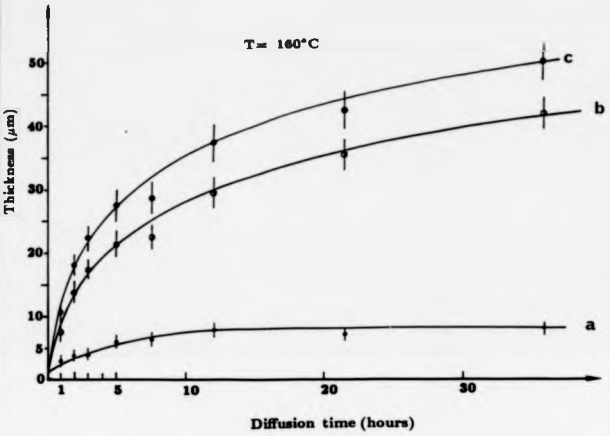

Fig. 4. 8 Variation with time at 160°C diffusion temperature of the thicknesses of the intermetallic layers in a Au/62Sn36Pb2Ag diffusion couple; (a) $AuSn_2$, AuSn and δ-layer, (b) $AuSn_4$, (c) all the intermetallic phases.

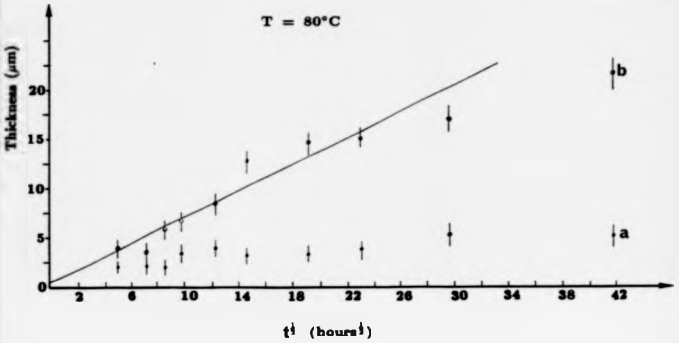

Fig. 4. 9 Plot of the thicknesses of the intermetallic layers in a Au/62Sn36Pb2Ag diffusion couple against the square root of the diffusion time at 80°C; (a) $AuSn_2$, AuSn and δ-layer, (b) $AuSn_4$.

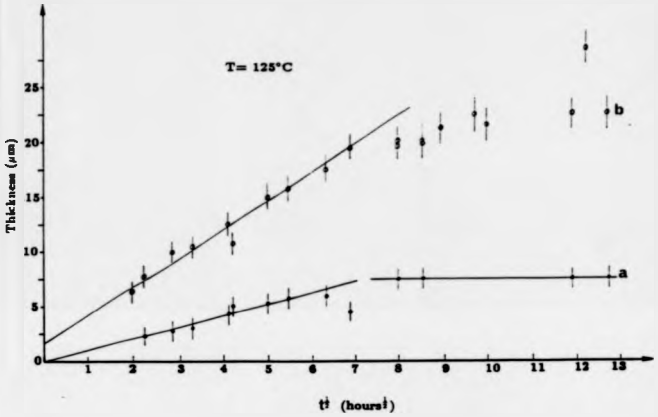

Fig. 4. 10 Plot of the thickneses of the intermetallic layers in a Au/62Sn36Pb2Ag diffusion couple against the square root of the diffusion time at 125°C; (a) $AuSn_2$, AuSn and δ-layer, (b) $AuSn_4$.

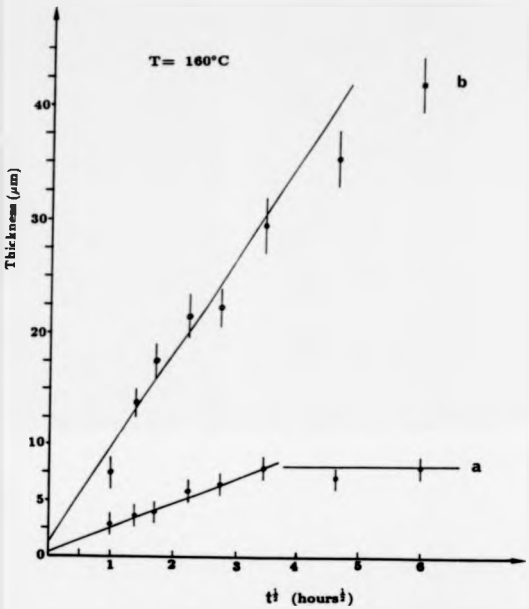

Fig. 4. 11 Plot of the thicknesses of the intermetallic layers in a Au/62Sn36Pb2Ag diffusion couple against the square root of the diffusion time at 160°C; (a) $AuSn_2$, AuSn and δ-layer, (b) $AuSn_4$.

since the parabolic law of growth was expressed in the usual way:

$$d^2 = Kt$$

where d is the layer thickness at the annealing time t and K the growth rate constant. The values of K determined in this way are listed in Table 4.1. These values are smaller than those obtained in the case of pure solder (Table 3.2), as the ratios K^*/K given in Table 4.1 show, where K^* and K are respectively the growth rate constant of an intermetallic layer in a Au/60Sn-40Pb diffusion couple and in a Au/62Sn36Pb2Ag joint.

-The late stage

In this stage, the thickness of the $AuSn_4$ layer continues to increase with diffusion time while that of the layer of the other intermetallics appears to be constant except at 80°C.

4.5 Effect of silver

The distribution of the silver content of the solder within Au/PbSnAg couples was investigated in detail at different anneal times at each aging temperature studied. An enhancement of the silver concentration was observed at the intermetallic compound/solder interface. For instance, after 6 hours of annealing concentrations of silver in the range 12 to 25 at.% were measured at the $AuSn_4$/solder interface. Energy dispersive X-ray analysis in the SEM indicated that the silver was present as precipitates of Ag_3Sn which is an intermetallic phase of tin and silver whose melting temperature is 480°C [65]. This was detected in the solder even before the heat treatment of the samples had begun and occurs during the soldering process because 2 wt.% silver is much greater than the Ag solubility limit in tin which is < 0.1% by weight even at 200°C [65]. No intermetallic phase exists between silver and lead [66] and the solubility of Ag in Pb is very restricted as well; the maximum solubility of Ag in Pb has been reported [67] as 0.19 at.% at the eutectic temperature of 304°C.

Table 4. 1 Growth rate constants of the intermetallic layers in Au/62Sn36Pb2Ag diffusion couples during the initial stage of interdiffusion.

annealing temperature (°C)	K (cm^2/s)	$K(AuSn_4)$ (cm^2/s)	$\frac{K^*}{K}$	$\frac{K^*(AuSn_4)}{K(AuSn_4)}$
80		$(1 \pm 0.2) \times 10^{-12}$		1.3 - 2.45
125	$(2.5 \pm 0.5) \times 10^{-12}$	$(0.19 \pm 0.02) \times 10^{-12}$	1.16 - 2.04	1.52 - 2.58
160	$(0.13 \pm 0.03) \times 10^{-10}$	$(2 \pm 0.2) \times 10^{-10}$	0.85 - 1.76	1.22 - 1.83

K^* and K are the growth constants of the layer of ($AuSn_2$ + AuSn + δ-layer), respectively in Au/60Sn-40Pb and Au/62Sn36Pb2Ag diffusion couples

Ag_3Sn particles were also found incorporated in the $AuSn_4$ layer but not in the $AuSn_2$ layer or any other layer. The detection of these particles within the $AuSn_4$ layer was not always possible as the intermetallic compound deforms plastically during mechanical polishing and covers the Ag_3Sn particles. These become visible in the microscope only in the case where the $AuSn_4$ compound layer surface breaks up during polishing. An example is shown in Fig. 4. 12a and the Ag_3Sn particles are indicated. It must be said that these particles were seen only in the layer region next to the solder. Two layer regions can be distinguished in the SEM micrograph shown in Fig. 4. 12b. Scan analyses performed on the surface of the outer region of the intermetallic layer, after the cross-section had been electropolished, gave 8 at. % silver and 8 at. % lead.

Point analyses in the SEM performed on the intermetallic layer surfaces and on the grain phases themselves by using the fracture surfaces (where the grain phases are clearly visible as can be seen on the micrographs shown in sub-section 4. 3. 2) did not give any trace of silver. Scan analyses done on the fracture surfaces did not give any trace of silver either.

The 2 wt. % silver in the solder had an effect on the growth rates of the Au-Sn intermetallic layers. The parabolic growth constant of a product layer in a couple made with pure 60Sn-40wt. %Pb solder is greater than that in a joint made with 62Sn-36Pb-2wt% silver (see Table 4. 1). Figure 4. 13 compares the thicknesses of the intermetallic layers,after 36 hours of annealing at 160°C, in a Au/60Sn-40Pb duffusion couple (Fig. 4. 13a) with those in a similar couple but with 2wt. % silver in the solder (Fig. 4. 13b). The effect of silver on the intermetallic layer thicknesses is clear from these figures. The overall compound layer in the joint made with the pure solder is thicker, by a factor of about 1. 3, than that in the couple made with the 2 wt. % silver-containing solder.

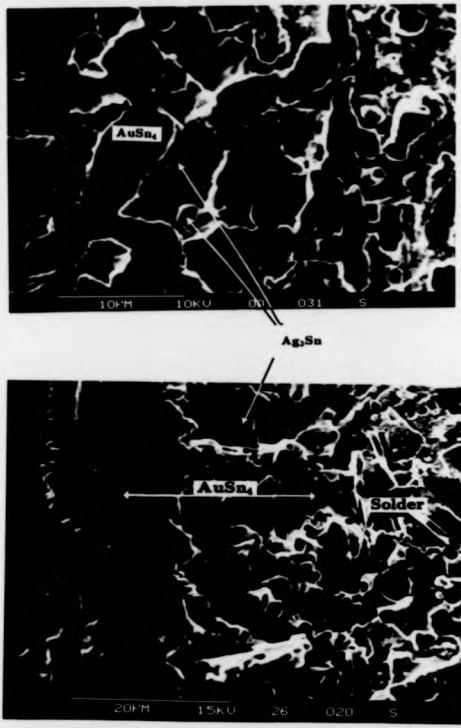

Fig. 4. 12. SEM micrographs showing the presence of Ag_3Sn particles within the layer of $AuSn_4$.

(a)

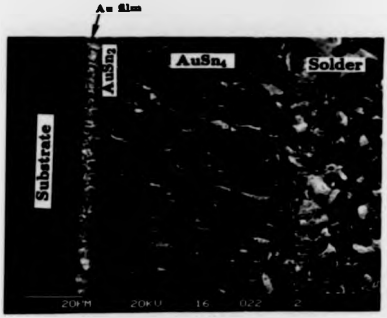

(b)

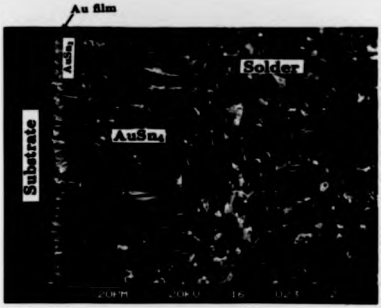

Fig. 4.13 This figure compares the intermetallic layer thicknesses in a Au/60Sn–40Pb joint (a) with those in a similar couple but with 2wt. % silver in the solder (b). Annealing temperature= 160°C, diffusion time= 36 hours.

4.6 Activation energy

Fig. 4. 14 shows the dependence of the growth rate constant of the $AuSn_4$ layer on the diffusion temperature, during the initial stage, in an Arrhenius plot. It can be seen on this figure that a straight line can be fitted to the experimental points. This means that the growth rate constant K_{AuSn_4} can be written in the form: $K_{AuSn_4} = K_0 \exp(-E_a/k_B T)$ where K_0 is a constant, k_B is Boltzmann's constant, T is the temperature on the Kelvin scale, and E_a is the activation energy of growth of the layer.

The activation energy E_a is given by the slope of the line on the Arrhenius plot and K_0 by the intercept of the line with the vertical axis. The least squares method which was used to fit the line to the experimental points yielded an activation energy $E_a = 0.87 \pm 0.04$ eV. The variation of k_{AuSn_4} (in cm^2/s), in the range of temperature [80-160°C], fits to the following expression:

$$K_{AuSn_4} = 2.59 e^{-0.87/k_B T} \qquad (4.1)$$

with $k_B T$ expressed in eV.

Within the experimental error, this value of the activation energy of growth of the $AuSn_4$ layer is equal to that in a couple made with silver-free 60Sn-40wt. %Pb solder (section 3.5.). This means that the type of diffusion (lattice or boundary diffusion) of the atoms through the $AuSn_4$ intermetallic layer is the same in the two Au/solder systems studied. Furthermore, it means that if the atoms migrate by lattice diffusion, the diffusion mechanism (vacancy, interstitial, etc ...) is the same.

An explanation of the effect of the silver of the solder on the diffusion rates of the atoms through the reaction products in the joint is given in section 7.2. In this model, the silver does not affect the activation energies for the diffusion of the atoms.

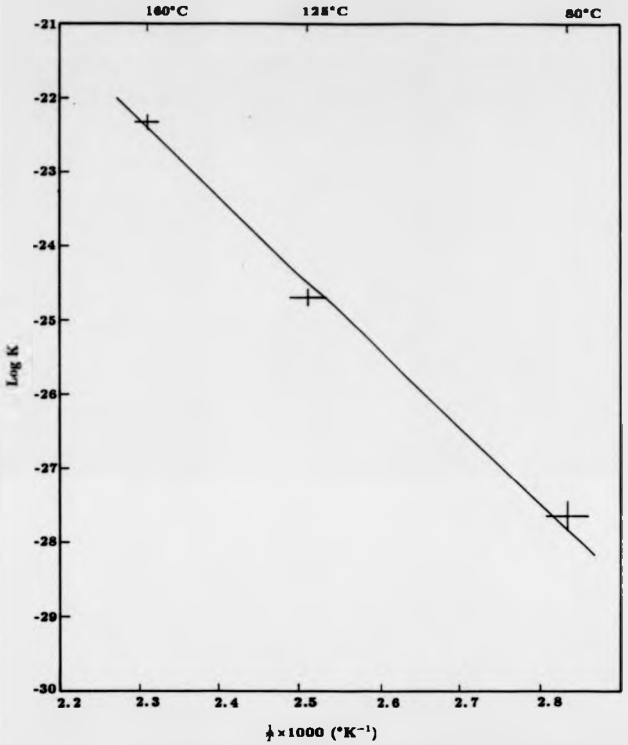

Fig. 4.14 Log K versus the inverse of the diffusion temperature where K is the parabolic growth constant, in a Au/62Sn36Pb2Ag diffusion couple, of the $AuSn_4$ phase layer. The straight line through the points which was fitted by the least squares method yielded an activation energy $E_a = 0.87 \pm 0.04$ eV.

4.7 Summary

Interdiffusion between gold films and eutectic tin-lead solder doped with 2wt.% silver has been studied at 80, 125 and 160°C using diffusion couples. The intermetallic layers which formed between the Au films and the solder were identified by X-ray analysis in the SEM and the intermetallic layer thicknesses were plotted as a function of diffusion time. It was found that silver has no effect on the growth of the Au-Sn phases which form between Au films and pure 60Sn-40wt.%Pb solder, identified in the previous study, and on the growth kinetics of the intermetallic layers. On the other hand the layer growth rates were smaller than those without silver in the solder. Ag_3Sn particles were detected in the $AuSn_4$ layer and are thought to be responsible of the reduction of the growth rates. An activation energy of growth of the $AuSn_4$ layer of 0.87 ± 0.04 eV was determined. The grain sizes of the intermetallic phases were found to increase with annealing time and temperature.

Chapter 5: INTERDIFFUSION IN Au/PbSnZn JOINTS

5.1 Introduction

The object of this study was to observe the effect of a small proportion of zinc added to 60wt.%Sn-40Pb solder on the growth rates of the intermetallic layers. The proportion of zinc added to the solder was 2wt.%. According to the published equilibrium phase diagrams for Sn-Zn alloys [68] and Pb-Zn alloys [69], Zn has a small solubility in tin and no apparent solubility in lead. At the eutectic temperature of 198.5°C, the maximum solubility of zinc in Sn is 0.6at.% and that of Sn in Zn is approximately 0.039at.%. No intermetallic compounds are formed with either tin or lead. In a 60Sn-40Pb alloy, up to 0.45at.%Zn (0.2wt.%Zn) may go into solid solution with Sn and above 0.45at.%, zinc rich regions form in the solder.

The effect of metallic contamination on the physical and on the wetting properties of tin-lead solders has been investigated [70]. Zinc in eutectic tin-lead solder is not harmful from the view point of resistivity but decreases the wetting power of the solder by increasing the dihedral angle. This is the angle formed between the solder in the liquid state and a solid substate; the smaller it is the better the solderability.

5.2 Experimental details

The PbSnZn solder was made in the laboratory. To prepare a small quantity of this alloy containing 2 weight percent zinc, 50.0g of the 60-40 tin-lead alloy and 1.0g of zinc nominally 99.999% pure were melted in an alumina crucible preheated at 500°C. The mixture was

stirred for a few minutes and then cooled quickly to room temperature. The composition of the as-made alloy was checked by X-ray analysis in the SEM. For that, pieces cut off at different regions of the material were polished.

For the manufacturing of Au/PbSnZn diffusion couples a soldering paste (fluxite) was used; the gold film was coated with a very thin layer of flux before melting the solder over it. The role of a flux is the cleaning of both the solder and the substrate by deoxidising and degreasing in order that a substrate/solder bond could be established. Another major role of the flux is to improve the wetting of the substrate by the liquid solder and the spreading of the latter over the substrate. With the use of the flux, the reaction between the gold films and liquid PbSnZn solder was quicker than without flux and the solder spread all over the 2 mm diameter gold film. Thus, intimate contact was obtained between the solder and the 2 mm diameter gold surface in a controllable time of a second or so.

For the purpose of promoting diffusion the Au/PbSnZn joints were annealed at 125°C. After a sample was given the desired anneal time it was cut through the joint interface. A flat surface of the joint cross-section was obtained by the metallographic techniques described in chapter 2. SEM examination of the prepared cross-sections plus EDX analysis provided both structural and compositional information of the joint.

5.3 Joint microstructure after aging

Figure 5.1 shows a SEM micrograph of a cross-section of a Au/PbSnZn sample annealed for 70 hours at 125°C. The Au-Sn intermetallic compounds observed in joints without zinc in the solder (chapter 3) occurred in this system also as can be seen on that picture. In addition, a compound layer has formed between the solder and the layer of $AuSn_4$. The microstructure of that compound layer is revealed in Fig. 5.1b. The chemical composition of the grains were determined by energy dispersive X-ray analysis in the SEM. Grains of composition

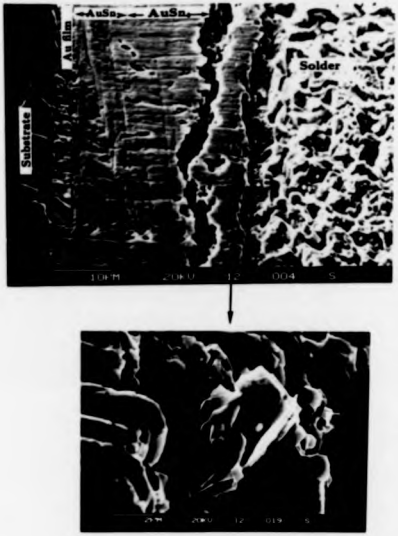

Fig. 5. 1. SEM micrographs (a) of a metallographic cross-section of a Au/PbSnZn diffusion couple annealed at 125°C for 70 hours, (b) of the grain structure of the compound layer formed between the $AuSn_4$ layer and the solder.

corresponding to the γ, γ_2, γ_3 and ϵ phases given by the equilibrium phase diagram for Au-Zn alloys shown in Fig. 5. 2 were detected. However, about 70 to 90% of the layer surface is composed of grains of composition $Au_{0.3}Sn_{0.2}Zn_{0.4}$. EDX analysis performed on the Au-Sn intermetallic layers have not shown any detectable quantity of zinc in the layers.

5.4 Growth kinetics of the Au-Sn phase layers

Figure 5. 3 shows the variation of the thicknesses of the Au-Sn phase layers in a Au/PbSnZn joint as a function of the annealing time at 125°C. As done in the previous cases, only the thickness of the $AuSn_4$ layer and the total thickness of the other intermetallic layers (for simplification called in the text $AuSn_2$ layer) were plotted as a function of diffusion time. It appears from the graph that the growth of the $AuSn_2$ layer is parabolic as in the cases studied earlier (chapter 2 and 3) but that of the $AuSn_4$ layer is not. A straight line seems to fit best to the experimental points. Still the thickest phase layer is $AuSn_4$. However, the ratio of the $AuSn_4$ thickness to that of the $AuSn_2$ is not constant and appears to be greater in the early stage of the layer formation than it is later on. For example, it is about 4 after 5 hours of annealing and only 1. 6 after 27 hours while in the previous cases it is constant during the early stage of the layer growth.

The growth rate of the $AuSn_2$ layer appears to become zero when the layer thickness has reached 10 μm or so. This behaviour is similar to that observed in Au/PbSn and in Au/PbSnAg diffusion couples.

The parabolic growth constant of the $AuSn_2$ phase layer is $(3.78 \pm 0.3) \times 10^{-12}$ cm^2/s and the linear growth constant of the $AuSn_4$ phase layer is $(1.75 \pm 0.25) \times 10^{-8}$ cm/s. Within experimental error the growth rate of $AuSn_2$ phase in a Au/PbSnZn joint is equal to that in a Au/60Sn-40Pb couple.

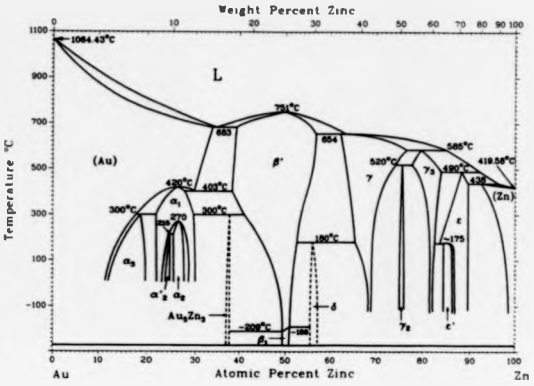

Fig. 5. 2 Equilibrium phase diagram of Au-Zn alloys[71].

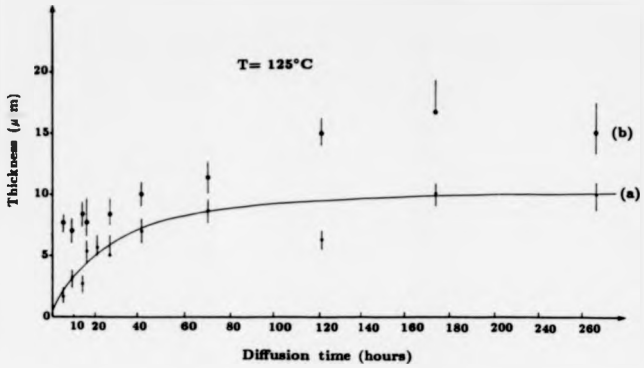

Fig. 5. 3 Variation with time at 125° diffusion temperature of the thicknesses of the intermetallic layers in a Au/PbSnZn diffusion couple: (a) $AuSn_2$, AuSn and δ-layer, (b) $AuSn_4$.

5.5 Effect of zinc

The addition of 2 weight per cent Zn in the solder remarkably reduced the growth rate of the $AuSn_4$ layer and changed its growth kinetics. This is apparent in comparison with Fig. 3.12 of chapter 3 relative to pure PbSn. On the other hand the growth kinetics of the $AuSn_2$ layer is unchanged by the presence of Zn in the solder and within experimental errors its growth rate is the same as in a Au/60Sn-40Pb diffusion couple.

The reduction of the growth rate of the $AuSn_4$ layer due to the presence of Zn in the solder could mean a slower dissolution rate of the gold film of the joint. This may be known by calculating the quantity of the reacted gold, at a given diffusion time and annealing temperature, in a Au/PbSnZn joint and compare it with that in a Au/PbSn couple. In a Au/PbSnZn joint the gold consumed by the solder elements (Sn, Zn) is given by the formula 3.2 plus a term taking into account the compound layer formed at the $AuSn_4$/Solder interface. 70 to 90% of this compound layer is made of $Au_{0.3}Sn_{0.3}Zn_{0.4}$, the rest is made of the Au-Zn alloys mentioned earlier plus a few percent lead . The density ρ of the $Au_{0.3}Sn_{0.3}Zn_{0.4}$ compound is not known but can be estimated by Vegard's law:

$$\rho = \frac{n_i m_i}{n_i \Omega_i} = 10.40 \text{ g/cm}^3, \tag{5.1}$$

where n_i is the fraction of atoms of the element i in the compound, m_i the atomic mass of the element i, and Ω_i the volume per atom of the element i.

After 70 hours of anneal, for example, the $AuSn_2$ phase layer has the same thickness in both Au/PbSn and Au/PbSnZn joints but the $AuSn_4$ phase layer is 18 μm greater in the first case than in the second. So the gold thickness transformed into Au-Sn intermetallics is greater in a Au/PbSn joint than in a Au/PbSnZn couple; the difference is roughly equal to $\frac{18 \times 0.3 \times 0.327}{19.3} = 1.72$ μm. However, in the Au/PbSnZn joint there is, between the $AuSn_4$ layer and the solder, a layer of $Au_{0.3}Sn_{0.3}Zn_{0.4}$ compound of about 8 μm $\times$ ($\frac{80}{100} \pm 0.1$) thick.

The gold film transformed into this compound layer is equal to $(6.4 \pm 0.8)\ 0.3 \times \frac{14.1}{4.1} = (1.03 \pm 0.13)\mu m$. The gold film transformed into Au-Zn intermetallics is less than $0.2\ \mu m$ and therefore one can conclude that at 125°C the rate of dissolution of gold films in joints made with 60Sn-40Pb solder doped with 2wt.% zinc is smaller than in joints made with pure 60Sn-40Pb solder.

5.6 summary

Interdiffusion between gold films and 60Sn-40wt.%Pb solder doped with 2wt.% zinc has been studied at 125°C using diffusion couples. The intermetallic compounds which formed in the diffusion zone were identified by X-ray analysis in the SEM. In addition to the Au-Sn intermetallic layers which form between Au films and 60Sn-40wt.%Pb solder (previous studies), a layer of $Au_{0.3}Sn_{0.3}Zn_{0.4}$ compound was found to form between the solder and the $AuSn_4$ layer. Au-Zn intermetallics which exist in the equilibrium phase-diagram of the Au-Zn system were also detected in that layer. The growth kinetics of the $AuSn_4$ layer was affected and its growth rate reduced. The dissolution rate, at 125°, of Au films in joints made with 60Sn-40Pb solder doped with 2wt.% zinc was found to be smaller than in joints made with pure 60Sn-40Pb solder.

Chapter 6: Au/SOLDER BOND STRENGTH

As explained in chapter 1, intermetallic formation not only consumes metals from the joints but reduces their mechanical strength. therefore, experiments to study Au/Solder bond strength after aging were undertaken.

6.1 Experimental details

In order to simulate the effect of aging on the bonding of copper wires soldered to gold film in an integrated circuit, copper wires 0.5 mm diameter were used to fabricate the samples for pull strength measurements. The gold film was 2 mm diameter disc, approximately 6 μm thick, well bonded to an alumina (Al_2O_3) substrate. The preparation of the gold discs on Al_2O_3 substrate is described in chapter 1. A typical sample for tensile testing is shown schematically in Fig. 6.1.

Prior to the sample fabrication, the wires, about 3 cm long, were thoroughly cleaned and their ends to be attached to the Au films were coated with the solder. Thereafter the samples were made; the wire was placed perpendicular to the substrate, held so it was in contact with the gold film, and soldered to the metal by melting additional solder over the assembly. The joints were then subjected to thermal aging in furnaces controlled to $\pm$ 3°C and set at 50 , 80 and 125°C. Pull strength measurements were taken at room temperature on samples from each of the three groups initially and after a range of aging times.

The solders used were those reported on earlier, i.e. 60Sn-40wt. %Pb, 62Sn36Pb2wt. %Ag and 60Sn-40wt. %Pb alloy to which 2 wt. % zinc were added. Intermetallic formation between

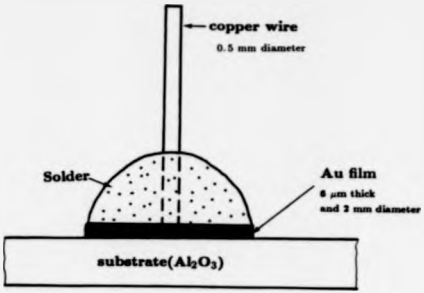

fig. 6. 1 Schematic diagram of the typical specimen for tensile testing the gold film/solder bond strength.

these solders and Au films are described in chapter 3, 4 and 5 respectively.

The measurements of the joint bond strength were made using an Instron tensile testing machine, model 1122. The specimen to be tested was attached between the fixed and the moving cross-head of the machine frame. The alumina substrate was rigidly clamped to the fixed cross-head and the Cu wire end to the moving cross-head. The alignment of the wire with the axis of pulling was optimized to avoid shear stresses on the joint and the load cell was calibrated. The tests were carried out, for all the samples, with the cross-head speed of 1 mm/minute. The joint pull strength to fracture was read on the Chart Recorder Unit.

After a sample was pulled to fracture EDAX together with SEM were used to determine where the failure occurred in the joint and to examine the microstructure of the materials present at the weak interface during pull testing.

6.2 Experimental results for Au/PbSnAg joints

6.2.1 Bond strength after aging

Figure 6.2 shows how the solder bond strength tested at room temperature varies with the aging time at 125 , 80 , and 50°C. Each point on the figure represents the average for 2 or 3 tensile specimens. It can be seen on that figure that after aging the pull strength of the joint is not much lower than that of the unaged specimen. Even, after some aging times at the lower temperatures the strength of the joint is greater than that of the unaged specimen. However, after long annealing times at the higher temperatures (125, 80°C) the joint reduced in strength. After 7×10^3 hours (nearly 10 and half months) at 125° and 12500 hours (nearly 17 months) at 80° the joint strength reduced to the half of the joint strength before aging.

Fig. 6. 2 Variation with aging time at 125°C, 80°C and 50°C of the tensile load at the fracture point of a Au/62Sn36Pb2Ag joint.

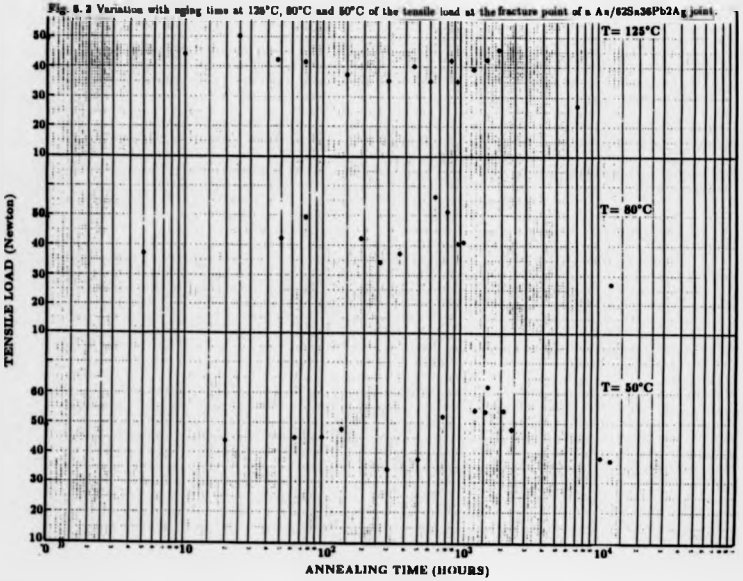

6.2.2 Failure mode

To identify the weak region(s) within the joint during pull testing, the fracture surfaces in the as-prepared and the aged joints were examined in the SEM and analysed. The Energy Dispersive X-ray Analyser fitted to the microscope was used to analyse the compositions of the fracture surfaces.

-Failure mode before aging

When as-prepared joints were tested, failure occurred through the intermetallic layer formed during the soldering process. The composition of the materials present on the fracture surface on the wire side of the joint (Fig. 6. 3a) corresponds to that of the $AuSn_4$. Spot analyses carried out on the fracture surface on the substrate side which is shown in Fig. 6. 3b revealed two intermetallic phases: $AuSn_2$ and AuSn.

-Failure mode after 80°C aging

Scanning electron micrographs of the fracture surfaces of joints pulled to fracture after aging at 80° are shown in Figs. 6. 4-6. The joints were fractured after 188 hours (Fig. 6. 4a), 266 hours (Fig. 6. 4b), 650 hours (Fig. 6. 5a), 1053 hours (Fig. 6. 5b) and 12500 hours (Fig. 6. 6). Results from EDX analysis of the fracture surfaces are given. All of the many joints annealed at this temperature fractured during the pull test both at the $AuSn_2/AuSn_4$ interface and within the solder for annealing times up to about 500 hours. The fracture at the $AuSn_2/AuSn_4$ interface occurred in the part of the joint situated between the copper wire and the solder, and the fracture in the solder occurred in the outer regions of the joint. The relatively high concentration of lead (up to 60 at. % Pb) detected on the fracture surfaces of this part of the joint suggests that the fracture occurred in the tin depleted region of the solder adjacent to the intermetallic compound. It has been observed when studying the nature and the kinetics of the product phases in Au/PbSn diffusion couples (chapter 3 and 4) that as a consequence of the growth of the intermetallic compound layers, a tin-depleted

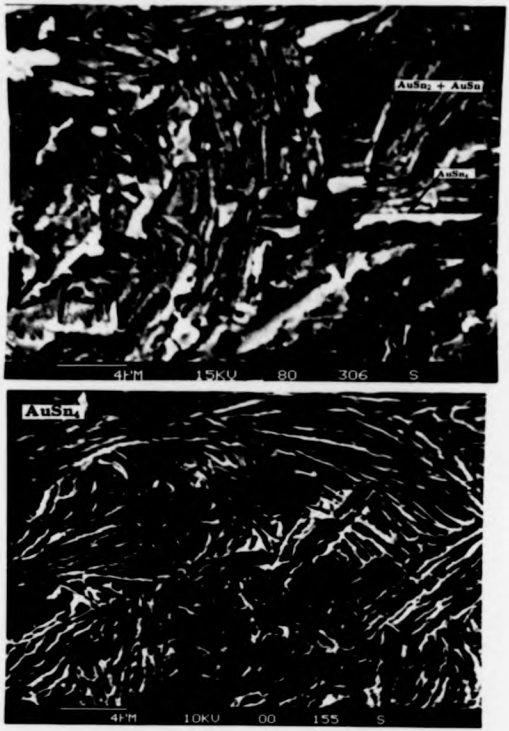

Fig. 6. 3 SEM micrographs of the fracture surfaces of an as-prepared Au/PbSnAg joint pulled to fracture; (a) fracture surface on the wire side of the joint, (b) fracture surface on the substrate side of the joint.

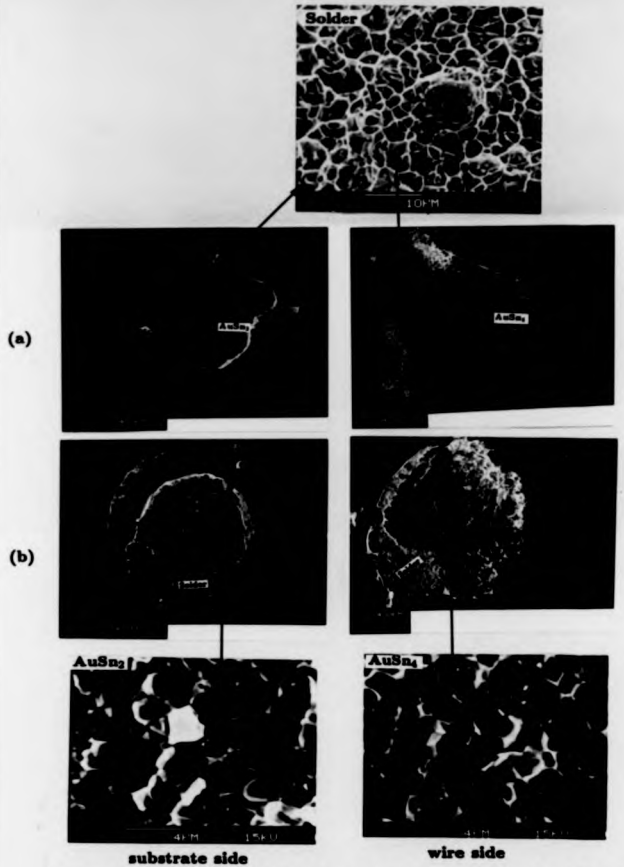

Fig. 6. 4. SEM micrographs of the fracture surfaces of a Au/62Sn36Pb2Ag joint pulled to fracture after aging at 80°C for (a) 188 hours, (b) 262 hours.

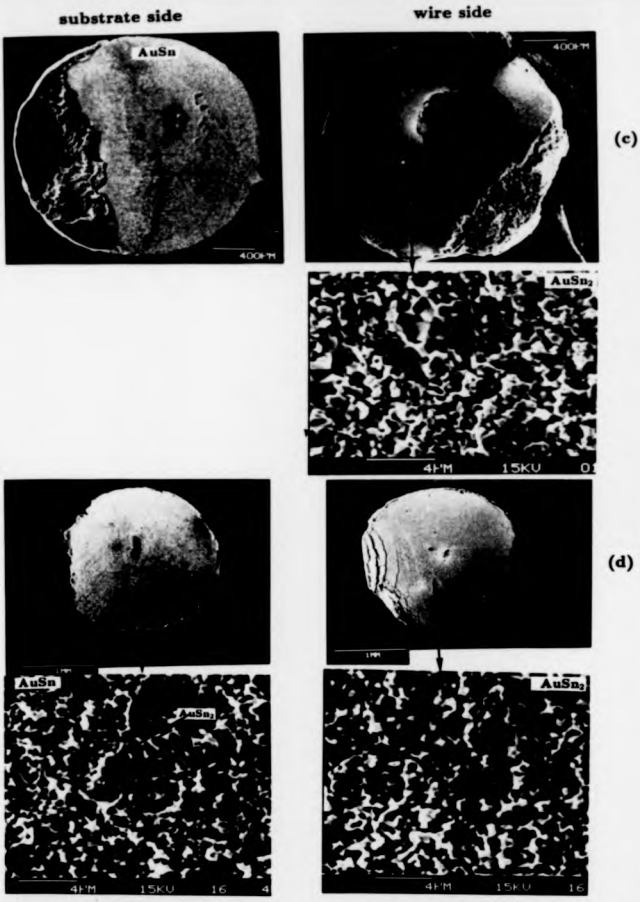

Fig. 6. 5. SEM micrographs of the fracture surfaces of a Au/62Sn36Pb2Ag joint pulled to fracture after aging at 80°C for (c) 650 hours, (d) 1053 hours.

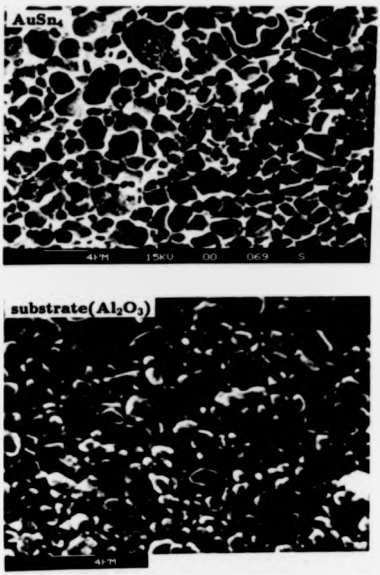

Fig. 6. 6. SEM micrographs of the fracture surfaces of a Au/62Sn36Pb2Ag joint pulled to fracture after aging at 80°C for 12500 hours (nearly 18 months).

layer of solder forms adjacent to the intermetallic layer.

SEM examination of cross-sectional diffusion couples showed that the only phases which formed within the joints at those aging times were $AuSn_2$ and $AuSn_4$. The grain sizes of the $AuSn_2$ and $AuSn_4$ phases were found to increase with annealing time, as previously mentioned in sub-section 4.3.2, but no variation of the phase compositions with annealing time could be detected. The increase of the phase grain sizes with aging time does not appear to affect the pull strength of the joint as can be seen on Fig. 6.2.

Joints which were subjected to annealing times between 650 and 1050 hours fractured during pull testing at the $AuSn_2$/AuSn interface. The fracture was exclusively at this interface (see Fig. 6.5) in contrast with that occurring at the shorter aging times.

After a long aging time (12500 hours) the joint fractured at the substrate/$AuSn_4$ interface. The gold film had of course been consumed by this stage. The time the 6 μm gold film completely transforms into Au-Sn intermetallics is about 2400 hours in a joint made with 60Sn-40Pb solder and annealed at this temperature (see Fig. 3.18), that in a joint made with 62Sn-36Pb-2Ag solder and annealed at the same temperature is not expected to be longer than 3000 hours. Even so the joint pull strength remained high. The microstructure of the $AuSn_4$ compound surface which pulled of the substrate is shown in Fig. 6.6.

-Failure mode after 125°C aging

SEM-EDX analyses of the fracture surfaces of joints pulled to fracture after annealing at 125°C showed that before degradation of the gold film the joint fractures during pull testing either both within the layer of intermetallic compounds and at the compound layer/solder interface or exclusively within the layer of intermetallics. While the fracture within the layer occurs at a boundary between two compound layers, sometimes it occurs in the same sample at two or three boundaries. After complete dissolution of the gold film the joint fractures at the substrate/$AuSn_2$ interface, then at the $AuSn_4$/substrate interface.

SEM micrographs of fracture surface are shown in Fig. 6. 7 and in Fig. 6. 8 along with the compositions of the elements present on the fracture areas. The micrograph in Fig. 6. 7a shows that the joint failed at the AuSn/δ-phase interface, that in Fig. 6. 7b shows that the joint failed at both the $AuSn_2$/AuSn and $AuSn_4$/$AuSn_2$ interfaces. The micrographs in Fig. 6. 7c of the fracture surfaces of a joint pulled to fracture after 150 hours of annealing show that the failure occurred at the AuSn/δ-phase and at the alumina substrate/$AuSn_4$ phase interfaces. It must be said that the composition detected does not correspond exactly to the δ-phase of the Au-Sn system but spreads within a wide range of compositions between 10 and 20 at. %Sn (the balance Au). Whether this was due to spurious X-ray signals or that the fracture surface contained the δ' or the δ' and δ phases of the Au-Sn system could not be known. So what we called δ-phase is that range of compositions. The fracture at the AuSn/δ-phase interface occurred in the region of the joint situated between the substrate and the copper wire and that at the boundary between the $AuSn_4$ compound and the substrate occurred outside this region. From the intermetallic layer thicknesses versus annealing time curves shown in Fig. 4. 7, the life time of the 6 μm gold film at the annealing temperature of 125°C, calculated by using equation 3. 2 is approximately 120 hours. Also it is known that after degradation of the gold film, tin atoms from the solder diffusing towards the substrate transforms the gold rich phases ($AuSn_2$, AuSn, δ-phase) into $AuSn_4$. Therefore, it is not surprising to find the $AuSn_4$ phase next to the substrate in that region of the joint. The presence of the AuSn and δ-phase, and may be some gold under the δ-phase layer, in the region of the joint situated between the copper wire and the substrate is due to the smaller amount of solder accessible to the gold in this region than elsewhere in the joint and consequently to a slower dissolution rate of the gold film. The micrograph in Fig. 6. 8a of the fracture surfaces of a joint pulled to destruction after 1250 hours of annealing show that the joint failed within the $AuSn_4$ intermetallic compound. The magnified view of a typical area of the fracture surface on the

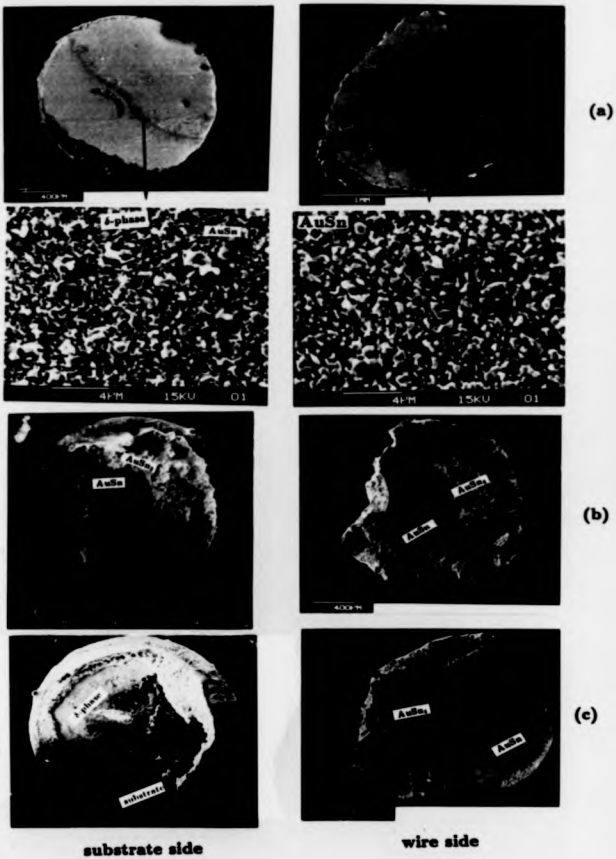

Fig. 6. 7. SEM micrographs of the fracture surfaces of a Au/62Sn36Pb2Ag joint pulled to fracture after aging at 125°C for (a) 10 hours, (b) 47 hours, (c) 150 hours.

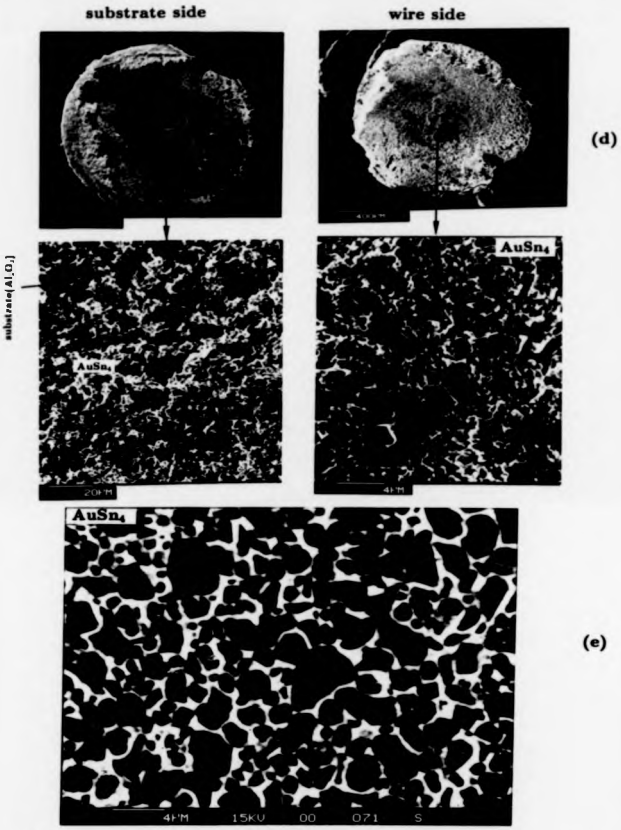

Fig. 6. 8. SEM micrographs of the fracture surfaces of a Au/62Sn36Pb2Ag joint pulled to fracture after aging at 125°C for (d) 1250 hours, (e) 7000 hours.

substrate side reveals that the fracture occurred very near the substrate and in some areas it occurred at the substrate/$AuSn_4$ interface. It is evident, as Fig. 6. 8a shows, that the $AuSn_4$ phase has a different and finer structure from that exhibited in the early stage of annealing and shown in Fig. 4. 5b. The microstructure of the $AuSn_4$ compound which pulled off the substrate is revealed in Fig. 6. 8b.

After a long aging time (7×10^3 hours) the joint completely failed at the boundary between the substrate and $AuSn_4$ layer. The microstructure of the $AuSn_4$ at this boundary is shown in Fig. 6. 8b. A comparison between this figure and that shown in Fig. 6. 8a suggests that grain growth of the $AuSn_4$ compound occurred during aging times from 1250 to 7000 hours. The decrease of the adherence of the $AuSn_4$ compound to the alumina substrate appears to be responsible of the decrease of the joint pull strength after the long aging time. That decrease of $AuSn_4$ adherence to the substrate might be due to the $AuSn_4$ grain growth with annealing time.

-Failure mode after 50°C aging

A noticeable difference between the failure mode of joints annealed at this temperature and the ones aged at the other temperatures was observed. Most of the joints annealed at 50°C failed during pull testing through the copper wire/solder interface, i.e. the Cu wire pulled away from the solder. The weak bond in the region between the gold film and the Cu wire end was identified as $AuSn_2/AuSn_4$ interface. Up to the longest anneal time used (12500 hours) the fracture in that region occurred at this interface.

6.3 Results for Au/PbSn joints

-Pull strength and failure mode

Tensile specimens as shown in Fig. 6. 1 made with 60Sn-40wt. %Pb solder were also pull tested initially and after aging at 125°C. The specimens were not annealed for as long as the

previous ones, however. It was observed from a limited tensile data that the joint strength was the same as for the joint made with 62Sn36Pb2Ag solder. Also, as was expected, the failure mode was similar to that of the Au/PbSnAg joint, i.e. the joint failed within the layer of Au-Sn intermetallics. So the presence of 2wt. % silver in the near-eutectic PbSn solder has no effect on the Au/PbSn joint strength. It only increases the gold film life time by reducing the growth rates of the reaction products in the joint.

6.4 Results for Au/PbSnZn joints

-Pull strength and failure mode

Joints of Cu wire and Au film soldered with the near-eutectic PbSn solder containing 2 weight percent zinc showed a substantial weakness under tensile stress compared to those made with 60Sn-40Pb or 65Sn36Pb2Ag solder . The results of the pull test carried out on as-prepared samples and after aging at 125°C are shown in Fig. 6. 9. There is a clear decrease in the joint pull strength with aging time in contrast with the pull strength of a joint made with a near-eutectic PbSn solder with or without 2wt. % silver and annealed at the same temperature. The loss in strength of the Au/PbSnZn joint is considerable (about 75% of its initial strength) after an anneal time as short as 68 hours at 125°C).

It has been noticed during pull test experiments that the Cu wires soldered to gold films with the PbSnZn alloy pulled out of the solder, before aging as well as after. Energy diapersive X-ray analysis in the SEM of the wire ends and the fracture surfaces on the substrate sides showed that the fracture occurs almost always within the solder trapped between the wire and the gold film. Two compositions [(63±2)at. % Zn-(37±2) Cu] and [(50 ± 3) at. % Zn - (49±2) Cu] suggesting formation of intermetallics between copper and zinc of the solder were detected on some pulled off wires. SEM micrographs of the fracture surfaces of Au/PbSnZn joints are shown in Fig. 6. 10. In figure 6. 10a of a sample annealed for 16 hours and pulled to

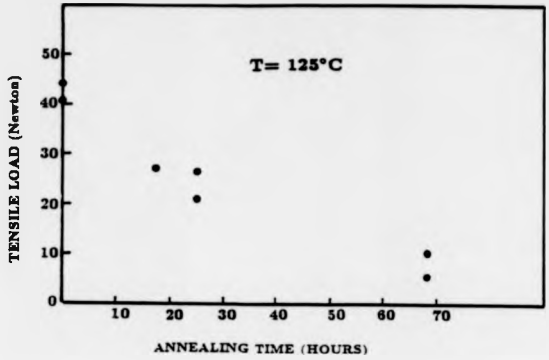

Fig. 6. 9 Variation with aging time at 125°C of the tensile load at the fracture point of a Au/PbSnZn joint.

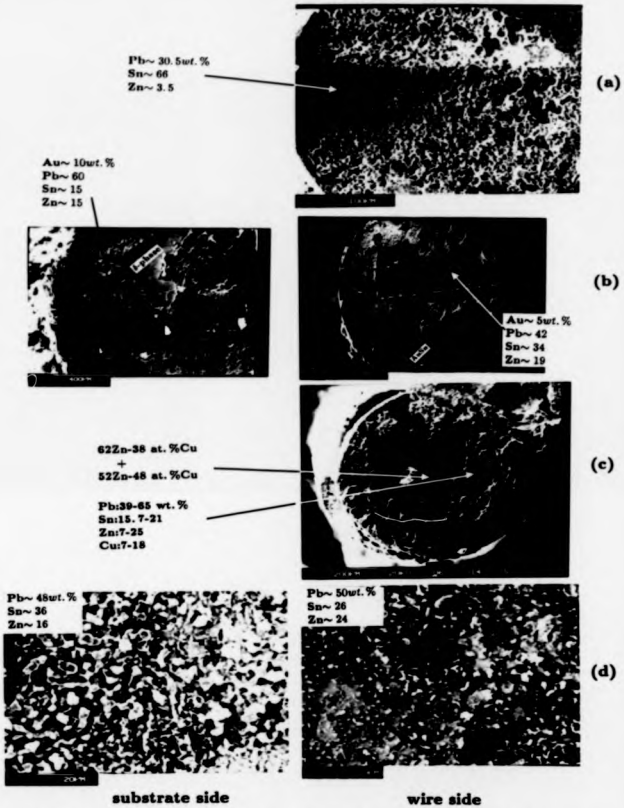

Fig. 6. 10. SEM micrographs of the fracture surfaces of a Au/PbSnZn joint pulled to fracture before aging (a) and after aging at 125°C for (b) 16 hours, (c) 25 hours, (d) 68 hours.

fracture two areas can be distinguished: The smooth and the rough area which includes most of the surface. X-ray analysis in the smooth areas gave the approximate atomic percentages: 82 Au, 3 Pb, 15 Sn on the substrate side and 50 Au, 1.5 Pb, 48.5 Sn on the other face, thus showing the fracture to be at AuSn/δ'- phase interface. The other part of both fracture surfaces which exhibits a relatively rough microstructure contains a small quantity of Au in addition to the elements present in the solder. The concentrations of the elements obtained by scanning the electron beam over the surfaces are given in Fig. 6. 10. In figures 6. 10c and d are shown the fracture surfaces on the wire sides after 25 hours of annealing (Fig. 6. 8c) and 68 hours (Fig. 6. 8d). The analytical results are included in those figures. High concentrations of zinc at the fracture surfaces are noticed in Figs. 6. 10b-d.

6.5 summary

The tensile strength of solder bonds to Au films has been evaluated before and after aging for various times and temperatures. Three solders (62Sn36Pb2wt. %Ag, 60Sn-40wt. %Pb and 60Sn-40wt. %Pb doped with 2wt. % zinc) were tested. The annealing temperatures were 50, 80 and 125°C for the first cited solder and 125°C for the remainder. The experimental results were as follows. First, the solder bonds with and without silver in the solder had similar tensile strengths. Second, after temperature aging the Au/62Sn36Pb2Ag joints broke during pull testing both within the intermetallic compound, at the boundaries between the intermetallic layers, and at the $AuSn_4$ layer/solder interface. After depletion of the gold film, they broke at the intermetallic compound/substrate interface. The tensile strength of the joint was independent of the number of intermetallic layers formed and their thicknesses. Third, the Au/solder bonds with 2wt. % zinc in the solder broke at the copper wire/solder interfaces and the tensile strength of the joint reduced very rapidly with the annealing time.

Chapter 7 : DISCUSSION

This chapter is divided in three sections. The first section deals with the formation of intermetallic layers in the gold/PbSn system, the second with the effect of silver in the solder on their growth rates, the third with the type of diffusion.

7.1 Intermetallic formation in gold/PbSn systems

7.1.1 Summary of experimental observations

When Au/60Sn-40Pb diffusion couples were annealed at 80, 125, 140 and 160°C, intermetallic layers of Au-Sn phases formed. The predominant and first phases which appeared in the diffusion couples were $AuSn_4$ and $AuSn_2$. AuSn phase and δ-layer (δ' or δ' plus δ phases of the Au-Sn system) appeared in the couples only after long annealing times, greater at the lower temperatures, and their thicknesses remained very small at all diffusion times. Two stages were observed in the variation with diffusion time of the thickness of the $AuSn_4$ layer and the total thickness of the other intermetallic phases (see Figs. 3.10-13). In the initial stage, up to a certain diffusion time which decreases with increasing temperature, both layers grow parabolically with time. In the second stage the thickness of the $AuSn_4$ layer continues to increase while the total thickness of the other intermetallic layers remains constant. The growth rate in the second stage is smaller than in the first stage. With 2wt.% zinc in the solder, in addition to the Au-Sn intermetallic phases a layer of a ternary compound of composition $Au_{0.3}Sn_{0.3}Zn_{0.4}$ formed between $AuSn_4$ layer and the solder (see

Fig. 5. 1). Au-Zn intermetallic phases were also detected in that layer. The growth rate of the $AuSn_2$ layer was unchanged as a consequence of the addition of zinc in the solder but that of the $AuSn_2$ did change. The thickness of this layer is less than in a Au/60Sn-40Pb couple for corresponding times and temperatures. The growth kinetics of the intermetallic layers in Au/62Sn36Pb2wt.%Ag couples (plotted in Figs. 4. 6-8) were similar to those in Au/60Sn-40Pb couples but the growth rates were smaller (see Table 4. 1 and Fig. 4. 13). Particles of the Ag_3Sn phase were detected in the $AuSn_4$ layer (see Fig 4. 12).

7.1.2 Theoretical treatment of intermetallic formation in binary diffusion couples

Numerous theories [72-78] which deal with the formation of reaction products in binary diffusion couples have been proposed. Multilayer diffusional growth theories in which the interface velocities are expressed in terms of the fluxes of the reactants at the interphase interfaces have been proposed [75-77]. Different approaches, however, have been used by these authors [75-77] for the determination of the growth rate of a compound layer. In reference 75, the growth rate of a compound layer is defined by the rates of accumulation of the diffusing species at the layer boundaries. In reference 77, it is related both to the rates of accumulation of the diffusing species at the layer boundaries and also to the accumulation of the diffusing species within the volume between the two layer boundaries. The theory given elsewhere [16] considers the dissolution of the phases at each interphase interface in addition the rates of accumulation of the diffusing species at the layer boundaries. All these theories [72-77], which are based on the assumption that the growth of a product phase is diffusion controlled, predict parabolic layer growth under conditions of quasi-steady state diffusion. Diffusion-controlled kinetics have been observed in many multiphase diffusion systems [79-81] but examples of non-parabolic product growth exist [79,82]. The disagreement between the diffusional theories and

existing non parabolic layer growth is thought [78] to be due to neglect of chemical reactions taking place at the interfaces between the reacting phases and a model has been proposed. In this model [78] the growth rate of a product phase is not only determined by the rates of diffusional transport of the reacting species through the growing layers but also by the rates of chemical reactions taking place at the interphase interfaces. The model gives analytical equations for layer growth rates which differ from those given by the diffusional theories [75,76], which become similar only in the limiting cases where the rates of chemical reactions are very high compared to the rates of diffusion of the reacting species.

The validity of the different theories [74-76] has been tested [79] experimentally. For that, diffusional growth experiments were performed on Ag-Zn binary alloys and the growth rates of the different phase layers evaluated in terms of the different theories [79]. The accuracy with which theses theories describe diffusion-controlled growth is good. A good agreement has also been obtained [77] between the reported experimental results on Ag-Zn binary alloys and the layer growth rates predicted by the published theory [77].

7.1.3 Solid-state growth of the intermetallic layers in Au/PbSn systems

-Description of the possible interfacial reactions

Figure 7.1 is a schematic diagram of a Au/PbSn couple within which the layers of $AuSn_2$ and $AuSn_4$ have formed and are growing as a result of reactions at the phase layer interfaces. The concentration profiles of the reactants are also shown.

The change of the thickness of the β phase layer, for example, with diffusion time could be due to five simultaneous reactions taking place at the phase layer boundaries, 2 and 3 in Fig. 7.1.

(a) At the interface 3 the Au atoms arrive by diffusion through the β phase layer and

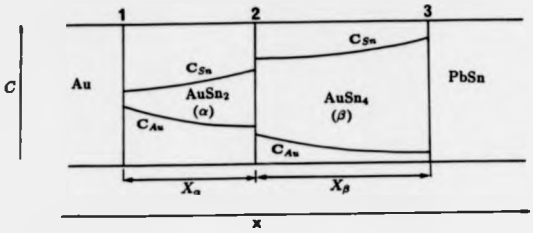

Fig. 7.1 Schematic diagram of a Au/PbSn diffusion couple annealed for some time.

combine with Sn atoms to form new $AuSn_4$ according to the equation:

$$Au + 4Sn \longrightarrow AuSn_4 \tag{7.1}$$

The Au atoms might be supplied by the gold film or by dissolution of $AuSn_2$ into $AuSn_4$ according to the equation 7.7 written later. Thus, the reaction of one atom of Au forms one molecule of $AuSn_4$. The number of atoms of Au arriving to the interface 3 per unit time and unit area of surface, J_a, may be given by Fick's first law:

$$J_a = -(D^{\beta}_{Au}\frac{\partial C^{\beta}_{Au}}{\partial x})_3 \tag{7.2}$$

where D^{β}_{Au} is the lattice diffusion coefficient of Au atoms within the β phase and C^{β}_{Au} the concentration in atoms per unit volume of Au in the β phase. The subscript 3 indicates the value of the quantity existing at interface 3.

At the interface 2, there are four possible reactions.

(b) The Au atoms arrive by diffusion through the α phase and combine with β to form new α phase according to the equation:

$$Au + AuSn_4 \longrightarrow 2AuSn_2 \tag{7.3}$$

Thus, the reaction of one atom of Au consumes one molecule of $AuSn_4$ and forms 2 molecules of $AuSn_2$. The number of atoms of Au arriving to the interface 2 per unit time and unit area of surface, J_b, may be given by Fick's first law:

$$J_b = -(D^{\alpha}_{Au}\frac{\partial C^{\alpha}_{Au}}{\partial x})_2 \tag{7.4}$$

wherein D^{α}_{Au} is the lattice diffusion coefficient of Au atoms within the α phase and C^{α}_{Au} is the concentration in atoms per unit volume of Au in the α phase. The subscript 2 indicates the value of the quantity existing at interface 2.

(c) The Sn atoms arrive by diffusion through the β phase and combine with α phase to

form new β phase according to the equation:

$$Sn + \frac{1}{2}AuSn_2 \longrightarrow \frac{1}{2}AuSn_4. \tag{7.5}$$

The reaction of one atom of Sn forms $\frac{1}{2}$ molecule of $AuSn_4$ and consumes $\frac{1}{2}$ molecule of $AuSn_2$. The number of atoms of Sn arriving to the interface 2 per unit time and unit area of surface, J_c, may be given by:

$$J_c = (D^{\beta}_{Sn}\frac{\partial C^{\beta}_{Sn}}{\partial z})_2, \tag{7.6}$$

wherein D^{β}_{Sn} is the lattice diffusion coefficient of Sn atoms within the β phase and C^{β}_{Sn} is the concentration in atoms per unit volume of Sn in the β phase.

(d) Transformation of $AuSn_2$ to $AuSn_4$ by departure through the β phase of Au atoms from $AuSn_2/AuSn_4$ interface according to the equation :

$$2\ AuSn_2 \longrightarrow Au + AuSn_4. \tag{7.7}$$

The departure of one atom of Au through the β phase forms one molecule of $AuSn_4$ and consumes 2 molecules of $AuSn_2$. If this reaction is diffusion controlled the number of atoms of Au which leave the $AuSn_2/AuSn_4$ interface per unit area of surface and unit time, J_d, would be :

$$J_d = -(D^{\beta}_{Au}\frac{\partial C^{\beta}_{Au}}{\partial z})_2. \tag{7.8}$$

(e) Transformation of $AuSn_4$ to $AuSn_2$ by departure through the α phase of Sn atoms from $AuSn_2/AuSn_4$ interface according to the equation :

$$\frac{1}{2}AuSn_4 \longrightarrow Sn + \frac{1}{2}AuSn_2. \tag{7.9}$$

The departure of one atom of Sn through the α phase consumes half a molecule of $AuSn_4$ and forms half a molecule of $AuSn_2$. If this reaction is diffusion controlled the number of atoms of Sn leaving the $AuSn_2/AuSn_4$ interface per unit area of surface and unit time would be given by:

$$J_c = (D^{\alpha}_{Sn}\frac{\partial C^{\alpha}_{Sn}}{\partial z})_2, \tag{7.10}$$

with D^{α}_{Sn} the lattice diffusion coefficient of Sn atoms and C^{α}_{Sn} the concentration per unit volume of Sn in the α phase.

-Layer growth kinetics

Assuming that the reactions at the interfaces 2 and 3 are diffusion controlled and the cross-section area of the diffusion couple invariant, the rate of change of the thickness of the β phase, X_β, may be written:

$$\frac{dX_\beta}{dt} = \Omega^{\beta}_{3} J_a - \Omega^{\beta}_{2} J_b + \Omega^{\beta}_{2} \frac{J_c}{2} + \Omega^{\beta}_{2} J_d - \Omega^{\beta}_{2} \frac{J_c}{2}, \tag{7.11}$$

where Ω^{β}_{3} and Ω^{β}_{2} are the volume per molecule of the β phase at interface 3 and 2 respectively. Substitution of the expressions of the fluxes J_a, J_b... into the equation above yields the following equation:

$$\begin{aligned}\frac{dX_\beta}{dt} &= -\Omega^{\beta}_{3}(D^{\beta}_{Au}\frac{\partial C^{\beta}_{Au}}{\partial x})_3 + \Omega^{\beta}_{2}(D^{\alpha}_{Au}\frac{\partial C^{\alpha}_{Au}}{\partial x})_2 + \frac{1}{2}\Omega^{\beta}_{2}(D^{\beta}_{Sn}\frac{\partial C^{\beta}_{Sn}}{\partial x})_2 \\ &\quad -\Omega^{\beta}_{2}(D^{\beta}_{Au}\frac{\partial C^{\beta}_{Au}}{\partial x})_2 - \frac{1}{2}\Omega^{\beta}_{2}(D^{\alpha}_{Sn}\frac{\partial C^{\alpha}_{Sn}}{\partial x})_2.\end{aligned} \tag{7.12}$$

The growth rate of the α phase layer, $\frac{dX_\alpha}{dt}$, can also be determined by considering the reactions which might occur at the layer boundaries, 1 and 2 in Fig. 7. 1. Taking into account that the AuSn and δ-layer growth rates are almost nil it can easily be shown that the overall reaction at interface 1 contribute to the α phase layer growth rate by $\frac{1}{2}(D^{\alpha}_{Sn}\frac{\partial C^{\alpha}_{Sn}}{\partial x})_1\Omega^{\alpha}$.

$$\begin{aligned}\frac{dX_\alpha}{dt} &= \frac{1}{2}\Omega^{\alpha}_{1}(D^{\alpha}_{Sn}\frac{\partial C^{\alpha}_{Sn}}{\partial x})_1 + \frac{1}{2}\Omega^{\alpha}_{2}(D^{\alpha}_{Sn}\frac{\partial C^{\alpha}_{Sn}}{\partial x})_2 - 2\Omega^{\alpha}_{2}(D^{\alpha}_{Au}\frac{\partial C^{\alpha}_{Au}}{\partial x})_2 \\ &\quad + 2\Omega^{\beta}_{2}(D^{\beta}_{Au}\frac{\partial C^{\beta}_{Au}}{\partial x})_2 - \frac{1}{2}\Omega^{\alpha}_{2}(D^{\beta}_{Sn}\frac{\partial C^{\beta}_{Sn}}{\partial x})_2.\end{aligned} \tag{7.13}$$

If the growth of the intermetallic phases occur by quasi-steady state diffusion the gradients of the concentrations of Au and Sn at the boundaries may be written as follows:

$$(\frac{\partial C^{\beta}_{Au}}{\partial x})_2 = (\frac{\partial C^{\beta}_{Au}}{\partial x})_3 = -\frac{\Delta C^{\beta}_{Au}}{X_\beta} = -\frac{(C^{\beta}_{Au})_2 - (C^{\beta}_{Au})_3}{X_\beta}, \tag{7.14}$$

$$(\frac{\partial C^{\alpha}_{Au}}{\partial x})_2 = -\frac{\Delta C^{\alpha}_{Au}}{X_\alpha} = -\frac{(C^{\alpha}_{Au})_1 - (C^{\alpha}_{Au})_2}{X_\beta}, \tag{7.15}$$

$$(\frac{\partial C^{\beta}_{Sn}}{\partial x})_3 = \frac{\Delta C^{\beta}_{Sn}}{X_\beta} = \frac{(C^{\beta}_{Sn})_3 - (C^{\beta}_{Sn})_2}{X_\beta} \quad (7.16)$$

$$(\frac{\partial C^{\alpha}_{Sn}}{\partial x})_2 = \frac{\Delta C^{\alpha}_{Sn}}{X_\alpha} = \frac{(C^{\alpha}_{Sn})_2 - (C^{\alpha}_{Sn})_1}{X_\alpha} \quad (7.17)$$

In general, diffusion coefficients are concentration dependent. Therefore, the diffusion coefficients of the reactants within a compound layer may be variable. However, if the compound has a narrow composition range, which is the case for $AuSn_2$ and $AuSn_4$ phases, that variation may be neglected. Then it can be assumed that $(D^{\beta}_{Au})_3 \cong (D^{\beta}_{Au})_2 \cong D^{\beta}_{Au}$; $(D^{\alpha}_{Au})_2 \cong (D^{\alpha}_{Au})_1 \cong D^{\alpha}_{Au}$; $(D^{\beta}_{Sn})_3 \cong (D^{\beta}_{Sn})_2 \cong D^{\beta}_{Sn}$; $(D^{\alpha}_{Sn})_2 \cong (D^{\alpha}_{Sn})_1 \cong D^{\alpha}_{Sn}$. In that case the approximations $\Omega^{\beta}_3 \cong \Omega^{\beta}_2 \cong \Omega^{\beta}$ and $\Omega^{\alpha}_1 \cong \Omega^{\alpha}_2 \cong \Omega^{\alpha}$ are also justified. Thus the growth rates of the β and α intermetallic layers may be written in the following forms:

$$\frac{dX_\beta}{dt} = \Omega^{\beta}[2D^{\beta}_{Au}\frac{\Delta C^{\beta}_{Au}}{X_\beta} + \frac{1}{2}D^{\beta}_{Sn}\frac{\Delta C^{\beta}_{Sn}}{X_\beta} - (D^{\alpha}_{Au}\frac{\Delta C^{\alpha}_{Au}}{X_\alpha} + \frac{1}{2}D^{\alpha}_{Sn}\frac{\Delta C^{\alpha}_{Sn}}{X_\alpha})], \quad (7.18)$$

$$\frac{dX_\alpha}{dt} = \Omega_\alpha[D^{\alpha}_{Sn}\frac{\Delta C^{\alpha}_{Sn}}{X_\alpha} + 2D^{\alpha}_{Au}\frac{\Delta C^{\alpha}_{Au}}{X_\alpha} - (2D^{\beta}_{Au}\frac{\Delta C^{\beta}_{Au}}{X_\beta} + \frac{1}{2}D^{\beta}_{Sn}\frac{\Delta C^{\beta}_{Sn}}{X_\beta})]. \quad (7.19)$$

For simplification let us write: $2D^{\beta}_{Au}\Delta C^{\beta}_{Au} = A$; $\frac{1}{2}D^{\beta}_{Sn}\Delta C^{\beta}_{Sn} = B$; $D^{\alpha}_{Au}\Delta C^{\alpha}_{Au} = C$; $\frac{1}{2}D^{\alpha}_{Sn}\Delta C^{\alpha}_{Sn} = D$. Then:

$$\frac{dX_\beta}{dt} = \Omega_\beta(\frac{A+B}{X_\beta} - \frac{C+D}{X_\alpha}), \quad (7.20)$$

$$\frac{dX_\alpha}{dt} = \Omega_\alpha(2\frac{C+D}{X_\alpha} - \frac{A+B}{X_\beta}). \quad (7.21)$$

The general solutions, $X_\beta = g(t)$ and $X_\alpha = h(t)$, of these equations may not be found in the form of simple analytical functions. The best way to solve these equations may be that suggested in reference 78: Dividing Eq. 7.20 by Eq. 7.21 yields an equation of the form $\frac{dX_\beta}{dX_\alpha} = f(X_\beta, X_\alpha)$; the solution of this equation gives X_β as a function of X_α; substitution of this function into Eq. 7.21 gives a differential equation of the form $\frac{dX_\alpha}{dt} = f(X_\alpha)$; integration of this equation gives X_α as a function of t. The $X_\beta - t$ relationship results from $X_\beta = f(X_\alpha)$.

It can easily be shown that $X^2_\beta = K_\beta t$ and $X^2_\alpha = K_\alpha t$ can be solutions of Eqs. 7.20 and

7.21 with the constants K_β and K_α solutions of the two following equations:

$$\frac{1}{2}K_\beta^{1/2} = \Omega^\beta\left(\frac{A+B}{K_\beta^{1/2}} - \frac{C+D}{K_\alpha^{1/2}}\right), \tag{7.22}$$

$$\frac{1}{2}K_\alpha^{1/2} = \Omega^\alpha\left(2\frac{C+D}{K_\alpha^{1/2}} - \frac{A+B}{K_\beta^{1/2}}\right). \tag{7.23}$$

The constants, K_β and K_α, given by the resolution of these two equations, have the following expressions:

$$K_\beta = \frac{1}{2\Omega_\alpha}[\Omega_\beta^2(C+D)^2 + \Omega_\alpha^2\Omega_\beta^2(A+B)^2 + 6\Omega_\alpha\Omega_\beta^2(A+B)(C+D)]^{1/2} + \frac{\Omega_\beta^2(C+D) + 3\Omega_\beta\Omega_\alpha(A+B)}{2\Omega_\alpha}, \tag{7.24}$$

$$K_\alpha = \frac{1}{\Omega_\beta}[\Omega_\alpha^2(A+B)^2 + \Omega_\alpha^2\Omega_\beta^2(C+D)^2 + 6\Omega_\alpha^2\Omega_\beta(A+B)(C+D)]^{1/2} + \frac{\Omega_\alpha^2(A+B) + 3\Omega_\alpha\Omega_\beta(C+D)}{\Omega_\beta}. \tag{7.25}$$

It can be seen that K_β and K_α are complex combinations of A, B, C and D, in other words of D^β_{Au}, D^β_{Sn}, D^α_{Au} and D^α_{Sn}.

7.1.4 Analysis of observations

The $X_\beta - t$ and $X_\alpha - t$ relationships, determined experimentally, are of the form $X_\beta^2 = K_\beta t$ and $X_\alpha^2 = K_\alpha t$ in the initial stage of the layer growths. This parabolic growth of the layers was observed at different diffusion temperatures. So, if the β and α intermetallic layers grow by the combination of processes described earlier the variation with temperature of K_β and K_α would be related by the corresponding equation given above to D^α_{Au}, D^α_{Sn}, D^β_{Au} and D^β_{Sn}.

In the late stage of interdiffusion the thickness of the β phase layer continues to increase with diffusion time while that of the α phase layer remains constant ($\frac{dX_\alpha}{dt} = 0$). It follows from Eq. 7.19, for $\frac{dX_\alpha}{dt} = 0$, that:

$$D^\alpha_{Sn}\Delta C^\alpha_{Sn} + 2D^\alpha_{Au}\Delta C^\alpha_{Au} = \frac{X_\alpha}{X_\beta}(2D^\beta_{Au}\Delta C^\beta_{Au} + \frac{1}{2}D^\beta_{Sn}\Delta C^\beta_{Sn}). \tag{7.26}$$

The term $2D^\alpha_{Au}\Delta C^\alpha_{Au}$ represents combination of Au atoms with $AuSn_4$ at $AuSn_2/AuSn_4$ interface, according to equation 7.3 and the term $2D^\beta_{Au}\Delta C^\beta_{Au}$ represents transformation of

$AuSn_2$ into $AuSn_4$ according to equation 7.7. The term $D^{\alpha}_{Sn}\Delta C^{\alpha}_{Sn}$ takes into account the transformation of $AuSn_4$ into $AuSn_2$ according to equation 7.9 plus the combination of tin atoms with Au atoms at interface 1. The term $\frac{1}{2}D^{\beta}_{Sn}\Delta C^{\beta}_{Sn}$ takes into account the reaction of Sn atoms with $AuSn_2$, at $AuSn_2/AuSn_4$ interface, according to equation 7.5.

The ratio, $\frac{X_\alpha}{X_\beta}$, in the Eq. 7.26 just above, varies with time and so that equality cannot be true unless the two terms are nil which would mean that all reactions at $AuSn_2/AuSn_4$ interface, at interface 2 in Fig. 7.1, and the reaction at interface 1 ceased. There is no apparent reason for the reaction described by equation 7.7 and for the reaction described by equation 7.9 to occur in the early stage of interdiffusion but not in the late stage. There is no apparent reason either for the reaction described by equation 7.3 to occur in the early stage of interdiffusion but not in the late stage. On the other hand, occurrence of reaction (7.5) and that at interface 1 in the early stage of interdiffusion but not in the late stage would be justified by the depletion of tin at the β phase layer/solder interface. Therefore one may ignore the reactions (7.3), (7.7) and (7.9) because they certainly do not occur. After ignoring the terms which describe them in Eqs. 7.20 and 7.21 the layer growth rates for the initial stage of interdiffusion may be rewritten as follows:

$$\frac{dX_\beta}{dt} = \Omega^{\beta}\frac{\frac{A}{2}+B}{X_\beta} = \Omega^{\beta}\frac{D^{\beta}_{Au}\Delta C^{\beta}_{Au} + \frac{1}{2}D^{\beta}_{Sn}\Delta C^{\beta}_{Sn}}{X_\beta}, \tag{7.27}$$

$$\frac{dX_\alpha}{dt} = \Omega^{\alpha}(\frac{D}{X_\alpha} - \frac{B}{X_\beta}) = \Omega^{\alpha}(\frac{\frac{1}{2}D^{\alpha}_{Sn}\Delta C^{\alpha}_{Sn}}{X_\alpha} - \frac{\frac{1}{2}D^{\beta}_{Sn}\Delta C^{\beta}_{Sn}}{X_\beta}). \tag{7.28}$$

Then:

$$K_\beta = 2\Omega^{\beta}(\frac{A}{2}+B) = 2\Omega^{\beta}(D^{\beta}_{Au}\Delta C^{\beta}_{Au} + \frac{1}{2}D^{\beta}_{Sn}\Delta C^{\beta}_{Sn}), \tag{7.29}$$

$$K_\alpha = \frac{\Omega^2_\alpha B^2 + 4\Omega^4_\alpha B^4 + 64\Omega^2_\alpha\Omega^2_\beta D^2(A+B)^2 - 4\Omega^3_\alpha B^3}{2\Omega_\beta(A+B)} + \frac{32\Omega^3_\alpha DB^2(A+B) - 16\Omega^2_\alpha\Omega_\beta BD(A+B)}{2\Omega_\beta(A+B)}. \tag{7.30}$$

Thus, the variation with temperature of K_β is related to the variations with temperature of the diffusion coefficients of Au and Sn atoms within the β layer. That of K_α is related to

the diffusion coefficients of Sn atoms within both the α and β intermetallic layers. Now it was found that values of K_β determined experimentally from layer thickness measurements and plotted against the absolute temperature on an Arrhenius graph could be fitted quite well by a straight line (see Fig. 3. 20). This is only possible if the activation energies of Au and Sn atoms within the β layer are not too different from one another or if one term dominates over the other or if one term only exists in the equation of K_β. It is not impossible that the activation energies of Au and Sn atoms within the β layer are not too different from one another. There is an indication which suggests that the reaction (7. 1) occurs during the β layer growth. The indication is the smaller layer thickness in a Au/PbSnZn diffusion couple than in a similar couple made with zinc-free solder. It seems clear that gold atoms diffuse towards the solder and because they do not react exclusively with tin atoms to form $AuSn_4$ phase as in a diffusion couple made with zinc-free solder that the layer thickness is thinner. The proof that Au atoms do not react exclusively with Sn atoms in this system is the formation of Au-Zn intermetallics and a compound layer of $Au_{0.3}Sn_{0.3}Zn_{0.4}$ at the β layer/PbSnZn interface (see Fig. 5. 1). There is no indication which suggests that tin atoms react with $AuSn_2$ phase, at interface 2 in Fig. 7. 1, to form $AuSn_4$ phase during the β-phase layer growth but it is thought that they do. This is because after exhaustion of the gold film that reaction is known to occur since the remaining intermetallic compound in the joint is $AuSn_4$. Thus, the activation energy of the β-phase layer growth might reflect the activation energy for the diffusion of Au and Sn atoms, or of Au atoms only, within the $AuSn_4$ intermetallic layer.

The values of K_α, displayed on an Arrhenius graph, could not be fitted by a straight line. This was certainly due to the complex expression of K_α as a function of $D = \frac{1}{2}D^{\alpha}_{Sn}\Delta C^{\alpha}_{Sn}$ and $(A + B) = (D^{\beta}_{Au}\Delta C^{\beta}_{Au} + \frac{1}{2}D^{\beta}_{Sn}\Delta C^{\beta}_{Sn})$ and hence of temperature.

-Late stage of layer growth

The zero growth rate of the $AuSn_2$ layer in this stage of interdiffusion implied that all reactions at interface 2 must not occur in this stage. The only possibility for the β layer to grow is then at the expense of diffusing Au atoms from the gold film to the solder face. If the diffusion of Au atoms through the β layer controls the layer growth, the growth rate, $\frac{dX_\beta}{dt}$, may be written:

$$\frac{dX_\beta}{dt} = -\Omega_\beta D^\beta_{Au} \frac{\partial C^\beta_{Au}}{\partial x}, \tag{7.31}$$

and if the layer growth still occurs by quasi-steady state diffusion the growth rate may be written:

$$\frac{dX_\beta}{dt} = \Omega_\beta (D^\beta_{Au} \Delta C^\beta_{Au}) \frac{1}{X_\beta}. \tag{7.32}$$

Integration of this equation with respect to time from t_1, the time ending the initial stage, to the diffusion time t gives:

$$X^2_\beta = X^2_{\beta_1} + 2\Omega_\beta D^\beta_{Au} \Delta C^\beta_{Au} (t - t_1), \tag{7.33}$$

where X_{β_1} is the layer thickness at the diffusion time t_1.

The results of the diffusion experiments, $X^2_\beta - X^2_{\beta_1}$, appear to lie on a straight line when plotted against the diffusion time $(t - t_1)$ (see Fig. 7.2). This means that the layer growth occurs by quasi-steady state diffusion. If the diffusing species is Au, the slopes of the lines which are given in Table 7.1 would be equal to $2\Omega_\beta D^\beta_{Au} \Delta C^\beta_{Au}$. The variation with temperature of this quantity, on an Arrhenius graph, is not a straight line, however. This makes it impossible to determine the activation energy of the diffusing species.

7.1.5 Model for intermetallic formation in Au/PbSn systems

On the basis of the results discussed above, it seems that the most probable model for the solid-state growth of the Au-Sn intermetallic layers in Au/60Sn-40Pb diffusion couples can

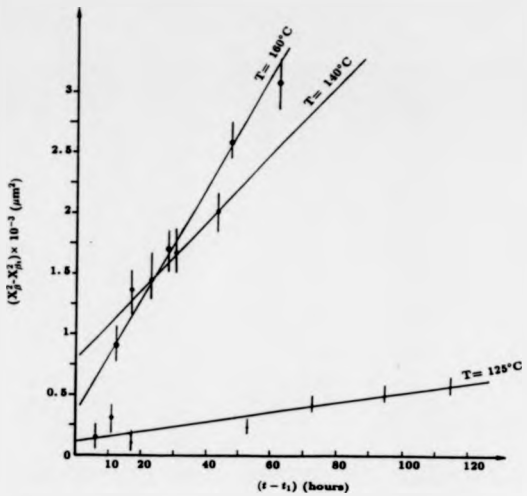

Fig. 7.2 Plot of $(X_\beta^2 - X_{\beta_1}^2)$ versus $(t - t_1)$ where X_β is the thickness of the $AuSn_4$ layer in a Au/60Sn-40Pb diffusion couple at a diffusion time t and X_{β_1} its thickness at the diffusion time t_1 which ended the initial stage of the layer growth.

Table 7.1 Slopes, K , of the straight lines which were fitted to the experimental points plotted in Fig. 7.2 above.

T(°C)	k ($\times 10^{10}$ cm^2/s)
160	1.27
140	0.79
125	0.104

be described as follows. A flux of tin atoms from the solder towards the gold film occurs between the joined materials. At the interface of the formed $AuSn_2$ and $AuSn_4$ layers, some of the diffusing tin atoms react with $AuSn_2$ phase to form $AuSn_4$ and the remainder diffuse across that interface, into $AuSn_2$ intermetallic layer. By diffusion through this intermetallic layer the unreacted tin atoms reach the other side of the $AuSn_2$ layer. The majority of the intermetallic compound which forms on this side, as a result of the arrival of Sn atoms, is $AuSn_2$. At the same time there is a flux of gold atoms from the gold film towards the solder. In contrast to the tin atoms, the diffusing Au atoms do not react at $AuSn_2/AuSn_4$ interface with $AuSn_4$phase to form $AuSn_2$ but react at $AuSn_4$ layer/solder interface with Sn atoms to form $AuSn_4$ phase. Thus, the growth of the $AuSn_2$ phase layer is governed by the diffusion of tin atoms and that of the $AuSn_4$ phase layer by both the diffusion of tin atoms and the diffusion of gold atoms. That is valid in the early stage of interdiffusion. In the late stage of interdiffusion, the diffusion of tin does not occur, due to depletion of tin at the intermetallic compound/solder interface, but that of Au atoms continues until the complete exhaustion of the gold film. As a consequence, the growth rate of the $AuSn_2$ phase layer is nil in this stage while that of the $AuSn_4$ phase layer is positive. A schematic diagram illustrating the growth processes of the intermetallic layers is shown in Fig. 7. 3.

7.2 Effect of silver on the growth rates of the intermetallic layers

The growth rate constants , K_β and K_α, in a Au/40Pb-60wt. %Sn diffusion couple and in a Au/36Pb-62Sn-2wt. %Ag couple have been determined in the temperature range [80-160°C] and are compared in Table 4. 1. It can be seen that the growth rate constants in a Au/PbSnAg diffusion couple are smaller than those in a Au/PbSn couple. The amount of tin in the silver-containing alloy is 2 wt. % greater than in the silver-free one. Excluding the proportion of tin

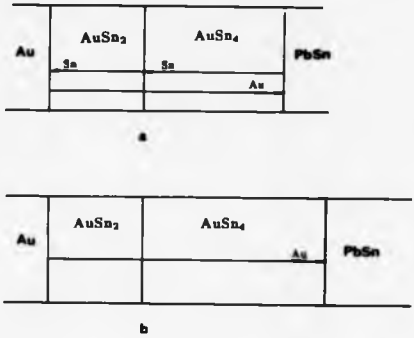

Fig. 7.2. Schematic diagram illustrating the growth of the $AuSn_2$ and $AuSn_4$ in a Au/PbSn diffusion couple: (a) in the initial stage of interdiffusion. (b) in the late stage of interdiffusion. The arrow-heads indicate where reactions occur.

which reacts with silver to form Ag_3Sn phase the difference is about 1.4 wt.% tin in favour of the silver containing alloy. Therefore, a bit more tin is available for intermetallic layer growth in a Au/PbSnAg diffusion couple than in a Au/PbSn couple. The slower growth of the intermetallic layers in a silver-containing couple than in a silver-free couple must be due in some way to the Ag_3Sn particles which were detected in the $AuSn_4$ layer. It is thought that such inclusions in the layer influence the diffusion rates in the following manner. Let us consider the diffusion of atoms through a layer of a material A containing inclusions of another material C. On its way across the layer, a diffusing atom may encounter one or more inclusions. Whenever this occurs, the atom might cross the inclusion or pass round it. If the activation energy for the diffusion in the inclusion is higher than that for the diffusion in the material A , the diffusing atoms will pass round the inclusions. In that case, as shown in fig. 7.4 for one atom, the path lengths of the migrating atoms, inside the layer, become longer than those in an inclusion-free layer of material A. Consequently, the time the atoms take to cross the layer becomes longer. During a diffusion time t, the average distance $\overline{X_1}$ covered by an atom in the direction X across the layer is smaller than $\overline{X_2}$ in the inclusion-free layer. The number of diffusing atoms per unit area of surface which reach the interface B (see Fig. 7.5) during the infinitesimal period of time δt is approximately equal to $\frac{1}{2}c_0\overline{X_1'}$ in the layer 1 and $\frac{1}{2}c_0\overline{X_2'}$ in the layer 2, where c_0 is the average concentration per unit volume of the diffusing atoms in the slices of thicknesses $\overline{X_1'}$ and $\overline{X_2'}$; $\overline{X_1'}$ and $\overline{X_2'}$ are the average distances covered by the diffusing atoms during the diffusion time δt in the layer 1 and 2 respectively. Since $\overline{X_1'} < \overline{X_2'}$ the number of atoms per unit surface attaining the interface B, during δt, in the case 1 is smaller than that in the case 2. Hence the growth rate of the layer 1 is smaller than that of the layer 2 since the growth rate of a layer depends on the magnitude(s) of the atomic flux(es) at its boundary(ies). As explained in sub-section 7.1.5, the growth of the layers of $AuSn_2$ and $AuSn_4$ occurs by the diffusion of Au and Sn atoms which must occur through the

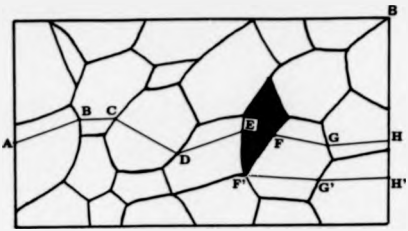

Fig. 7. 4. Scheme showing the effect of an inclusion (black on the picture) on the penetration of a diffusing atom. The letters A, B, ..., E, F, G, H represent possible positions of the atom inside the layer after successive intervals of diffusing times δt if the atom can go through the inclusion. If the atom cannot go through the inclusion its possible positions are A,B, ...,E,F',G',H'. It can be seen that in this case an extra-walk must be made by the atom to reach the point H' of the interface B.

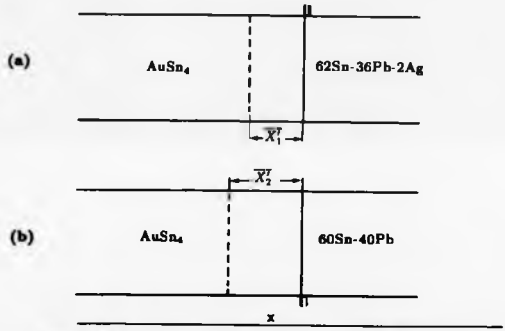

Fig. 7. 5. $\overline{X_1'}$ and $\overline{X_2'}$ are the average distances of migration, in the direction x, of a diffusing atom during an interval of time δt. $\overline{X_1'}$ must be inferior to $\overline{X_2'}$ because of presence of inclusions, Ag_3Sn in this case, in the $AuSn_4$ layer as explained above. All the diffusing atoms inside the slices of thicknesses $\overline{X_1'}$ and $\overline{X_2'}$ can cross the interface B after a diffusing time δt. The concentration of the diffusing atoms in a slice varies with x but for small $\overline{X'}$ it can be approximated by its value c_0 in the middle of the slice. In a random walk the number of atoms which cross the interface B per unit area of surface during δt is equal to $\frac{1}{2}c_0\overline{X_1'}$ and $\frac{1}{2}c_0\overline{X_2'}$ in (a) and (b) respectively. Therefore, in the case (a) the atomic flux at interface B is smaller than that in the case (b).

layer of $AuSn_4$. The Ag_3Sn particles present in this layer , in the Au/62Sn36Pb2Ag system, are thought to reduce the atomic fluxes in the described manner.

7.3 Type of diffusion

There are two types of diffusion, lattice and grain boundary diffusion, through which the atoms of Sn and Au can be transported through the intermetallic layers in Au/solder diffusion couples. The equations describing the growth rates of the intermetallic layers given earlier for lattice diffusion can be used for grain boundary diffusion under the condition that each term of the equations is multiplied by the corresponding ratio $\frac{a_i}{S}$ where a_i is the effective cross-sectional area for intergranular diffusion of the layer i and S the total cross-sectional area of the diffusion couple. For example, Eq. 7.11 can be written for grain boundary diffusion as follows:

$$\frac{dX_\beta}{dt} = (\Omega_2^\beta J_a + \Omega_2^\beta \frac{J_c}{2} + \Omega_2^\beta J_d) \times \frac{a_\beta}{S} - (\Omega_2^\beta J_b + \Omega_2^\beta \frac{J_a}{2}) \times \frac{a_\alpha}{S}, \qquad (7.34)$$

where a_β and a_α are the effective cross-sectional area for grain boundary diffusion of the β and α phase layer respectively.

Only for constant a_β and a_α does the integration, with respect to diffusion time, of Eq. 7.34 give $X_\beta = Kt^{1/2}$ under quasi-steady state diffusion conditions, where K is a constant. Because of the variation (decrease) of a_β and a_α with diffusion time due to the β and α layer grain growth, one may be tempted to conclude that the correlation of the experimental data with the equation $X_\beta = Kt^{1/2}$ is indicative of lattice diffusion. Because of uncertainty on the determined value, 1/2, of the exponent of t from the experimental results, it could be wrong to make such a conclusion. However, the low value of the activation energy (0.84 ± 0.02 ev) for the diffusion in the $AuSn_4$ layer may suggest that the type of diffusion is intergranular.

CONCLUSIONS

On the basis of the work presented in this thesis the following conclusions may be drawn pertaining to intermetallic formation in Au/60Sn-40Pb couples, the tensile strength of the Au/solder couple after aging, and the effects of additives (Ag, Zn) in the solder.

1) *Intermetallic phases* - The intermetallic phases are gold-tin compounds. Regardless of time and temperature the predominant phases are $AuSn_4$ and $AuSn_2$ with $AuSn_4$ predominating over $AuSn_2$. The gold richer phases of the Au-Sn system form after a certain diffusion time which decreases with increasing temperature and their amounts remain very small even after long diffusion times.

2) *Growth kinetics of the intermetallic layers* - Two stages occur in the variation of the thicknesses of the intermetallic layers with diffusion time. In the early stage, both the thickness of the $AuSn_4$ layer and the total thickness of the other intermetallic layers increase parabolically with time. In the late stage, the thickness of the $AuSn_4$ layer continues to increase with time and that of the other intermetallic layers ceases. The growth rate is greater in the early stage than in the late stage. The temperature dependence of the growth rate constant of the $AuSn_4$ layer obeys in the early stage to the equation:

K_{AuSn_4} (cm^2/s) = $1.7 \times \exp(-0.84/k_BT)$ with k_BT expressed in eV.

3) *Growth mechanisms of the intermetallic layers* - In the early stage, the growth of the intermetallic layers occur by both Au and Sn diffusion through them and reactions at the layer boundaries. While Au atoms react at the $AuSn_4$/solder interface only, Sn atoms react at both $AuSn_2$/$AuSn_4$ and Au film/$AuSn_2$ interfaces. In the late stage, because of depletion of the solder in tin, Sn diffusion through the intermetallic layers ceases. The growth rates of the intermetallic layers are diffusion controlled. The diffusions of Au and Sn atoms through the layers are probably grain boundary diffusion.

4) *Tensile strength of Au/solder bonds* - The tensile strength of Au/60Sn-40Pb joints, with or without silver in the solder, is independent of the number of intermetallic layers formed and their thicknesses as long as the gold film of the joint is not depleted. Before depletion of the gold film, the joint fractures during pull testing either both at the boundaries between the intermetallic layers and the $AuSn_4$/solder interface or at the intermetallic layer interfaces. After depletion of the gold film, the fracture occurs at the substrate/intermetallic compound interface. The adherence of the $AuSn_4$ compound to the substrate weakens slowly with aging time.

5) *Effects of impurities in the solder*

a) *Effect of silver* - The presence of 2 wt. % silver in the solder decreases the growth rates of the intermetallic layers but does not affect the forms of the layer thicknesses-diffusion time curves. The silver forms Ag_3Sn phase with tin. Particles of this phase incorporate in the $AuSn_4$ layer and hinder the diffusion of Au and Sn atoms through the intermetallic layer. The silver has no effect on the strength of the Au/solder joint.

b) *Effect of zinc* - Zinc in the solder forms a layer of a ternary compound of composition $Au_{0.3}Sn_{0.3}Zn_{0.4}$ and Au-Zn intermetallic phases between the $AuSn_4$ layer and the solder. It decreases the growth rate of the $AuSn_4$ layer but has no effect on the other intermetallic phases. The rate of degradation of the gold film also decreases. The tensile strength of the Au/solder joint after aging at 125 °C is very weak. The weakest region of the joint under a tensile stress is the wire/solder interface.

FUTURE WORK

Since Au/60Sn-40Pb joints appeared to weaken only after the gold film had been completely consumed and that the gold film life time is dependent on the fluxes of Au and Sn atoms across the joint , it may be possible to reduce these by:

1) Changing the microstructure of the gold film. This can be achieved by choosing the

adequate electroplating conditions (plating current, plating temperature, gold concentration in the solution, hardening additives in the solution, etc...). Therefore, it may be interesting to investigate how the growth rates of the intermetallic layers between gold films and the 60Sn-40Pb solder vary with the microstructure of the Au film.

2) Decreasing the amount of the solder in the joint in order to decrease the tin abundance. Therefore, it may be interesting to study how the gold film life time varies with the amount of the solder in the joint.

REFERENCES

L. S. Castleman and L. L. Seigle, Trans. TMS-AIME, 212 (1958) 589.

2 - E. Philofsky, Intermetallic formation in gold-aluminium systems, Solid-State Electronics, 13 (1970) 1391.

3 - P. M. Hall and J. M. Morabito, Diffusion problems in microelectronic packaging, Thin Solid Films, 53 (1978) 175.

4 - F. G. Foster, Embrittlement of solder by gold from plated surfaces, A. S. T. M. Special Technical Publication, no. 319 (1962) 13.

5 - W. G. Bader, Dissolution of Au, Ag, Pd, Pt, Cu, and Ni in a molten Tin-lead solder, Welding Journal,supplement, 1969 p. 551.

6 - J. A. Cunningham, Expanded contacts and interconnections to monolithic silicon integrated circuits, Solid State Electronics, 8 (1965) 735.

7 - T. B. Massalski, Binary Alloy Phase Diagrams, Vol. 2, p. 1848, American Society for Metals, Ohio, 1986.

8 - T. B. Massalski, Binary Alloy Phase Diagrams, Vol. 1, p. 293, American Society for Metals, Ohio, 1986.

9 - T. B. Massalski, Binary Alloy Phase Diagrams, Vol. 1, p. 316, American Society for Metals, Ohio, 1986.

10 - M. L. Ackroyd and C. A. Mackay, Circuit World, 3 (1977) 6.

12 - H. N. Keller,Temperature Aging of External Connection Condensations soldered to Ti-Pd-Au Thin Films, IEEE Trans., CHMT-2 (1979) 180.

13 - H. N. Keller, Reliability of Clip-On Terminals soldered to Ta-Ta_2N-NiCr-Pd-Au Thin Films, IEEE Trans., CHMT-2 (1979) 294.

14 - H. N. Keller, Significant Features of Solder Connections to Gold-Plated Thin Films, IEEE Trans., CHMT-5 (1982) 408.

15 - P. M. Hall and L. W. Condra, Aging of Solder Connections to Ti-Pd-Au Films, IEEE Trans. CHMT-2 (1979) 279.

16 - C. R. Jackson, Circuits Manufacturing, 13 (1973) 40.

17 - Unpublished work quoted by Ref. 18.

18 - C. Wright, The Effect of Solid-State Reactins upon Solder Lap Shear Strength, IEEE Trans., PHP-13 (1977) 202.

19 - L. Buene, T. Finstad, K. Rimstad, O. Lonsjo and T. Olsen, Thin Solid Films, 34 (1976) 149.

20 - V. Simic and Z. Marinkovic, J. Less Com. Met. ,51 (1977) 177.

21 - L. Buene, Thin Solid Films, 43 (1977) 285.

22 - L. Buene, Thin Solid Films, 47 (1977) 159.

23 - L. Buene, H. Falkenberg-Arell , J. Gjonnes and J. Tafto, Thin Solid Films, 67 (1980) 95.

24 - S. Nakahara and R. J. McCoy, Thin Solid Films, 72 (1980) 457.

25 - S. Nakahara and R. J. McCoy, Appl. Phys. Letter, 37 (1980) 42.

26 - L. Buene, H. Falkenberg-Arell and J. Tafto, Thin Solid Films, 65(1980) 247.

27 - S. Nakahara, R. J. McCoy, L. Buene and J. M. Vandenberg, Thin Solid Films 84 (1981) 185.

28 - D. Gregersen, L. Buene, T. Finstad, O. Lonsjo and T. Olsen, Thin Solid Films, 78 (1981) 95.

29 - B. Hugsted, L. Buene, T. Finstad, O. Lonsjo and T. Olsen, Thin Solid Films, 98 (1982) 81.

30 - R. W. Balluffi and J. M. Blakely, Thin Solid Films, 25 (1975) 363.

31 - W. J. Tomlinson, P. A. Rogers, J. Mater. Sci., 22 (1987) 2416.

32 - L. Quan, D. Frear, D. Grivas, J. W. Morris Jr, J. Elect. Mat. Vol. 16, no. 3, (1987) 203

33 - D. Frear, D. Grivas, J. W. Morris Jr., J. Elect. Mat., Vol. 16, no. 3, (1987) 181.

34- J. O. G. Parent, D. D. L. Chung, I. M. Berastein, J. Mat. Sci., 23 (1988) 2564.

35 - R. V. Penney, "current-induced mass transport in aluminium", J. Phys. Chem. Solids, 28 (1964) 335.

36 - P. S. Ho and H. B. Huntington, "electromigration and void observation in silver", J. Phys. Chem. Solids, 27 (1966) 1319.

37 - J. E. McDonald and J. G. Eberhat, "Adhesion in aluminium oxide-metal systems", Trans. Metall. Soc. AIME, 233 (1965) 512.

38 - I. R. Christie and W. Maaur, Gold Bulletin Vol. 19 no. 2 (1986) 40.

39 - P. Wilkinson, Gold Bullitin, Vol. 19, no. 3, (1986) 75.

40 - E. Raub and K. Muller, Fundamentals of Metal Deposition, (1967) Elsvier.

41 - Lea Ronal Technical Report (1976).

42 - D. K. Bowen and C. R. Hall, Microscopy of Materials, Macmillan 1975.

43 - P. J. Goodhew, Electron Microscopy and Microanalysis, Wykham Publications Ltd, London and Winchester 1975.

44 - F. Weinberg, Tools and Techniques in Metallurgy, Marcell Dekker, INC., New York Vol. 2, page 1-513.

45 - P. Duncumb and S. J. B. Reed, Quantitative Electon Probe Microanalysis, ed. K. F. J. Heinrich: N. B. S Spec. Publ. 298, 1968 page 133-54.

46 - S. J. B. Reed, J. Phys. D : Appl. Phys. 4 (1971) 1910.

47 - G. Love, M. G. Cox and V. D. Scott, J. Phys. D: Appl. Phys. ,11 (1978)7.

48 - H. A. Bethe, Ann. Phys. Lps. 5 (1930) 325.

49 - M. Green and V. E. Cosslett, Proc. Phys. Soc. 78 (1961) 1206.

50 - J. Philibert, X-Ray Optics and Microanalysis, Third Int. Symo. Stanford, 1963, page 379, ed. Pattee et al. Academic Press, New York.

51 - G. Love and V. D. Scott, J. Phys. D : Appl. Phys., 11 (1978) 1369.

52 - D. A. Sewell, G. love and V. D. Scott, J. Phys. D: Appl. Phys., 18 (1985) 1245.

53 - D. A. Sewell, G. Love and V. D. Scott, J. Phys. D: Appl. Phys. 20 (1987) 1567.

54 - R. Castaing, Ph. D. Thesis, University of Paris, 1951.

55 - S. J. B. Reed, J. Appl. Phys. 16 (1965) 913.

56 - D. R. Beaman, Anal. Chem. 39 (1967) 418.

57 - J. V. P. Long, unpublished work quoted by W. J. M. Salter, J. Phys. D, Ser. 2, 1, (1968) 541.

58 - D. M. Poole and P. M. Martin, Metall. Rev. 14 (1969) 61.

59 - C. J. Smithells, Metals Reference Book, Vol. 1, 4 ed., London Butterworths 1967, p. 324.

60 - Z. Kotrba, Microscopica Acta, Vol. 82, no. 1, (1987) 59.

61 - D. R. Beaman and L. F. Sololaky, Proc. 9th Ann. Conf. M. A. S. Ottawa, Canada, 1974, 26A-26E.

62 - Handbook of lattice spacings and structures of metals, W. B. Pearson, volume 2, Pergamon Press (1967).

63 - S. K. Tarby, M. R. Notis, Metall. Trans. B, Vol. 17B, no. 4 (1986) 829.

64 - D. R. Andrews, "Soldering, Brasing, Welding, and Adhesives", published by the institution of production engineers, 1978, p. 14.

65 - T. B. Massalski, Binary Alloy Ahase Diagrams, Vol. 1, p. 71, American Society of Metals, Ohio, 1986.

66 - T. B. Massalski, Binary Alloy Phase Diagrams, Vol. 1, p. 53, American Society of Metals, Ohio, 1986.

67 - K. Kusunoki, K. Tsumuraya, and S. Nishikawa, Trans. Jpn. Inst. Met. 22 (1981) 501.

68 - T. B. Massalski, Binary Alloy Phase Diagrams, vol. 2, p. 2086, American Society of Metals, Ohio, 1986.

69 - T. B. Massalski, Binary Alloy Phase Diagrams, Vol. 2, p. 1861, American Society of Metals, Ohio, 1986.

70 -H. H. Manko, Solders and Soldering, 2nd ed. (1979) McGraw Hill, New York.

71 - T. B. Massalski, Binary Alloy Phase Diagrams, Vol. 1, p. 338, American Society of Metals, Ohio, 1986.

72 - J. D. Baird, J. Nucl. Energy, part A, 11 (1960) 81.

73 - J. Colwell, G. W. Powell, J. L. Ratliff, J. Mater. Sci., 12 (1977) 543.

74 - C. Wagner, Acta Metall. ,17 (1969) 99.

75 - G. V. Kidson, J. Nucl. Mater., 3 (1967) 21.

76 - S. R. Shatynski, J. P. Hirth, and R. A. Rapp, Acta Metall. ,24 (1976)1071.

77 - Guan-xing Li and G. W. Powell, Acta Metall., 33 (1985) 23.

78 - V. I. Dybkov, J. Mater. Sci. 21 (1986) 3085.

79 - D. S. Williams, R. A. Rapp, and J. P. Hirth, Metall. Trans. A., 12A (1981) 639.

80 - M. M. P. Janssen, Metall. Trans. 4 (1973) 1623.

81 - A. J. Hickl and R. W. Heckel, Metall. Trans. A, 6A (1975) 431.

82 - F. J. J. Van Loo and G. D. Rieck, Acta Metall., 21 (1973) 73.

BEST COPY
AVAILABLE